

STUDIES OF THE DEVELOPMENT OF FABRICS IN
SOME NATURALLY DEFORMED LIMESTONES

Thesis by
James Ekstedt Conel

In Partial Fulfillment of the Requirements
For the Degree of
Doctor of Philosophy

California Institute of Technology
Pasadena, California

1962

ACKNOWLEDGMENTS

I am indebted to Professor W. Barclay Kamb of the California Institute of Technology for suggesting the problem treated herein, providing some of the materials used in the research, and for making his initial results available to me. His continued help and encouragement during practically all phases of the study, and his careful criticism of several manuscripts have helped me immeasurably. The work presented here could not have been completed in this form without his aid.

I also wish to thank Professor Ernst Cloos of the John Hopkins University for offering me the facilities of the geology department during my brief visit there, and also for his personal guidance on a field trip through western Maryland, during which materials of major importance for this research were collected.

Mr. W. M. Chapple took time from his own research to program for the computer some of the results given in a section of the thesis dealing with microtwinning lamellae. Numerous helpful discussions with him have also been greatly appreciated. Professor Clarence R. Allen criticized part of an early edition of the manuscript and has also given freely of his time in many discussions. Professors D. S. Wood, California Institute of Technology and J. F. Nye, University of Bristol, England, discussed problems with me relating to the dislocation mechanism of twinning in calcite.

I am very grateful for generous financial support in the form of fellowships and research funds from the Standard Oil Company of California, and fellowships from the Pan American Petroleum Foundation and California Institute of Technology (Harvey Mudd Summer fellowship).

Mr. R. von Huene prepared many special thin sections and also advised me on photographic problems. Judith A. Sidwell helped in drafting some of the illustrations.

ABSTRACT

The purpose of this investigation has been to study in detail the development of deformation fabrics in some naturally deformed limestones, with a view of testing the geological applicability of experimentally deduced origins of such fabrics in these materials. Flexurally folded limestones have been used to make comparisons between experiment and nature, by taking advantage of the approximately known character and variation of strain in these structures and using this information to deduce theoretically the deformation fabrics from place to place to compare with those actually observed in the structures. Two kinds of fabric problems are treated, ones dealing with gross changes in crystal orientation accompanying large strain, and those treating the origin of twinning lamellae in carbonate rocks in relation to applied stress, the so-called dynamic analysis. An extension of this analysis is made which allows quantitative information as to rock strain due to twinning (and translation gliding) to be obtained from thin sections.

Current theoretical treatments used in predicting fabric changes with strain in marble are found inadequate for predicting fabric changes with strain in flexure folds. Exact derivations of these fabrics for folds have not been made. Instead, an implication of a more general theory treating development of fabrics in metal aggregates is used to derive approximately the changes in c -axis orientations with large strain by analogy with fabrics obtained from experimental deformed Yule marble. Well defined fabric changes with large strain involving both twinning and translation gliding in individual crystals have not been observed in the folds studied.

Predicted results for the dynamic analysis of an aggregate with isotropic c -axis distribution are derived with special reference to one of the folds studied. The stress distribution in plane strain is calculated for the structure starting with an already partly folded unconfined layer of circular cross-section, and assuming it to be loaded elastically with simple compressive forces applied in the limbs directed normal to the axial plane. Twinning deformation in individual crystals is treated by assuming that the law of maximum resolved shear stress determines an active twin set in each grain. The results obtained are compared favorably with those observed in a natural fold.

Deformation fabrics from two small folds are given. The first fold occurs in a large anticlinorium in western Washington County, Maryland, in thinly bedded limestones and shales of the Silurian McKenzie Creek formation. The second is a drag fold on the eastern limb of a north-trending anticline in Carboniferous limestones and shales located in upper Darwin wash, Darwin Hills, Inyo County, California. In the Maryland fold, c -axis fabrics obtained from the axial region show no preferred orientation due to deformation, but a dynamic analysis of the twinning lamellae is in good agreement with that expected in theory. The dynamic analysis is shown to be sensitive in depicting small changes in twinning deformation throughout portions of the body examined. The strains due to twinning are compatible with bending in part of the structure. More quantitative comparisons of the observed and expected deformation have shown that under a derived system of stress at the axial plane, twinning deformation in 80% of the grains in the aggregate has followed the law of maximum resolved shear stress. The amount of twinning strain within individual crystals varies with their orientation in the stress field. The calculated visible (twinning) strains of about 0.01 are considerably less than the strains computed from the geometry of the fold of 0.25, and much of this discrepancy may be due to fracturing (slip on planes parallel to bedding) during folding.

In the fold from Darwin wash, observed fabrics cannot be related simply to the megascopic deformation in the fold. Preferred orientations of c -axes are thought to be partly due to veining in the rock. Fabric changes due to twinning are however qualitatively correlated with shortening in the fold perpendicular to the axial plane, and a shear similar to that necessitated by the relation of the drag fold to the major anticline with which it is associated. Calculated visible strains are considerably less than those approximately deduced from fold geometry, but can be partially correlated with the observed deformation in the structure. Analysis of the deformation in nonhomogeneously strained individual crystals of these aggregates (Appendix II) shows that in addition to $e \{01\bar{1}2\}$ twinning, translation gliding has occurred on most types of glide planes deduced for calcite from laboratory experiments. Microscopically these rocks appear to have undergone large deformation, exhibiting local cataclastic texture, much twinning and warping of individual crystals. However, well defined formation fabrics due to large strain have not been observed in them.

A second part of this investigation has dealt with the so-called nontwinned lamellae in calcite and dolomite. From these studies it has been concluded that such structures are extremely thin (a few microns) but otherwise normal twin lamellae parallel to $e\{01\bar{1}2\}$ in calcite and $f\{02\bar{2}1\}$ in dolomite, and are for this reason renamed micro-twinned lamellae. In addition to interference colors, these lamellae exhibit four different types of interference fringes. A new method is presented, which utilizes the optical properties of the twins, for obtaining the orientation of lamellae inclined at small angles to the plane of a thin section. The utility of this technique lies in the fact that it may be used to eliminate the central "blind-spot" in twin lamellae fabric diagrams. Some measurements of twin thicknesses, made using the new orientation method, are given, together with calculations which show that only an average and not a cumulative optical thickness for a stack of lamellae superposed in thin section may be obtained using the method.

TABLE OF CONTENTS

TITLE	PAGE
INTRODUCTION AND PURPOSE OF THE INVESTIGATION	1
PREVIOUS WORK	7
BASIC CONCEPTS AND METHODS	17
Nature of the Structures Selected for Study	17
Choice of folded limestones as subject	17
Detailed requirements for the folds	19
Strain Distribution in Folds	21
Simple model for the bending strains in flexure folds	21
Approximate calculation of strains in fold	29
Principles for the Comparison of Theoretical and Observed Fabrics in Folds	34
Types of fabric comparisons	34
Gross changes in crystal fabric arising from strain	34
Dynamic interpretation of deformation lamellae	44
Calculation of Bulk Strain from Petrofabric Data	55
Visible bulk strain due to twinning	56
Strain due to translation gliding	61
Accuracy of the strain calculations	65
Relation between the strain calculations and dynamic analysis	70

TITLE	PAGE
Petrofabric method for determining the bulk rheological properties of limestone under deformation in nature	71
Petrographic Techniques Employed	74
Petrofabric analysis procedure	74
New developments in carbonate petrofabric study	76
FABRIC STUDIES OF FOLDED LIMESTONES	79
Introduction	79
Localities Examined	81
Folds from the Cacapon Mountain Anticlinorium	90
Geologic setting	90
Detailed description	93
Petrographic character of the rock	97
Fabrics from the fold	101
<u>c</u> -axis fabrics	101
<u>e</u> -lamellae preferred orientation	101
Dynamic analysis results	105
<u>c'</u> -axis orientations	110
Calculation of strains due to twinning	111
Fabrics of highly deformed vein material	121
Application of the law of maximum resolved shear stress	124
Fold from the Darwin Hills, Inyo County, California	131
Geologic setting	131
Description to the fold studied	139
Petrographic character of the rock	143

TITLE	PAGE
Results of the fabric studies	147
<u>c</u> -axis fabrics	147
<u>c'</u> -axis fabrics	149
<u>e</u> {01 $\bar{1}$ 2} orientation data	153
Dynamic analysis of <u>e</u> -lamellae	155
Calculation of strain due to mechanical twinning .	158
Interpretation of the Darwin fabric results and	
comparisons with experimental studies	166
Summary and Conclusions Drawn from the Fabric Studies	169
Future Studies	173
NATURE AND PROPERTIES OF <u>e</u> {01 $\bar{1}$ 2} LAMELLAE IN CALCITE	
AND <u>f</u> {02 $\bar{2}$ 1} LAMELLAE IN DOLOMITE	174
Introduction	174
Previous Studies	176
Description of Microtwinning Lamellae	178
Interference colors and fringes	179
Origin of the fringe features and interference	
colors	184
A New Method for Measuring Orientations of	
Twinning Lamellae	192
The "blind spot" problem	192
Physical principles of the method	194
Method for measuring orientation of lamellae used	
in practice	196
Difficulties in the method	197
Principle use of the orientation method	198

TITLE	PAGE
Determination of Lamella Thickness	199
Optical Effects Produced by Superposition of Several Thin Lamellae	204
Introduction	204
Exact calculation for the two-lamellae case . . .	207
Experimental test of the results for two superposed lamellae	216
Extension of the calculations to the case of three or more lamellae	218
Summary of results of previous sections	222
APPENDIX I. CRYSTALLOGRAPHIC NOTATION AND A SUMMARY OF EXPERIMENTALLY DETERMINED GLIDING ELEMENTS IN CALCITE	224
APPENDIX II. GLIDE MECHANISMS OBSERVED IN THE DARWIN FOLD	228
APPENDIX III. DISLOCATION MODEL FOR THE GROWTH OF MECHANICAL TWINS IN CALCITE	235
REFERENCES	250

LIST OF FIGURES

FIGURE	PAGE
1.	23
2.	25
3.	43
4.	48
5.	52
6.	58
7.	91
8.	92
9.	94
10.	95
11.	99
12.	102
13.	103
14.	109
15.	120
16.	123
17.	126
18.	129
19.	132
20.	133
21.	137
22.	138
23.	145

FIGURE

PAGE

24.	148
25.	151
26.	152
27.	154
28.	157
29.	161
30.	161
31.	180
32.	182
33.	186
34.	186
35.	187
36.	195
37.	202
38.	206
39.	212
40.	212
41.	212
42.	226
43.	245
44.	248

LIST OF TABLES

TABLE	PAGE
1.	33
2.	189
3.	203
4.	227
5.	232
6.	234
7.	243

INTRODUCTION AND PURPOSE OF THE INVESTIGATION

The purpose of this study is to test in detail the applicability of experimental studies on the origin of deformation fabrics in carbonate rocks to the origin actually observed in such rocks in nature.

The geological literature contains abundant petrofabric data bearing on the problem of preferred crystal orientation in many kinds of deformed rocks. Investigations of this type were first carried out by Sander (1911) who applied the methods of petrofabric analysis to complexly deformed rocks in the eastern Alps. The purpose of these investigations was to understand the deformational history of the rock as defined by their fabrics. The central problem in interpreting all fabric data has been to understand how preferred crystal orientations arise in nature--whether intracrystalline plastic deformation, cataclasis, recrystallization, or some combination of these processes is responsible for the fabrics. Such understanding is obviously necessary if any certain conclusions are to be drawn from the fabrics either as to the strain the rock has undergone or as to the forces that acted upon it during deformation. Prior to the efforts of Griggs (1936, 1939) most experimental data on the mechanism of plastic deformation of a poly-crystalline material pertained to metals. It was natural therefore to look to deformed metal textures to provide insight as to how deformation fabrics arise in rocks.

Close comparisons between rock and metal fabrics have been justified on the grounds that both rock forming minerals and metal crystals deform by the same mechanisms, translation gliding and twinning, and through recrystallization. Rock and metal deformation is also similar in that both types of material show plastic flow, work hardening, and creep, and both may be annealed at high temperatures after cold working (Griggs, 1940; Griggs et al., 1960). On the other hand, the atomic structure and bonding of metals is profoundly different from that of most common rock forming minerals. Nevertheless the results of 25 years of experimental work have largely shown the validity and usefulness of these comparisons.

Griggs et al. (1960, p. 104) thus conclude:

Our [experimental] results with rocks and rock forming minerals without exception follow the empirical laws developed in the study of metals. This implies that the vast body of data collected in experiments on metals may be applied in some detail to the interpretation of deformed rocks

In accord with experience in metals we find that flow by intracrystalline gliding obeys the law of maximum resolved shear stress and that deformation is nearly homogeneous. It follows that if the active glide systems of the component crystals are known fabric changes resulting from plastic strain without recrystallization may be predicted for any stress and strain system.

As an example, Turner et al. (1956) have had great success in predicting fabric changes which occur in Yule marble during uniaxial testing under laboratory conditions using methods akin to those of the metallurgist.

The present work is an effort to gain further understanding of how crystal fabrics develop in nature by attempting to test the geological applicability of the experimental fabric studies of marbles. Comments of DeSitter (1956, p. 112) are pertinent to the argument for this kind of study:

In my opinion the [fabric] interpretation problems can be solved only by careful fabric studies of structures whose major features and microstructures are both well known beforehand. The tendency to depend on deformation experiments in the laboratory in order to find the solution is to my mind a wrong road; we have . . . not the slightest guarantee that the experiment arrives at an identical structure by the same path as in nature.

There are well recognized reasons for believing that some differences exist between laboratory experiments and nature. Strain rates in the laboratory are probably in most cases much greater than those experienced by naturally deformed rocks, and this may determine that the magnitudes of the stress differences involved in the flow of rocks under natural circumstances may be small, below experimentally determined yield stresses. Extending the analogy with metallurgical findings, it can be said that if rocks do deform naturally in slow creep and at elevated temperatures with prolonged times of loading, opportunity is given for processes to operate which have larger than average activation energies (Cottrell, 1953, p. 213). Thus recovery, recrystallization, grain growth, diffusion, and slip at grain boundaries could contribute to the deformation of rocks during high temperature creep, in addition to the various intracrystalline slip processes which are active to some extent at all temperatures

and which provide the dominating mechanism of deformation in laboratory experiments on carbonate rocks.

Carbonate rocks are the most advantageous types of geological material one might choose for the comparative investigation pursued here for several reasons. (1) Of greatest importance is the fact that the mechanical behavior and the corresponding development of crystal fabrics in response to strain in the laboratory are rather well understood in calcite and dolomite rocks. Detailed comparisons between laboratory and natural experiments are thus possible. (2) Calcite and dolomite aggregates in thin section show a variety of intragranular features which are direct evidence of mechanical deformation, and which permit detailed studies of how individual grains have participated in the deformation of the aggregate. (3) Calcite and dolomite are also comparatively simple minerals structurally and this fact makes feasible a study of their deformational properties in terms of the atomic mechanisms involved.*

The present investigation proceeded in the following steps:

- (1) A search was first made for naturally deformed

*In Appendix III e $\{01\bar{1}2\}$ mechanical twinning in calcite is treated using a dislocation mechanism like that applied to twinning in body centered cubic and hexagonally close packed metals. Though this study is not of direct concern to the major topic dealt with here, a geologically important reason for establishing such a twinning mechanism for calcite is to form a basis upon which a structural theory of recovery creep might be established for this material.

limestone having approximately known strain distributions, and in which observable fabric changes produced by the deformation could be expected.

(2) For ostensibly suitable samples, c-axis* and e-lamellae fabrics were measured and the degrees of fabric change as a function of the estimated amount and character of the strain were evaluated. These data should make it possible in principle to distinguish syn-tectonic fabrics from pre- and post-tectonic ones, and enable fabrics predicted on the basis of laboratory experiments to be compared with the fabrics observed in the naturally deformed specimens that have been subjected to approximately known strain.

(3) The "dynamic analysis" technique of Turner (1953) was then applied to the fabric data. An extension of this technique was also developed that made possible a quantitative determination of the strain history recorded in the rock. The results obtained in this step make possible an evaluation of the geological applicability of both the qualitative (Turner, 1953) and quantitative approaches (p.56 this thesis).

(4) From the data obtained in investigation of (2) and (3), an attempt was made to draw conclusions about the mechanics of limestone deformation under natural conditions. In particular, the following questions were treated:

- (a) Can the mechanisms of plastic deformation of calcite crystals in nature be distinguished

* Crystallographic notation is explained in Appendix I.

from those known from laboratory experiments?

(b) To what extent may the fundamental assumptions embodied in predicting fabrics for experimentally deformed Yule marble be shown to apply in nature? For example, is the "law of maximum resolved shear stress" applicable to both twinning and translation gliding in naturally deformed aggregates?

(c) To what extent can the macroscopic rheological laws governing the deformation of limestone under natural conditions be determined from the petrofabric data?

(5) A natural but unexpected outgrowth of the above studies has been an investigation of the optical properties and crystallographic significance of the so-called non-twinned lamellae of calcite and dolomite (Turner et al., 1956, p. 896), a type of intragranular structure that is a conspicuous feature of the deformed rocks studied. In this work a useful new technique for carbonate petrofabric measurement has been discovered.

The material outlined above may be rather naturally divided into two parts, one dealing with the detailed fabric studies and the other with microscopically observable features in naturally deformed carbonate aggregates. In the first part, pertinent experimental studies and previous applications of the laboratory investigations to petrofabric problems are first summarized. Basic concepts and methods relating to the

fabric studies are then developed, viz., the nature of the geologic structures selected for this study--flexurally folded limestones, a discussion of the strain distribution in flexure folds, principles upon which comparisons of theoretical and observed fabrics are based, the development of a method for calculation of bulk strain from petrofabric data, a method for obtaining the rheological laws of natural limestone deformation in nature, and the various petrofabrics techniques used in the investigation are then treated in this order. The detailed fabric results are then given. Following the fabric studies attention is devoted to the problem of the non-twinned lamellae, and other microscopic deformation features observed in the rocks studied here. Glide mechanisms observed in individual crystals of naturally deformed rocks studied here, and the problem of a dislocation mechanism of mechanical twinning in calcite are treated in appendices.

PREVIOUS WORK

From the various experimental and supporting microscopic studies of Griggs, Turner, and co-workers (Griggs and Miller, 1951; Handin and Griggs, 1951; Turner and Ch'ih, 1951; Griggs et al., 1951; 1953; Turner et al., 1954; Turner et al., 1956; Griggs and Handin, 1960; Handin et al., 1960) a good understanding has emerged of the mechanical behavior and development of preferred crystal orientations with strain in Yule marble. The following results are of importance to

the present study. Many of these matters are treated in more detail later and are only summarized here.

(1) For confining pressures of from 3,000-10,000 kgm/cm² and over a temperature range of 24°-500° C, both Yule marble and single calcite crystals deform by intracrystalline gliding, the principal mechanisms being twinning on \underline{e} {01 $\bar{1}$ 2}* and translation gliding on \underline{r} {10 $\bar{1}$ 1}. At 24° C and between 500° and 600° C, \underline{f} {02 $\bar{2}$ 1} translation gliding also has been found active to some extent, but never dominant over \underline{r} translation gliding. At 800° C \underline{c} (0001) gliding may occur.

(2) In both single crystals and with aggregates the law of maximum resolved shear stress has been found to apply approximately. This law states that from all accessible glide systems in a crystal of a given type, the system which operates during deformation is that one upon which the resolved shear stress is greatest. For the available glide systems in calcite, the critical resolved shear stress for \underline{e} twinning is lower by a factor of about 10² than that for translation gliding on \underline{r} . With increasing temperature the difference decreases and between 500°-600° C the critical values for each type of glide are equal approximately.

(3) In deformed marble, each crystal of the aggregate undergoes the same microscopic strain as the strain of the aggregate in bulk. This is the homogeneous deformation hypothesis of Taylor (1938).

* Experimentally determined glide mechanisms are crystallographically defined and summarized in Appendix I.

(4) In predicted fabric studies supporting the experimental work, it has been found satisfactory to assume for purposes of calculation that each grain of a marble aggregate experiences the same stress as the aggregate as a whole during deformation.

(5) Experimental deformation of Yule marble in uniaxial compression and extension causes significant reorientation of the original strongly preferred optic-axis orientation of the marble. For deformation of 40% or greater in compression, strong preferred orientations of c-axes develop at 10-30° to the axis of compression. With elongations of 90-120%, axes concentrate at 60-80° to the principal axis of extension. In each case the symmetry of the deformed fabric corresponds to the symmetry of the developed strain. Preferred orientations become more sharply defined with increasing temperature and corresponding increases in deformation.

From time to time general summaries in English of the relationship between the experimental deformation of rocks and the evolution of tectonite fabrics have been compiled (Knopf and Ingerson, 1938; Turner, 1948; Fairbairn, 1949; Turner, 1952). More recently there have been several attempts to apply results of experimental carbonate deformation to some particular geologic problems. (Turner, 1952; McIntyre and Turner, 1953; Gilmour and Carman, 1954; Weiss, 1954; Crampton, 1956; Turner, 1957; Christie, 1958; Nickelsen and Gross, 1959).

However, as far as I have been able to discern from the abundant and widely scattered petrofabric literature, there has been no attempt to make a detailed comparative study of the type contemplated here. Petrofabric applications of the experimental work on calcite deformation are summarized below.

Turner (1952) provides some qualitative comparisons between experimental and natural fabrics. He suggests that fabrics resulting from various degrees of laboratory deformation are to be compared with fabrics from three kinds of natural marbles: (a) marbles showing cataclastic microstructures, cloudy grains, numerous warped twinning lamellae, a single strong lineation and no foliation (the B-tectonites). Rocks of this class have strong c-axis girdle fabrics with the girdle plane normal to the lineation. These rocks are thought, by analogy with experimental studies, to be the subject of squeezing on all sides (Einengung) at right angles to the lineation, and extension parallel to the lineation. (b) Marbles comprised of clear equant grains showing no cataclastic effects and only limited twinning. Fabrics are considered the result of post- or para-kinematic recrystallization and show c-axis girdles with the pole to the girdle plane parallel to the b-lineation (fold axes). (c) Other marbles with fabrics resulting from recrystallization, have a well defined foliation and no lineation, and show single c-axis maxima which may or may not coincide with directions of maximum compression.

More specific comparisons between experimental and natural fabrics have been made by Turner et al. (1956, p. 1292) in noting that c-axis fabrics obtained by Sander (1950, D60,61) closely resemble those resulting from 40% shortening of Yule marble in uniaxial compression normal to its initial foliation. However these authors feel that the resemblance may be fortuitous. This in fact must be the case unless Sander's material had a pre-tectonic fabric similar to that of Yule marble and was subsequently naturally deformed in a similar manner to the experiments. Sander's fabric is discussed below (p. 44).

Another comparison is made by McIntyre and Turner (1953), who maintain that observed c-axis preferred orientations in marbles from Mid-Strathspey and Strathavon, which conform to a B-tectonite pattern (a symmetry axis (B) coincident with the b-axis of the megascopic fabric of lineation and fold axes) are, by analogy with experimental studies, the result of a regional compression normal to the regional tectonic axis (B).

Weiss (1954) has studied in detail a highly complex area of folded marbles and quartzites, part of a roof pendent lying in granite near Barstow, California. He believes that preferred orientations of c-axes in the calcite marbles investigated coincide in orientation with an axis of maximum compressive stress immediately before cessation of deformation in the area, an opinion based on analogy with results from the experimental studies. All c-axis maxima are approximately

normal to the foliation, and normal to the trend of fold axes throughout the area.

Many studies have also been made using the "dynamic" interpretation of deformation lamellae in calcite, a technique due to Turner (1953). The method is used to determine simple systems of stress that could account for observed deformation in twinning in carbonate rocks. It is discussed in greater detail later (p. 44). Turner (1953) has applied the dynamic analysis technique to Yule marble and to marbles from Sonora, California, and Moray Firth, Scotland. In each case it was concluded that the twinning lamellae resulted from a late minor deformation unrelated to the deformation responsible for the major c-axis patterns observed in the rocks. A number of other workers have since applied the technique to some specific structural problems, and have attempted to show that the results obtained are not incompatible with the grosser aspects of the structural environment from which the specimens were obtained. With one exception, none of these investigations deal with details of the structures examined. For example Crampton (1956) compares fabrics of coexisting calcite and dolomite in the Loch Shin limestone. The c-axis fabrics for both calcite and dolomite are isotropic. He finds that the dolomite is much less twinned than the calcite, an observation consistent with the experimental deformation of these materials (Turner et al., 1954; Griggs et al., 1953).

Dynamic analysis of the twinning lamellae fabric indicates a compression normal to foliation in the marble and a direction of tension parallel to a lineation defined by elongated grains in the rock. Crampton (1958) has also studied limestones (both calcite and dolomite) adjacent to thrust faults in the northwest highlands of Scotland. He maintains that the dynamic analysis defines an axis of rotation (this axis being normal to the plane of a compression axis girdle) which is consistent with the generally accepted direction of movement on the thrusts--northwest-southeast. However, other results obtained from the same area and specimens also suggest movements in a nearly perpendicular direction.

Gilmour and Carman (1954), using the dynamic analysis, suggest that the sense of movements on the northwest limb of a northeast trending (Cowal) anticline in the Strachur region (southwest Highlands of Scotland) are not inconsistent with shapes of associated minor folds and strain-slip cleavages.

Results of a dynamic interpretation of the marble fabric obtained by Weiss (1954) from the Barstow area disclose no obvious or consistent relations with either foliation or c-axis maxima in the rocks (pp. 56-57 of his report).

Christie (1958) has applied the dynamic analysis to a dolomite with mylonitic textures from the Moine thrust zone in northwest Scotland, and has concluded that the results of the analysis are statistically correlative with similar data obtained from an analysis of internally rotated lamellae in some

grains. The associated deformation is considered to be late, low temperature and post-crystalline in age, and is not directly correlative with known deformation associated with the Moine thrust.

McIntyre and Turner (1953) studied marbles from widely separated localities (maximum of 20 miles apart) in Mid-Strathspey and Strathavon. Results of the dynamic analysis indicate a sub-horizontal compression of the rocks from each locality in a direction transverse to a tectonic axis (the axis being defined by lineation and axes of overturned folds) plunging 30° southeast.

Nickelsen and Gross (1959) have made a petrofabric study of the Conestoga limestone from Hanover, Pennsylvania. A dynamic analysis of the twinning lamellae fabric of these rocks yields a direction of compression which is normal to slaty cleavage and normal to the plane of flattening of grains, pebbles, and boulders in associated limestone conglomerates. Directions of shear in the rock, constructed by plotting glide directions and glide planes in twinning, are parallel to the b-lineation defined as the intersection of bedding with slaty cleavage. Pebbles and boulders are elongated along the a-axis of the megascopic fabric, which is perpendicular to the b-axis in the cleavage plane. They conclude that the low grade (green-schist facies) rocks studied yield good preferred orientations of c-axes and compression and tension axes from the dynamic

analysis method, and that the methods of Turner (1953) are therefore definitely applicable to rocks on this metamorphic grade.

In neither type of fabric study discussed above, either comparisons of gross fabric between experiment and nature or applications of the dynamic analysis, has there been an attempt to correlate quantitatively rock fabric with deformation, although the work of Nickelsen and Gross (1959) with the dynamic analysis in an apparently secondary way, approaches this objective to some extent. In the present study the attempt is made to make such correlations.

To effectively carry out these correlations it is necessary, as in the case of Nickelsen and Gross (1960), to find rocks which have undergone a known strain. In the next section arguments for using flexure folds for this purpose are developed. Fabric studies involving folds have previously been made in carbonate rocks by Sander (1930, D 180, 181), and in quartzite by Ladurner (1954), Christie and Raleigh (1959) and most recently by Jones (1959). Sander's results are discussed below (p. 44). Christie and Raleigh (1959) have used folds as an index of deformation to study deformation lamellae in quartz. Jones has made detailed application of a technique used by Ladurner for analysing folding in quartzite. The method involves plotting c-axis orientation maxima from various parts of folded layers

relative to a line tangent to the layer at the places where fabrics are measured. By flattening out a stratum (or "unrolling" it) the combined effects of bending and folding due to shear parallel to the axial plane are assessed. If the angle between the directions of the maxima and the line tangent to the bed is constant, simple bending is indicated. If maxima are disposed at different angles, though tilted nearly symmetrically about a plane containing the axis of flexure, then shear parallel to the axial plane is thought to be involved. It is perhaps significant to this work that fabric changes (reorientation of c-axis maxima) due to bending in quartz are not observed in the crests of these folds.

BASIC CONCEPTS AND METHODS

Nature of the Structures Selected for Study

Choice of folded limestones as subject

A variety of possibilities can be considered in the search for deformed carbonate rocks that might be used in this investigation. The principal requirement with any such naturally strained body is to be able to discern from geometrical evidence the nature and spatial variation of the strain within the body so that observed fabrics can be compared with fabrics theoretically predicted to evolve under similar strain. The nature and amount of strain rocks have undergone may in some instances be indicated by boudinage, deformed fossils, oolites, pebbles, and the like (Cloos, 1947). However, in the present study small flexural folds have been chosen. The purpose here is to deal with a limestone body of a type that is available under a variety of geological conditions, a body in which the strain distribution can be approximately deduced from geometry on the basis of general mechanical principles, and in which the variation in character and amount of rock strain and rotation from place to place in the body can also be used as a tool to distinguish pre-deformation, syn-deformation, and post-deformation fabrics. Thus fabrics from relatively unstrained portions of a fold, i.e. the limbs, can be used as a guide to

the pre-deformational fabric of the rock which then in turn can be used as a basis for calculation of the fabric changes expected for strain in other portions of the structure, particularly the axial region. As will be examined in more detail below, it appears that fabric changes in a deformed rock should be functions of the strains imposed and not the deforming forces. In principle it should be possible to distinguish fabrics due to bending strains from post-deformational fabrics unrelated to bending. In the axial region of a fold two similar fabrics of different orientation will ideally emerge with strain, those due to shortening and extension perpendicular to the axial plane, the symmetry of the fabrics being that of the deformation. Because of the decrease in strain away from the axial region, deformation fabrics will be less sharply defined than those at the axial plane. These smaller strain fabrics will possess the same symmetry but will be symmetrically rotated about the fold axis. Ideally it is thus possible to obtain a variety of fabrics from a fold and to definitely relate these to the deformation within the layer. In following sections some general remarks are made concerning strains and related deformation fabrics in folds, but interest is primarily confined to the axial region for reasons of simplicity. First, mechanical and geometrical requirements are established for the structures used in this study.

Detailed requirements for the folds

Folded limestones actually selected for this study were ideally required to meet the following specifications to simplify the problems of determining the strain distribution and the carrying out of comparisons of observed and predicted fabrics. The requirements are that:

(1) The folds should be of the flexure type so that large variations of predominantly bending strain throughout the structure could reasonably be expected.

(2) The folds should have simple geometry, ideally with approximately circular cross-section in the axial region, to simplify calculation of the strains.

(3) The folds should have small radii of curvature relative to thicknesses of individual beds to assure large internal strains.

(4) Individual strata comprising the folds should be free of fractures, cracks, cleavage, joints, veinlets, etc., to insure that strain has not been accommodated by these means.

(5) Individual beds comprising the fold should be mechanically competent and intercalated with shales or other

less competent materials so that shear stresses on the boundaries of layers are low compared to shear stresses within the folded layers themselves. When the boundary shear stresses are reduced to negligible values, then, aside from normal pressures on the boundaries, only stresses acting on transverse sections of the beds need be specified in the boundary conditions for calculation of stresses and strains in the layer for an elastic or plastic material.

(6) The limestones should be homogeneous and equigranular with crystals sufficiently large to be accessible to measurement with the universal stage. To facilitate comparisons with experiments, rocks texturally similar to Yule marble would be ideal. There is an additional reason for choosing coarsely crystalline rocks, for as is discussed below (p.168), finely crystalline calcite rocks may deform by different mechanisms than ones with coarser crystal.

(7) The aggregates should ideally show some evidence of plastic deformation (twinned crystals, warped twin lamellae) to assure at least to some extent that effects of deformation have not been removed by an annealing recrystallization after deformation.

(8) After folding the limestones must not have undergone recrystallization of sufficient intensity to obliterate fabrics and microstructures produced by the deformation.

Strain Distribution in Folds

In the following sections a model of the distribution of strain throughout an unconfined layer that has been subjected to large bending will be developed as a basis for establishing theoretically predicted fabrics to compare with observed fabrics in actual folds. The question of calculating these strains which accompany large bending is then treated for the case of an elastic-plastic body.

Simple model for the bending strains in flexure folds

Consider a series of stratified sediments consisting of thin alternating strata of limestone and shale in which the limestone layers are of much greater competence than layers of intervening shale. Suppose that the sequence is warped into a series of regular folds, and that the folding represents an instability (buckling) developed during uniform squeezing of the whole sequence normal to the axial planes of the folds. Under these conditions it is possible to describe qualitatively the state of stress and strain in a particular limestone stratum, neglecting at first the effects of stresses imposed by the assumed weaker shales. As the tightness of folding increases, details of the stress distribution within the strata will change progressively. Initially, all strata experience compression parallel to the layering. As folds develop, the material in the crests and troughs of individual folds experiences a bending moment as well as compression, with the

moment increasing in magnitude as the folding becomes tighter. In the limb regions there are shearing and normal stresses on transverse cross-sections of the layer. In real folds, the surrounding sediments will also impose shearing and normal stresses over all bounding surfaces of the limestone strata. The resulting deformation in a single crest or trough will thus be the result of an interplay of all these stresses, but a simplified and useful picture is obtained if only the axial region of the fold is considered and the deformation there is imagined to result predominantly from bending. It is well known that the qualitative distribution of the bending strain is characterized by a relative extension of the layer normal to the axis of flexure near one boundary and shortening near the other, the amounts depending on the tightness of folding. A calculation of the exact distribution of strain in a layer which is not deformed in pure bending and which is not circular in cross-section can be a very complex problem. When the strains are finite and complicated distributions of surface forces and bending stresses are included in the analysis, an exact solution is not possible. The strain distribution will in any case depend upon the nature of the deforming forces, the allowed displacements at the boundaries of the folded stratum, and the rheological properties of the materials involved.

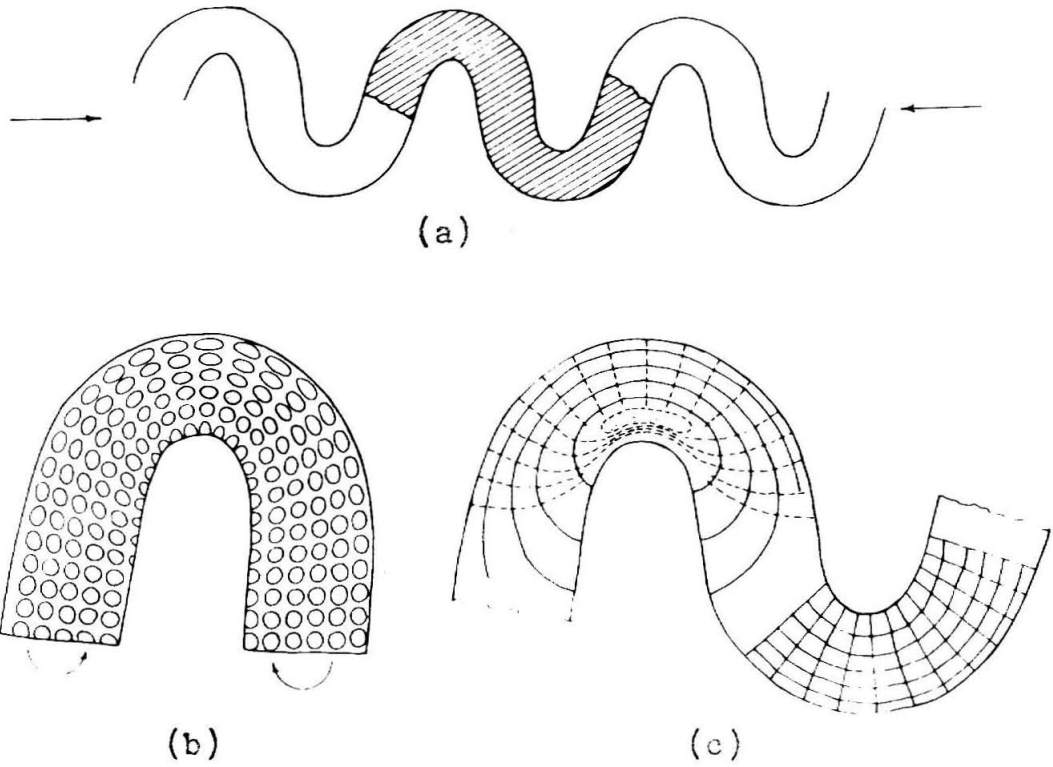


Figure 1. A simple model of the strains developed with large bending in a flexure fold. (a) Part of a long train of simple, regular folds in an unconfined layer; (b) strain distribution in a bent bar (after Sander, 1930); (c) schematic representation of strains in the hachured area of (a) for the compressive force applied as shown in (a) and (c) assuming mostly bending as in (b). Left half shows principal strain trajectories with dashed lines representing compressive strains, solid lines extending strain, the right half distortion of an originally (nearly) square grid of lines connecting centers of reference circles in the undeformed slab. Dotted portion represents a region of "no strain."

In order to obtain a more graphical picture of the possible distribution of strain in a fold a hypothetical example is presented. (See fig. 1.) The problem is reduced to its simplest form by considering an unconfined stratum (fig. 1a)--all boundaries stress-free--in which the deformation has been produced by a simple compressive force applied along the center line of the wave train shown in the figure. This set of boundary conditions leads to an unstable system of the kind shown because a slight departure from the regularity and symmetry of the strain distribution in any one fold or deflection of the series of folds from the supposed line of application of the deforming force will cause the system to change to another more stable configuration. Stability requires application of lateral constraining forces on the layer. These are neglected in this necessarily qualitative treatment, and this further restricts the results outlined below. Figure 1b forms the basis for further discussion of the strain distribution throughout the layer, and is taken from Sander (1930, p. 34). Sander's experiment consisted of bending slabs of plasticine (modeling clay) into the shape outline in the figure after first inscribing ink circles on one side of the slab. The resulting distribution of ellipses graphically depicts the amounts of strain, and directions of the principal axes of strain at points throughout the body. The description of this experiment is incomplete, for there is no mention of the precise manner in which the deformation was carried out or whether

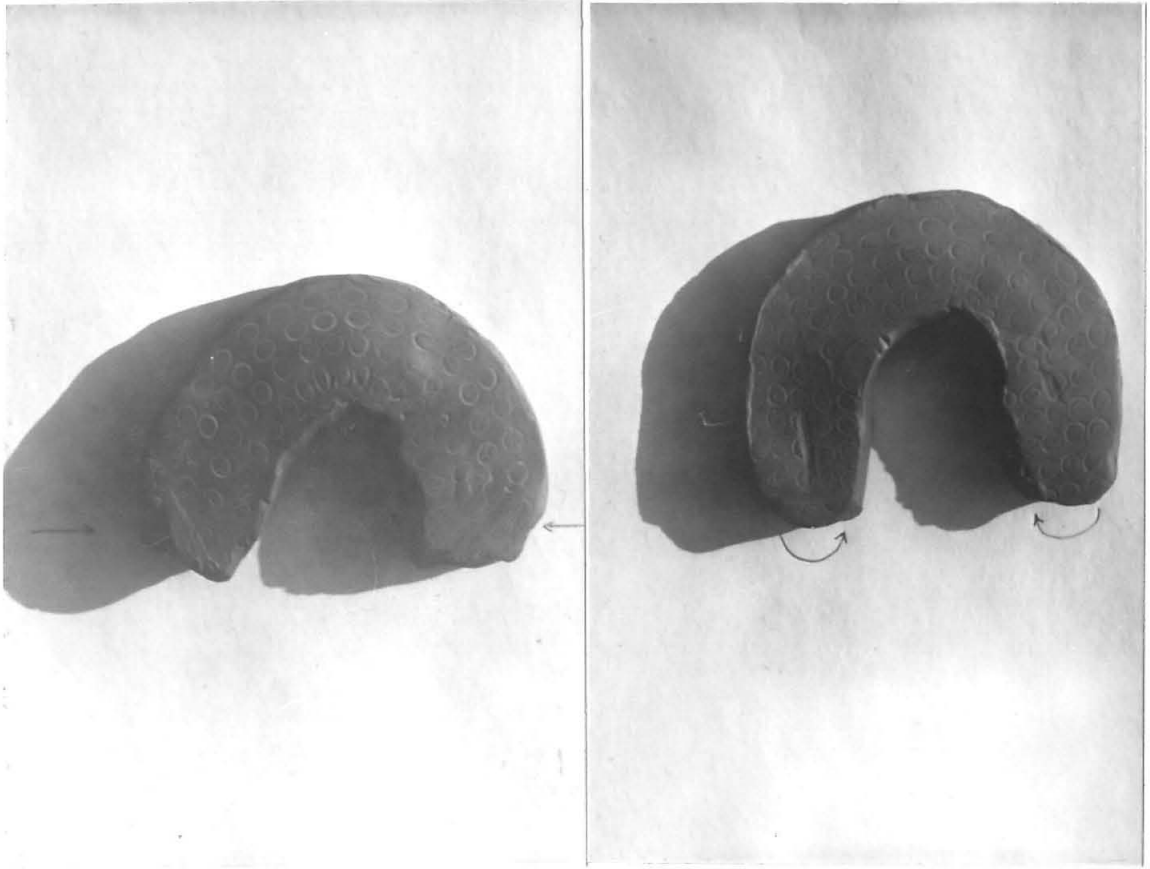


Figure 2. Simple experiments illustrating the distribution of strain in a bar deformed in buckling (left half) and through bending (right half). Plane strain parallel to the plane of bending. Reference markings were originally circular in shape. The material is plasticine. For details of the strains see Table I.

the bending was in plane stress or plane strain. There is also no discussion of the mechanical properties of plasticine and the extent to which this material might be expected to simulate the mechanical properties of rocks.* A series of very simple experiments of a type similar to Sander's were therefore carried out by this writer. Model slabs of plasticine approximately 8 inches long, 1 1/2 inches wide, and 1/2 inch thick were arranged between fixed glass plates lubricated with vaseline to simulate approximately plane strain conditions. Different kinds of deforming forces were then applied to the ends of the slabs. The results are shown in Figure 2, (2a) being the result obtained when the slab is grasped at the ends and bent about an axis normal to the drawing, and (2b) when the slab is pushed from the ends until a fold develops through buckling. The two patterns of strain differ in detail, particularly with regard to the position of the neutral line (line of no strain parallel to the longitudinal direction of the slab). In (2b) the neutral line is situated farther

* Plasticine might be useful in simulating the properties of rocks under certain conditions. Green (1951) has used plasticine models to simulate the plastic flow of metals. He shows that under conditions of plane strain, the material deforms similarly to an ideal, isotropic, non-hardening metal. Stress-strain curves depict a plastic-elastic behavior, and show a sharp bend after which the material deforms essentially at constant stress. The deformation characteristics are very sensitive to temperature. The permanent compressibility of plasticine is about 0.2%. It consists of finely ground calcite, mineral oil, and an organic dye. The tensile stress-strain curve of this substance is quite similar in shape to that obtained with "T-cylinders" of Yule marble and other rocks deformed at 5 kb. and 800° C (Griggs et al., 1960).

from the center of curvature than in (2a), an effect due to the presence of a longitudinal shortening as well as bending strain in the layer. The general agreement of these results with Sander's, except for the exact positioning of the neutral line, is apparent. In these experiments surfaces of the models are planes of principal strain, except near the ends. The principal axes of strain, depicted by the major and minor axes of the ellipses, are arranged so that axes of principal extension, which are parallel to one boundary, are perpendicular to the other boundary across the layer. Between the boundaries, the principal axes assume intermediate orientations. In the axial regions of these "folds," the deformation is symmetrical about the axial plane. As the amplitude of the bending deflection becomes greater, strains due to bending dominate over those due to compression of the layer for the case shown in Figure 2b. In a wave-like series of folds in nature this situation would arise only when the amplitude of the wave train becomes appreciably greater than the wave length.

Of course it cannot be argued that Figure 1b or Figure 2 describe with accuracy the strain situation to be expected in a real fold. However the pictures do qualitatively depict the strain which could be expected to accompany simple bending of large magnitude.

Figure 1c represents an attempt at further graphic portrayal of the orientation of principal strain axes throughout a fold. The left half of the drawing is a schematic

representation of the principal strain trajectories in the axial region, and the right half shows the strain as distortion of an originally square network of lines through centers of circles in the undeformed state. The strain trajectories are drawn so that the tangent and normal directions to any one of them at any point are the directions of the principal axes of an ellipsoid at that point. A trajectory is constructed by first drawing a line parallel to one of the principal axes of an ellipse, for instance an axis of extension, at some point in the fold. At a small distance from the original point along the line, another line is placed parallel to the greatest principal axis of the ellipse at that point. The same process is repeated until the particular trajectory is traced throughout the entire fold, or the regions for which the deformation data are available. If the orientations of the principal axes of these reference ellipses are single valued and continuous functions of position, which will be true if there are no fractures or faults in the body, then the strain trajectories as drawn are unique. As shown, these trajectories traverse regions of varying degrees of strain, and do not necessarily denote lines along which strains of a given type are equal in magnitude.

To summarize briefly, the idealized example given in Figure 1 shows a number of important properties of the expected strain distribution in a flexure fold: (a) symmetry of the strain to either side of the axial plane, (b) shortening of

one side of the layer and extension of the other, (c) a decrease in the amounts of strain discussed in (b) in the limbs, (d) the approximately linear change in strain along a transverse section of the layer in the axial region, (e) the small scale roughly homogeneous deformation, (f) the property of transverse cross-sections of the beam remaining nearly planar and perpendicular to the layer in the axial region during the deformation (g) the approximately circular shape of the slab in the axial region.

The approximate calculation of strains in folds

As discussed above, there is generally no easy method available for determining analytically the distribution of strain in a natural fold, and some sort of approximate calculation must be made. In practice deformed oolites, pebbles, and fossils may be used to determine the strain in a fold (Cloos, 1947), but lacking features such as these, independent estimates of the strain--particularly in the axial region--may be obtained only in special simple cases.

An analysis of the strain in a buckled unconfined thin slab could be made for small deformations proceeding in a manner similar to von Karman (1910). The distribution of strain in a transverse cross-section of the sheet follows from the conditions of static equilibrium provided that a stress-strain relationship for the material is known and reasonable values of the applied longitudinal compression can be selected. But for geologically interesting situations there

is usually no way a priori of estimating either of these unknowns. Kienow (1942) and more recently Ramberg (1961) have analysed the distribution of strain folds due to bending and buckling respectively, and both give expressions for the longitudinal strain for small deformation the same as Equation 1 below.

To obtain some idea of the magnitude of the strains associated with large bending in a fold, we proceed in the following manner. Consider an obviously oversimplified but straightforward example, the originally rectangular plate of thickness t , whose cross-sectional dimensions are not necessarily small compared with its length (L). Imagine that the plate is deformed by pure couples applied at its ends, and that there is no strain parallel to the axis of bending. Let all other surfaces of the plate be stress-free and suppose that the material is incompressible, isotropic, non-hardening, and elastic-plastic. For small elastic deflections, the transverse stresses are negligible compared to those induced by bending (Hill, 1956, p. 79). The neutral surface, where stresses and strains parallel to the longitudinal direction produced by bending vanish, is located in the center of the plate and can be considered circular with radius R (Hill, 1956). The strain E parallel to the surfaces of the plate are linearly distributed over the cross-section, that is,

$$E = \frac{z}{R} \quad (1)$$

where z is the distance measured normally away from the neutral surface. Suppose now that the bending is allowed to become

greater so that the induced stresses exceed the yield point of the material. Plastic zones first develop near the boundaries of the layer and move inward as the bending increases (Hill, 1956, p. 79-84). We now imagine that the bending is allowed to become very large under the pure terminal couples so that the plastic zones move inward and the material is yielding everywhere. Under these conditions it is possible to describe some general geometrical properties of the deformation (Hill, 1956, p. 290). If the angle of bending α (per unit length) is increased by an amount $d\alpha$, the displacements of elements in the plate are such that: (1) the surfaces of the plate remain cylindrical with further bending, (2) radial sections remain planar, (3) the thickness of the plate remains constant. Thus the strains at the boundaries of the layer may easily be found by equating the original and final areas of the plate. Doing this we find that the maximum strains at the inner and outer edges of radii \underline{a} and \underline{b} ($\underline{b} > \underline{a}$) respectively to be:

$$\begin{aligned} 1 + E_{\underline{a}} &= 2\underline{a}/(\underline{a} + \underline{b}) & (E_{\underline{a}} = \text{extension}) \\ 1 + E_{\underline{b}} &= 2\underline{b}/(\underline{a} + \underline{b}) & (E_{\underline{b}} = \text{shortening}) \end{aligned} \quad (2)$$

where the strains $E_{\underline{a}}$ and $E_{\underline{b}}$ are defined as $\Delta L(\underline{a})/L$ and $\Delta L(\underline{b})/L$, $\Delta L(\underline{a})$ and $\Delta L(\underline{b})$ being the changes in length of the inner and outer surfaces of the original rectangular plate of length L .

In order to derive the above conclusions and equations 2, it is not really necessary to assume that the material possesses any special rheological properties, only that it be incompressible and that circumferential displacements of elements within the plate at any stage of the bending be given by

$$\underline{u}_\theta = (\underline{r} - R) \frac{\theta}{\alpha} d\alpha .$$

That is, the displacements \underline{u}_θ of points with polar coordinates \underline{r} , θ (θ being measured positive clockwise from the plane of symmetry in bending) must be linearly distributed both about the instantaneous position of the neutral surface of radius R , and with the angle θ .

Undoubtedly most folds in nature cannot be the result of simple pure bending. In fact, it is hard to visualize a situation where this kind of deformation would prevail. However at present the above development appears to be the simplest geometrical argument which can be used to determine the strains of interest here. Equations 2 are used in subsequent sections to calculate the approximate maximum strains for the observed geometries of the structures studied (p. 112 and p. 141).

To get an idea of how well equations 2 might be expected to estimate bending strains, we have used them to calculate the deformations in the previous model experiments. The results are presented in Table 1.

For the case of the fold deformed in pure bending the agreement between observed and calculated strains, especially

TABLE 1

Original reference circle diameter	Change in diameter	Indicated strain	Calculated strain	Radius* of neutral surface, calc. & obs.
I. 0.19 (0.32)	at \underline{b} , ** (0.15)	0.32	0.33	R_{calc} 1.36 (3.45)
	at \underline{a} , ** (0.13)	-0.26	-0.33	R_{obs} 1.62 (4.10)
II. 0.19 (0.32)	at \underline{b} , ** (0.15)	0.26	0.37	
	at \underline{a} , ** (0.15)	-0.26	-0.37	
III.	at \underline{b} , (0.10)	0.33	0.46	R_{calc} 0.65 (0.16)
	at \underline{a} , (0.05)	-0.16	-0.46	R_{obs} 0.52 (0.13)

- I. Fold deformed in pure bending (fig. 2a); $\underline{a}^{**} = 1.09"$ (2.77 cm), $\underline{b}^{**} = 2.15"$ (5.46 cm)
 II. Fold produced in buckling (fig. 2b); $\underline{a} = 0.78"$ (1.98 cm), $\underline{b} = 1.68"$ (4.26 cm)
 III. Sander's experiment (fig. 1b); $\underline{a} = 0.36"$ (0.91 cm), $\underline{b} = 1.20"$ (3.21 cm)

* With pure bending, plane strain in a material obeying the Mises yield criterion
 $R = \sqrt{\underline{ab}}$, (Hill, 1956, p. 289)

** \underline{a} and \underline{b} here refer to radii of points where measurements of strain were made,
 not inner and outer radii of the bars
 Measurements given in inches and centimeters (parentheses)

at the "outer" boundary of the fold, is surprisingly good. In the "buckling" experiment the agreement is not as good, but this is perhaps to be expected considering the assumptions under which Equations 2 are valid. Agreement in the case of Sander's experiment is rather poor.

Principles for the Comparison of Theoretical and Observed Fabrics in Folds

Types of fabric comparisons

The foregoing discussion has attempted to show the purpose for using folds in these investigations, and has developed some of the expected properties of the strain distribution in these structures. The question of fabrics produced in response to the imposed strains in folds is now examined theoretically. Two types of carbonate fabric studies are considered in the present work. The first type is concerned with gross changes in crystal orientation which accompany large strains, while the second type, based on the "dynamic analysis," deals only with carbonate twinning lamellae in relation to applied stress. It is possible to treat twinning lamellae from the standpoint of the strain they represent rather than the applied stresses causing them, and this argument is developed in detail below (p. 44).

Gross changes in crystal fabric arising from strain

Metallurgists have long noted preferred crystal orientations resulting from cold working (sheet rolling, extrusion,

drawing) of metals (Barrett, 1952, p. 442-484). In an analogous manner changes in crystal fabric are also brought about in highly deformed marble. These have been extensively studied, and the way in which fabric changes develop in response to strain is now understood (Turner et al., 1956). In all experimental work with carbonate rocks it has been shown that the geometrical symmetry of the fabric of a deformed aggregate is the same as the symmetry of the strain the aggregate has undergone (Griggs et al., 1960, p. 104). For small strains, less than 10% in either extension or compression, fabric changes in Yule marble are negligible (Handin and Griggs, 1951, p. 882-884). With greater strain, stable orientations of crystals develop with respect to the principal axes of distortion, and these persist and become more sharply defined with higher deformation.

Generally speaking, theories for predicting deformation fabrics of polycrystalline aggregates are of two types depending upon whether assumptions are made as to the stress or the strain in each grain. Most of these can be criticised in several respects, and Bishop (1954) has made such an analysis. Two principal requirements must be met: (1) the aggregate must fit together after straining, i.e., the strain must be homogeneous and (2) stresses acting through grain boundaries must be continuous during deformation. In order to satisfy (1) it is necessary that at least five independent glide systems be available to operate in a crystal (Bishop, 1953). However it can be

shown that under these circumstances condition (2) cannot be met if the critical resolved shear stress law is to hold in each crystal (Bishop and Hill, 1951b). This in general leads to the conclusion that the strains in individual crystals will be nonhomogeneous (Bishop, 1954). Two separate treatments will be briefly outlined below, that of Bishop (1954) because of its possible application to the present work, and the theory of Handin and Griggs (1951) as modified by Turner et al. (1956), because of its prior application to prediction of deformation fabrics in Yule marble.

The theory of Bishop (1954) forms the most successful approach for predicting deformation fabrics in metals. The theory is an approximation as it does not incorporate effects due to possible grain boundary slip, changes in crystal size, or nonhomogeneity in the deformation of individual grains. It is assumed that each grain comprising the aggregate undergoes the same strain as the aggregate in bulk, an assumption originally due to Taylor (1938). The critical resolved shear stress law is also assumed to hold for glide in the individual crystals. On a microscopic basis crystals are required to deform by glide on at least five independent glide systems (assuming no volume change with deformation). Substances with fewer than five possible glide systems are not covered by the theory. The five systems actually operative during deformation are those which maximize the plastic work of deformation, or, phrased differently, satisfy the principle of maximum plastic

work (Bishop and Hill, 1951a), which can be written,

$$(\tau_{ij} - \tau_{ij}^*) de_{ij} \geq 0 . \quad (3)$$

In words Equation 3 states that the work done by stresses τ_{ij} in causing a crystal to deform plastically through a certain strain increment de_{ij} relative to the axes of the crystal, is not less than the work done by any other set of stresses τ_{ij}^* producing the same strain increment and not violating the maximum critical stress criterion in the current state of hardening for the crystal. For metals of high symmetry to which the theory has been applied (face centered cubic metals in particular) a range of possible engineering shear strains can be assigned to each of the available glide systems which satisfy this criterion (Bishop, 1954, p. 135). This means that the external rotations each grain undergoes (rotations of the crystal axes relative to the principal axes of strain) are not, in the absence of work hardening determined uniquely by the maximum work principle. Bishop argues that the actual choice of glide systems is determined by the amount of work hardening each suffers during deformation. Once shears have been determined for the various glide systems which give the strain increment de_{ij} , the rotation components of the crystals $d\omega_{ij}$ relative to the principal axes of strain can be obtained from geometrical considerations (Bishop, 1954, p. 135). Thus fabric changes associated with any desired macroscopic strain may be determined. It is not immediately obvious that this theory

cannot be applied to calcite aggregates. Individual crystals possess sufficient independent glide elements, even if e twinning and r translation are the only available glide mechanisms. One possible restriction lies in whether twinning in calcite obeys a critical resolved shear stress law. Experimental evidence indicates that it does approximately (p. 8, this thesis), but current theoretical treatments suggest otherwise (see Appendix III).

The importance for petrofabrics of the Bishop theory is that under the assumptions involved, changes in fabric are functions only of the deformation occurring, not the forces used to bring about the deformation. This is because the microscopic strains and rotations are determined from pure geometry, together with the maximum plastic work principle. By this last assumption, the permissible stresses in each grain are fixed during yielding.

A theory formulated by Handin and Griggs (1951), as modified by Turner et al. (1956), has been applied to deformed calcite aggregates, and also follows closely the ideas of Taylor (1938). In their analysis of uniaxial experiments with Yule marble, each crystal is considered to be strained the same amount as the aggregate in the direction of extension or shortening. The law of maximum resolved shear stress is also assumed to determine an active glide element in each grain. This particular assumption is applied by assuming further that each grain sees the same stress as the aggregate as a whole.

Work hardening is neglected. External rotations of crystals due to strain are computed from analogy with rotations in single crystal experiments. In uniaxial strain of single crystals, poles to glide planes move toward the axis of compression, and glide directions toward an axis of extension, the amounts of rotation depending on the strain. Appropriate formulas are given by Handin and Griggs (1951, p. 869) for computing these rotations. By specifying only one component of strain for each crystal, the theory only partly fulfills the condition that continuity of the aggregate be maintained after deformation.

The assumptions needed to compute fabric changes for calcite aggregates according to the method of Handin and Griggs (as modified by Turner et al., 1956) are:

(1) The law of maximum resolved shear stress determines the active glide system in each grain (this effectively adopts the maximum plastic work criterion). Only one glide system operates at any one time unless the resolved shear stress is equal on two or more systems, in which case multiple slip occurs on these systems.

(2) The available and potentially active glide systems are $\{10\bar{1}1\}$ translation gliding with the edges between $\{10\bar{1}1\}$ and $\{02\bar{2}1\}$ as glide directions, with glide sense negative;* $\{01\bar{1}2\}$ twinning, glide direction parallel to the edge between

* See Appendix I.

adjacent $\{10\bar{1}1\}$ planes, glide sense positive.* Other types of glide occurring at room temperature and above 500-600° C are neglected.

(3) A particular crystal will twin on $\{01\bar{1}2\}$ rather than translate on $\{10\bar{1}1\}$ when the resolved shear stress coefficient S_0 (the ratio of the resolved shear stress in the slip plane and in the direction of slip to the applied stress) for a particular $\{01\bar{1}2\}$ system is algebraically greater than -0.05 (negative sign refers to shear stress oriented in wrong sense on the twin plane). If a crystal cannot twin, it translates so that its deformation is equal to that of the aggregate as a whole.

The Handin-Griggs method, modified by Turner et al. (1956) to account for r-translation gliding rather than e-translation gliding, cannot be used in its present form to predict fabrics in folds, because the theory permits specification of only one component of strain in each grain, and therefore for the aggregate as a whole. In the axial region of a fold deforming in plane strain parallel to the fold axis, it is evidently necessary to specify the following strains:

$$E_{ij} = \begin{bmatrix} E & 0 & 0 \\ 0 & 0 & 0 \\ 0 & 0 & -E \end{bmatrix} \quad (4)$$

for the region of the fold which is extended parallel to the

*See Appendix I.

bedding, and

$$E_{ij} = \begin{bmatrix} -E & 0 & 0 \\ 0 & 0 & 0 \\ 0 & 0 & E \end{bmatrix} \quad (5)$$

for those portions where elements are shortened parallel to the bedding. The strains E_{ij} are referred to principal axes chosen so that \underline{x} is perpendicular to the fold axial plane, \underline{y} is parallel to the fold axis, and \underline{z} is perpendicular to the \underline{xy} plane. The material is considered incompressible. Strains (4) and (5) differ only by a rotation of 90° about the \underline{y} -axis.

The Bishop theory on the other hand allows specification of arbitrary strains, but because of the geometry of the calcite lattice, becomes extremely complicated when applied to this material. Unfortunately it has not been possible to carry through a detailed application of the theory for the strains (4) or (5) because of the time which would be required for such a calculation. However it is possible to gain an approximate picture of the fabrics to be expected for these strains in the following manner. As pointed out above, the theory suggests that fabric changes occurring during nonhomogeneous deformation of an aggregate should be functions of the strains imposed, not the forces used to bring about the deformation. Therefore we could use the experimental results as to development of deformation fabrics in Yule marble if the

strains in any of the experiments approximated those given in (4) and (5). This would of course restrict the results obtained so that they would strictly apply only in situations where the initial fabric of the undeformed rock was exactly the same as that of undeformed Yule marble. This fabric (Turner, et al., 1956) consists of a well defined maximum of c-axes normal to foliation in the marble, with no preferred orientation of the other axes (a₁, a₂, a₃) in the foliation plane. The strains (4) and (5) are those which approximately develop during homogeneous deformation of T-cylinders* of Yule marble (Turner, et al., 1956, figure 8 G,H) in compression and extension. That is, an originally circular cylinder becomes ellipsoidal in cross-section with one axis of the ellipse remaining approximately equal to the diameter of the original cylinder. The fabrics which evolve under these strains are shown in figures 3 a, b. Figure 3c is the fabric of undeformed Yule marble. Figure 3a is the c-axis fabric associated with extension parallel to the foliation and the c-axis fabric obtained from shortening parallel to the foliation. The fabrics consist of c-axis maxima lying in a plane perpendicular to the

* This nomenclature describes orientation of experimentally deformed cylinders with respect to the foliation (and geographic coordinates) in Yule marble (Turner et al., 1956). "T-cylinders" are those cut with longitudinal axis parallel to the foliation. The c-axis fabric thus consists initially of a maximum along a radius of a circular basal section.

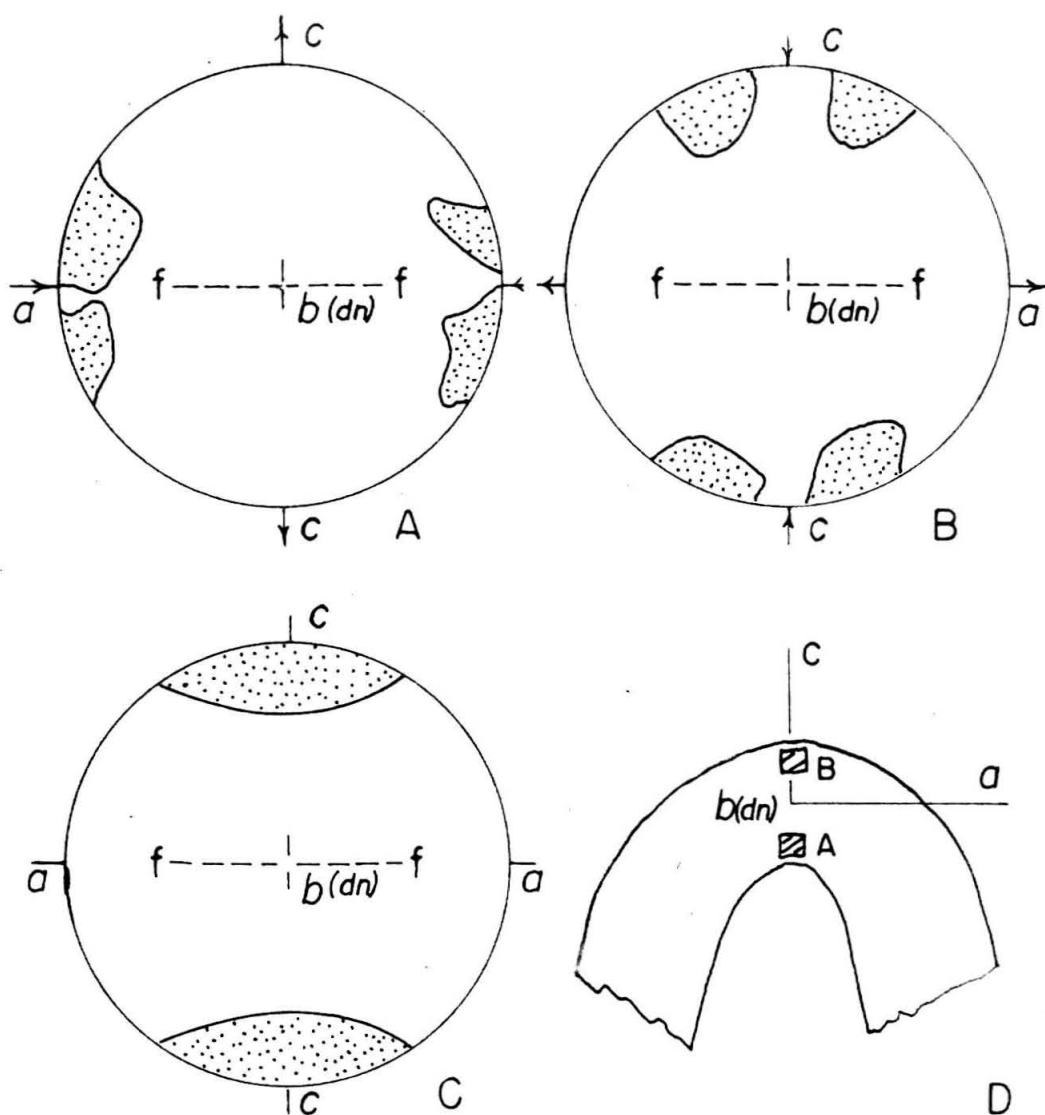


Figure 3. Approximate \underline{c} -axis fabrics to be expected with large deformation in a flexure fold. (A) Fabrics associated with the position marked "A" in the reference diagram (D); (B) fabrics from position "B" in (D); (C) assumed original (undeformed) \underline{c} -axis fabric of the material. In each diagram ff represents trace of bedding. Stippled regions are areas of high concentrations of \underline{c} -axes. Arrows denote senses of strain. The above diagrams were prepared by analogy with experimental results given by Turner (1957, p. 15). (See p. 42, this thesis for further details.) In particular (A) is the orientation diagram for \underline{c} -axes in a T-cylinder (see bottom p. 42), shortened 40.7% at 400°C, 3000 kgm/cm², (B) the diagram for \underline{c} -axes in a T-cylinder extended 118%, at 500°C, 5000 kgm/cm², (C) the fabric of undeformed Yule marble. All fabric diagrams plotted on equal area projections, lower hemisphere.

axis of approximately no strain in the specimen, situated in each case $10-30^\circ$ to the direction of shortening. The principal axes of strain in the deformed specimens in the two cases differ only by a rotation of 90° about the axis of least strain (or approximately zero strain).

We might then draw the following rough analogy between these experiments and fold fabrics. Start with a calcite aggregate having the initial c-axis fabric shown in Figure 3c. Subject the aggregate to strains given by the strain tensor matrices (4) and (5). The stable fabrics which evolve through operation of the deformation mechanisms prevalent in laboratory experiments will be very roughly those given in Figures 3a and 3b respectively. It is interesting to note that Sander (1930, D181) has measured a c-axis fabric from a tight fold in calcite phyllite from the southern Tirol essentially the same as that shown in Figure 3a.

Fabric changes associated with an incremental deformation of an initially isotropic c-axis fabric are considered in the next section.

Dynamic interpretation of deformation lamellae

The dynamic analysis of e-lamellae fabrics in calcite (and f-lamellae fabrics in dolomite) is due to Turner (1953). This method is based on the fact that twin gliding on e in calcite is most easily promoted by stresses which make the twin plane a plane of maximum shearing stress with the shear

having the sense favorable for twinning. This condition is fulfilled if either a tension is applied to a crystal at an angle of 19° to the c-axis or if the crystal is compressed at an angle of 71° to the c-axis, with these axes of stress lying in the plane containing the c-axis and the pole to e. Twinning may of course be induced by a combination of these stresses. Diagrams produced from the analysis may show clusterings of compression (C) axes and tension (T) axes (cf. Turner, 1953) and such groupings presumably center around the appropriate stress direction or directions which could be responsible for the observed twinning in the aggregate.

Since the C and T axes for a particular crystal are fixed geometrically with respect to the crystal lattice, a preferred crystal orientation automatically introduces a pattern into data derived from dynamic analysis of the twinning lamellae fabric. For example, in a calcite aggregate showing a single well defined c-axis maximum, a dynamic analysis will tend to give T-axis maxima which coincide with the c-axis pattern or are displaced from this pattern by about 20° . C-axes will form a girdle or will cluster into several maxima lying within a zone 20° from the plane which is normal to the direction of the c-axis maximum. Breached C-axis girdles may or may not be real features produced by the analysis. Such openings can in part be attributed to the central "blind-spot" in the associated e-lamellae diagram, which arises because of observational difficulties (p.192).

In strict terms, the stress state defined by the dynamic analysis for an individual crystal is not generally the actual state of stress at that point in the aggregate. If it is assumed that two adjacent crystals are at the yield point for twinning, with principal axes of stress in each defined by the analysis, then the stresses across their mutual grain boundary will generally not be in equilibrium, i.e., components of stress acting through the boundary will not be continuous from one crystal to the next. The analysis gives only the best possible distribution to promote twinning on a grain for grain basis, and it therefore might be expected that results will have meaning only if applied to a large number of grains in random orientation throughout the aggregate.

With this discussion of the method, we now proceed to develop theoretically the expected results for a dynamic analysis of an aggregate with an isotropic distribution of c-axes, which has undergone an increment of deformation under the system of stress prevailing in the axial region of a flexure fold. Knowing the stresses, the operative twin set in each crystal may be found from the law of maximum resolved shear stress. The particular model developed below is meant to apply specifically to one of the natural folds whose deformation fabrics are discussed later (p. 90). In particular, we start with an already deformed body, and consider only the elastic state of stress within it. This simplifying provision

is made because the observed plastic deformation in the natural fold is slight (p.111), and it is presumed that the material was always close to the elastic state during deformation. The body is assumed to be elastic, incompressible, homogeneous, and macroscopically isotropic.

Consider again the axial portion of a fold with circular cylindrical cross-section perpendicular to the fold axis (fig. 4). The inner radius of curvature is \underline{a} and the outer radius \underline{b} . For purposes of simplifying the calculation the ends of the structure considered are taken at right angles to one another. The angle θ is measured positively from the left side clockwise. The fold is imagined to be compressed by a force F directed along the normal to the axial plane. Referred to polar coordinates \underline{r} and θ the components of F parallel and perpendicular to the cross-section $\theta = 0$ are T and P respectively. For equilibrium these must be balanced by resultant forces $-P$ and $-T$ acting parallel and perpendicular respectively to the cross-section at $\theta = \pi/2$. The boundary conditions are:

$$\begin{aligned} @ \quad \theta = 0, \quad & \int_a^b \tau_{\theta\theta} \, dr = P ; \quad \int_a^b \tau_{r\theta} \, dr = T \\ @ \quad \theta = \pi/2, \quad & \int_a^b \tau_{\theta\theta} \, dr = -T ; \quad \int_a^b \tau_{r\theta} \, dr = -P \quad (6) \\ \tau_{rr} = \tau_{r\theta} = 0 & \text{ at } r = \underline{a} \text{ and } \underline{b} \text{ for all } \theta . \end{aligned}$$

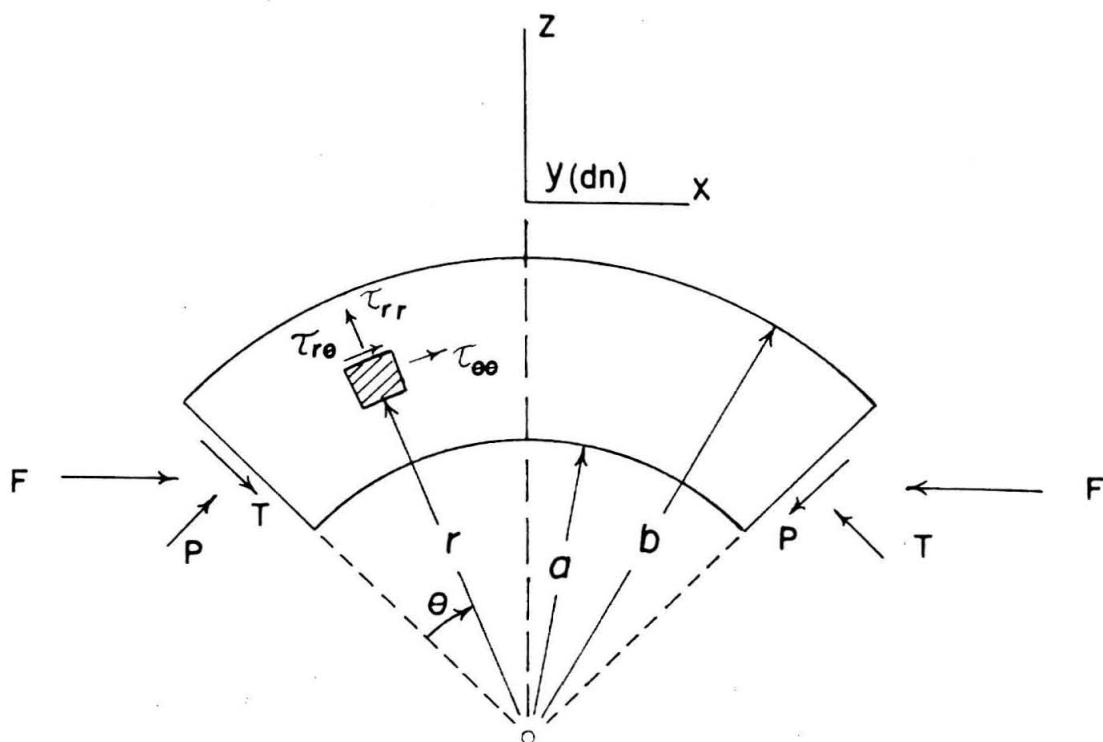


Figure 4. Model assumed in calculation of stress distribution in an already partially deformed layer of circular cross-section which is loaded elastically by the force F applied to the "ends" of the body. For $\theta = 0$, the components of F normal and tangential to the end of the beam are P and T respectively, and for $\theta = \pi/2$, T and P . In the case chosen, P is equal to T . This model is meant as an approximation to the situation in one of the natural folds discussed later (p. 90).

The stress distribution satisfying these conditions may be obtained by superposition of solutions to the following problems: (a) bending of a curved bar by a force applied tangentially at one end (Timoshenko, 1951, p. 73), (b) bending of a curved bar by a force applied normally to one end. The resultant stress distribution is

$$\begin{aligned}\tau_{rr} &= \frac{1}{N} \left(r + \frac{a^2 b^2}{r^3} - \frac{a^2 + b^2}{r} \right) (T \sin \theta + P \cos \theta) \\ \tau_{\theta\theta} &= \frac{1}{N} \left(3r - \frac{a^2 b^2}{r^3} - \frac{a^2 + b^2}{r} \right) (T \sin \theta + P \cos \theta) \\ \tau_{r\theta} &= \frac{1}{N} \left(r + \frac{a^2 b^2}{r^3} - \frac{a^2 + b^2}{r} \right) (P \sin \theta - T \cos \theta)\end{aligned}\quad (7)$$

where $N = a^2 - b^2 + (a^2 + b^2) \ln \frac{b}{a}$.

For purposes of dealing with the natural fold we consider the special case of the dimensions where $b = 2a$ and the stresses at the cross-section $\theta = \pi/4$. For $P = T$, Equation 7 reduces to

$$\begin{aligned}\tau_{rr} &= \frac{\sqrt{2} P}{N} \left(r + \frac{4a^4}{r^3} - \frac{5a^2}{r} \right) \\ \tau_{\theta\theta} &= \frac{\sqrt{2} P}{N} \left(3r - \frac{4a^4}{r^3} - \frac{5a^2}{r} \right) \\ \tau_{r\theta} &= 0\end{aligned}\quad (8)$$

In plane strain, τ_{yy} , the stress along the axis perpendicular to the plane of the fold is $\frac{1}{2}(\tau_{rr} + \tau_{\theta\theta})$. (Poisson's ratio is

equal to $\frac{1}{2}$ for an incompressible material.) We now evaluate these three non-zero components of stress for $\underline{r} = (5a)/4$ and $(7a)/4$, which are the approximate "mean" positions of thin sections examined in the natural fold the present analysis is intended to describe (p. 95, fig. 10). Thus

$$\begin{aligned}\tau_{rr} \left(\frac{5a}{4}\right) &\cong - \frac{7a \sqrt{2}}{10} \left(\frac{P}{N}\right) \\ \tau_{\theta\theta} \left(\frac{5a}{4}\right) &\cong - \frac{23a \sqrt{2}}{10} \left(\frac{P}{N}\right) \\ \tau_{yy} \left(\frac{5a}{4}\right) &\cong - \frac{3a \sqrt{2}}{2} \left(\frac{P}{N}\right)\end{aligned}\tag{9}$$

and

$$\begin{aligned}\tau_{rr} \left(\frac{7a}{4}\right) &\cong - \frac{4a \sqrt{2}}{11} \left(\frac{P}{N}\right) \\ \tau_{\theta\theta} \left(\frac{7a}{4}\right) &\cong \frac{18a \sqrt{2}}{11} \left(\frac{P}{N}\right) \\ \tau_{yy} \left(\frac{7a}{4}\right) &\cong \frac{7a \sqrt{2}}{11} \left(\frac{P}{N}\right)\end{aligned}\tag{10}$$

To compute the resolved shear stress on a slip plane in the direction of slip for a given crystal, it is necessary to use the transformation formulae for stresses (Sokolinkoff, 1956, p. 43)

$$\tau'_{\alpha\beta} = \sum_{i=1}^3 \sum_{j=1}^3 \lambda_{\alpha i} \lambda_{\beta j} \tau_{ij}$$

where the $\tau'_{\alpha\beta}$ are components of stress referred to Cartesian

Figure 5. Predicted results for the dynamic analysis of the twin lamellae fabric in a fold using the model shown in Figure 4 for the radial section at $\theta = \pi/4$. The original distribution of c -axes and lattice orientations chosen are those shown in Figure 12. In each diagram "C" refers to a compression axis and "T" to a tension axis. The operative twin set in a grain was assumed to be that for which S'_0 given by Equations 12 is greatest, with the sense of shear favorable for twinning (i.e. values of S'_0 algebraically greater than -0.05). Arrows on the diagram show the sense of the stress acting along the a -axis of the fold, or the x -axis as defined in Equations 12. Thus (a) is for the region which is compressed parallel to the layering during deformation and (b) for the region which is extended parallel to the layering.

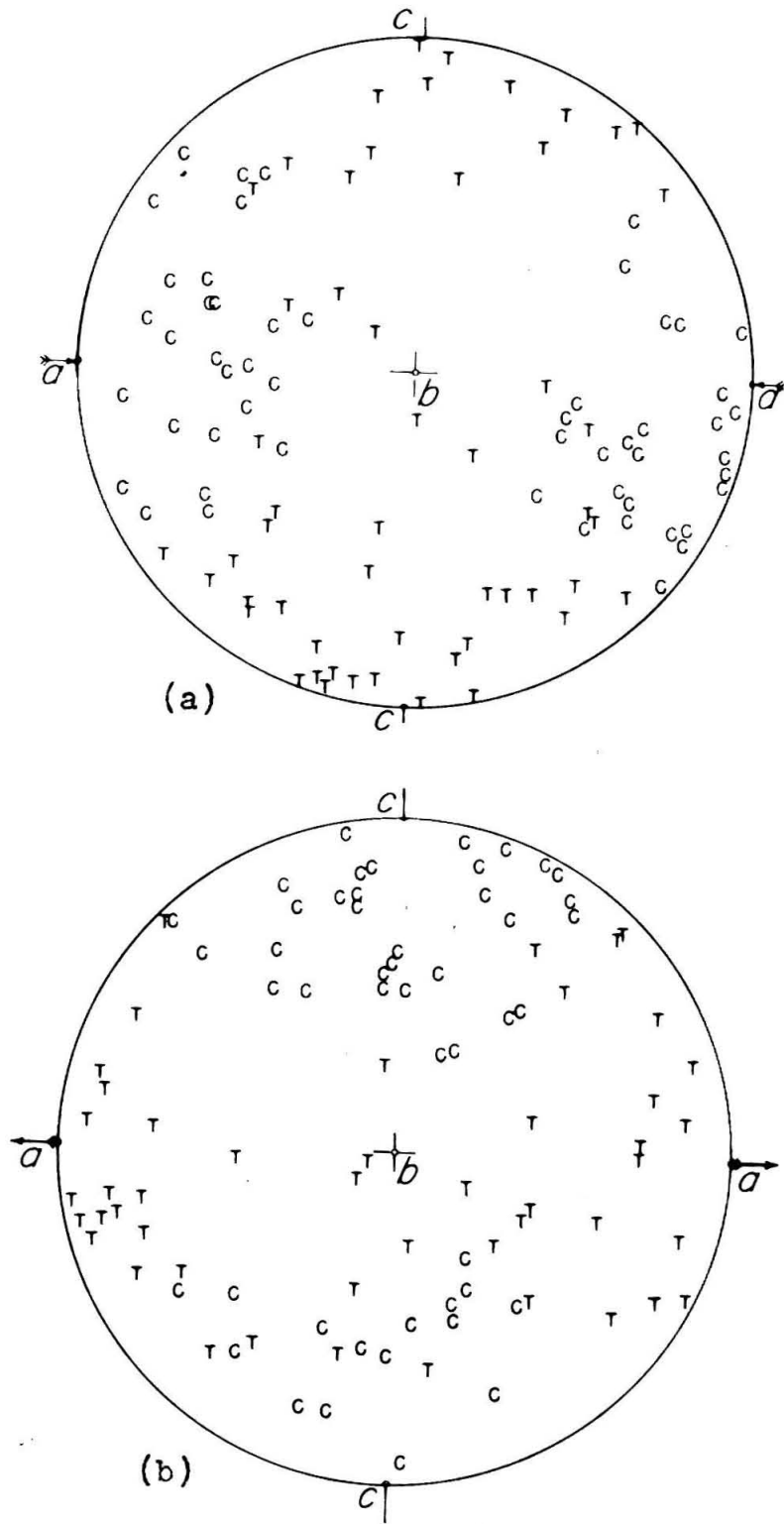


Figure 5

axes fixed with respect to the slip plane and slip direction and where the τ_{ij} are given by Equations 9 and 10, defined now with respect to a set of Cartesian axes with $+x$ parallel to the positive θ direction, $+y$ parallel to the fold axis and $+z$ parallel to $+r$. $\lambda_{\alpha i}$ is the cosine of the angle between the positive end of the α 'th coordinate axis fixed in the grain and the i 'th principal stress axis. Define the shear stress on a slip plane perpendicular to the x' axis in the direction of the y' axis as τ'_{xy} . Then

$$\tau'_{xy} = \lambda_{xx} \lambda_{yx} (\tau_{xx} - \tau_{yy}) + \lambda_{xz} \lambda_{yz} (\tau_{zz} - \tau_{yy}) \quad (11)$$

where the orthogonality relations between the direction cosines, $\lambda_{\alpha i} \lambda_{\alpha j} = \delta_{ij}$ (δ_{ij} = Kronecker δ), have been used. ($\tau_{xx} = \tau_{\theta\theta}$; $\tau_{yy} = \tau_{yy}$; $\tau_{zz} = \tau_{rr}$). Evaluating Equation 11 for each set of stresses given by Equations 9 and 10 we obtain as the values for the resolved shear stress coefficient written in terms of the stress τ_{xx}

$$\frac{\tau'_{xy}}{\tau_{xx}} = S'_0 \left(\frac{5a}{4}\right) \approx \frac{16}{23} (\lambda_{xx} \lambda_{yx} + \frac{1}{2} \lambda_{xz} \lambda_{yz})$$

$$S'_0 \left(\frac{7a}{4}\right) \approx \frac{11}{9} (\lambda_{xx} \lambda_{yx} + \frac{1}{2} \lambda_{xz} \lambda_{yz}) \quad (12)$$

For each product of λ 's on the right side of Equation 12 a graphical solution like that presented by Handin and Griggs

(1951, p. 868) may be used to obtain the final value for S'_0 for any particular plane in the lattice.

Consider now a calcite aggregate with isotropic c-axis distribution* subjected to the system of stresses given by Equations 9 and 10. Assume further that the operative twin plane in each crystal during deformation is that upon which the value of S'_0 is greatest, and that twin gliding does not occur unless S'_0 is algebraically greater than or equal to -0.05, in accordance with the assumptions in the Handin and Griggs (1951) and Turner et al. (1956). We may then construct C and T axes for the appropriate active twin set in each crystal. The results of this procedure are presented in Figures 5a and 5b. In the region where there is shortening parallel to the x-axis, the dynamic analysis gives a broad clustering of C-axes about this direction. T-axes form a general equatorial girdle in the axial plane (yz plane) of the fold. For the other case of extension parallel to the x-axis, the concentration of C-axes is about the y-axis with a T-axis girdle lying in the xy-plane. These results will be compared more fully with those obtained from the natural fold in a later section (p. 106). For the present it will only be remarked that the results obtained above show qualitative good agreement with those actually observed to develop in nature.

With the above picture of the dynamic method it is possible to go further and examine qualitatively the fabric changes

*The actual distribution used is that given in Figure 12a.

due to mechanical twinning which would develop for the deformation imagined above. For twinning in calcite the c-axis of the host and twin crystal are symmetrically disposed about the pole in the twin plane, $52\frac{1}{2}^{\circ}$ apart, and lie in the plane containing the original c-axis and pole to the twin plane. The C-axis derived from the dynamic analysis also lies in this plane, 71° from the host c-axis. Therefore as a first approximation a clustering of C-axis also depicts a general concentration of optic axes for the twinned part in each of the crystals, and the C-axis pattern will thus grossly conform to the major fabric change which develops through mechanical twinning. The optic axis patterns obtained in this manner are generally similar to the stable orientations of c-axes which have been discussed above (p. 43) for the special situation adopted here.

Calculation of Bulk Strain from Petrofabric Data

The problem of interpreting deformation lamellae in carbonate aggregates may be approached from a different and more natural standpoint than that suggested by the dynamic analysis. This approach involves consideration of the bulk strain* in an aggregate represented by twinning and/or internally rotated lamellae (Turner, et al., 1956) rather than the stresses involved in producing these features. As has

* Bulk strain is synonymous with macroscopic strain, and refers to the strain of a volume of material which includes many individual crystals. The microscopic strains are the strains of individual crystals.

already been discussed, the intragranular stress distribution defined by the dynamic analysis is not an actually possible distribution of stress for each crystal, and therefore the analysis is to some extent unreal. The new method presented below allows a quantitative estimate to be made of the amount of visible strain an aggregate has undergone, and also permits the directions of the principal axes of strain to be computed. Contributions of individual grains to the total strain are also weighted in a prescribed manner, thus allowing for non-homogeneity of grain size and distribution of strain among individual crystals to be taken into account.

Calculation of visible bulk strain due to twinning

When a crystal of calcite is deformed in twinning, it undergoes a shearing strain, the amount of strain depending on the degree of twinning. Twinning deformation in a grain is characteristically heterogeneous. That is, most grains are usually only partially twinned, and contain completely twinned layers separated by layers of the untwinned or host crystal. Within each twinned band the deformation is homogeneous by virtue of the atomic movements involved in the twinning process. The plane of shear in twinning is perpendicular to the twin plane and includes the twinning direction. A twinned crystal is thus in a state of plane strain (this is proved by Jaswon and Dove (1960) for deformation twins) parallel to the shear plane in twinning, provided that only one set of lamellae is developed in the crystal.

In a given partially-twinned grain, the average shear strain induced by partial twinning is computed by thinking of the deformation as uniformly distributed throughout the grain. The situation is depicted diagrammatically in Figure 6. An original rhombohedral shaped crystal ACDB viewed in the $(1\bar{2}10)$ plane, of height h , is deformed by twinning on layers of thicknesses h_1 and h_2 into the shape shown in dashed lines, AEFB. The average engineering shear strain in the plane of the drawing referred to the Cartesian axes \underline{x} and \underline{y} is

$$\gamma = \tan \psi = \frac{2(h_1 + h_2)}{h} \tan (\delta/2) \quad (13)$$

where $\delta/2$ is one-half the angle between $\underline{r}(10\bar{1}1)$ in the host crystal and $\underline{r}'(\bar{1}011)$ in the twinned crystal, and equal to $19^\circ 08.5'$ in calcite. In order to compute the average shear strain in a grain due to mechanical twinning, it is only necessary to measure the relative lengths of twinned and untwinned crystal traversed along a line normal to the operative twin plane.

For infinitesimal γ , the principal axes of strain for twinning lie at 45° to the twinning plane as shown in Figure 6a, and the magnitudes of the principal strains along these axes are,

$$\begin{aligned} e'_{\underline{x}} &= \frac{1}{2} \tan \psi \\ e'_{\underline{y}} &= -\frac{1}{2} \tan \psi \\ e'_{\underline{z}} &= 0 \end{aligned} \quad (14)$$

where $\tan \psi$ is given by Equation 13. These strains can be referred to any arbitrary set of coordinate axes, for example a

set parallel to the edges of and normal to a thin section, by using the infinitesimal strain transformation formulae,

$$e_{ij} = \sum_{\alpha=1}^3 \sum_{\beta=1}^3 \lambda_{i\alpha} \lambda_{j\beta} e'_{\alpha\beta} \quad (15)$$

where the e_{ij} are components of the strain tensor referred to the arbitrary coordinate system and the $e'_{\alpha\beta}$ are components of the strain tensor referred to the principal axes in each grain. The $e'_{\alpha\beta}$ written in matrix form are:

$$e'_{\alpha\beta} = \begin{bmatrix} \frac{1}{2}\tan\psi & 0 & 0 \\ 0 & -\frac{1}{2}\tan\psi & 0 \\ 0 & 0 & 0 \end{bmatrix} \quad (16)$$

$\lambda_{i\alpha}$ is the cosine of the angle between the positive end of the i 'th arbitrary axis and the positive end of the α 'th principal axis in each grain. In the present study the particular reference axes chosen for purposes of calculation are as follows:

- + \underline{x} = north universal stage direction in the thin section (long edge).
- + \underline{y} = east universal stage direction of the thin section (the short edge).
- + \underline{z} = normal to the plane of the thin section (\underline{xy}) with positive direction downward.

In a particular grain the axes, defined by their positions on the lower hemisphere of an equal area projection, are:

+ \underline{x}' = extension axis, positive end making an angle of 19° with the \underline{c} -axis position on the lower hemisphere, and lying on the great circle containing the poles of $\underline{c}(0001)$ and $\underline{e}\{01\bar{1}2\}$ away from the pole to \underline{e} .

+ \underline{y}' = compression axis, positive end making an angle of 71° with \underline{c} in the great circle containing \underline{c} and \underline{e} , and measured from \underline{c} in the direction of \underline{e} .

+ \underline{z}' = normal to the $\underline{x}'\underline{y}'$ plane.

The \underline{x}' and \underline{y}' axes are coincident respectively with the tension and compression axes of the dynamic analysis (p. 45).

Equations (5) and (5a) combined and written out in full are:

$$\begin{aligned}
 e_{\underline{xx}} &= \frac{1}{2}(\lambda_{\underline{xx}}^2 - \lambda_{\underline{xy}}^2) \tan \psi \\
 e_{\underline{yy}} &= \frac{1}{2}(\lambda_{\underline{yx}}^2 - \lambda_{\underline{yy}}^2) \tan \psi \\
 e_{\underline{zz}} &= \frac{1}{2}(\lambda_{\underline{zx}}^2 - \lambda_{\underline{zy}}^2) \tan \psi \\
 e_{\underline{xy}} &= \frac{1}{2}(\lambda_{\underline{xx}} \lambda_{\underline{yx}} - \lambda_{\underline{xy}} \lambda_{\underline{yy}}) \tan \psi \\
 e_{\underline{xz}} &= \frac{1}{2}(\lambda_{\underline{xx}} \lambda_{\underline{zx}} - \lambda_{\underline{yy}} \lambda_{\underline{zy}}) \tan \psi \\
 e_{\underline{yz}} &= \frac{1}{2}(\lambda_{\underline{yx}} \lambda_{\underline{zx}} - \lambda_{\underline{yy}} \lambda_{\underline{zy}}) \tan \psi
 \end{aligned} \tag{17}$$

For each set of twin lamellae visible in a grain the six angles whose cosines are $\lambda_{\underline{xx}}$, $\lambda_{\underline{xy}}$, ... etc., must be measured from the projection net. The factor $\tan \psi$ is equal to $0.69\underline{v}$, \underline{v} being the ratio of the width of twinned crystal to the total width of the crystal, that is, $(\underline{h}_1 + \underline{h}_2)/\underline{h}$ in the example of Figure 6.

The strain components given by Equation 17 represent the visible strains due to twinning in each grain referred to the arbitrary axes. Each grain does not deform independently of its neighbors, but the amount of observed strain and the grain size do vary from grain to grain in the aggregate. Thus in order to obtain an average for the deformation of the aggregate, contributions of individual grains to the total or bulk strain must be weighted in an appropriate way. This is done by multiplying the calculated components of strain e_{ij} for each grain by the ratio of the area of the grain to the total area of all the grains involved in the computation. The areal extent of each grain gives an unbiased estimate of its volumetric contribution (Chayes, 1956, p. 13), and the contributions of the individual grains to the bulk strain are in proportion to their individual volumes. The sum of the weighted individual components e_{ij} make up the components of what is here termed the bulk strain tensor E_{ij} . Once the E_{ij} have been obtained the three principal bulk strains and associated principal-strain-axis directions can be computed using either the procedure given by Sokolnikoff (1956, p. 17, 47) or an iterative procedure (Nye, 1957, p. 165).

Strain due to translation gliding

By a procedure exactly analogous to that described above, shearing strain due to translation gliding alone may be included in the analysis of strain provided its amount can

be determined through analysis of internally rotated lamellae (Turner, et al., 1954, p. 883-934), or by some other means. The engineering shear strain \underline{s} associated with such internal rotation is calculated from the following equation (Turner, et al., 1954, p. 900):

$$\cot \alpha - \cot \beta = \underline{s} \sin \xi , \quad (18)$$

where α and β are the angles between a given lamella and the operative glide plane before and after internal rotation (β arbitrarily chosen greater than α), and ξ is the angle between the glide direction and the axis of internal rotation which is the line of intersection of the lamella and glide plane. Under the assumption that \underline{s} is infinitesimal, the principal axes of strain for this deformation lie at 45° to the active glide plane in a plane normal to the plane of gliding which includes the glide direction. Which axis is the axis of extension or shortening depends on the sense of gliding. As an example, for negative* \underline{r}_1 translation gliding in calcite, with one glide system in operation, the principal axis of extension is 45° from the pole to \underline{r}_1 nearly coincident with the pole to \underline{m}_1 , and the axis of compression of the deformation is almost coincident with the \underline{c} -axis.

The strain tensor matrix for negative \underline{r}_1 translation gliding shear strain, written in a coordinate system defined by the particular axes given above is:

*See Appendix I.

$$e_{\alpha\beta}'' = \begin{bmatrix} \frac{1}{2}s & 0 & 0 \\ 0 & -\frac{1}{2}s & 0 \\ 0 & 0 & 0 \end{bmatrix} \quad (19)$$

For positive r_1 translation gliding, these two strains simply change signs. The components of strain given in Equation 18 may be referred to the arbitrary reference axes of the previous section by use of relations, Equation 5.

It must be emphasized that these strain calculations omit perhaps the majority of strain experienced by a given rock. If a grain has undergone translation gliding strain prior to the development of visible twin lamellae, then this strain is necessarily neglected. It is also not possible to detect readily the strain adsorbed as grain boundary slip, recrystallization, or through fracturing of the material. However these are probably not the major sources of the difficulty as will be discussed below. As has already been mentioned (p. 36), it is generally necessary that at least five glide systems operate in each grain for continuity of a deforming aggregate to be maintained. But, it is generally difficult to identify more than three operative systems in any grain of the deformed rocks studied here. It is therefore quite probable that translation gliding strains are not detected and hence remain unaccounted for in an evaluation of the bulk strains. The identification of translation gliding in calcite is ordinarily made by measurements of internally

rotated lamellae (Turner et al., 1954; see also appendix II). Sometimes such lamellae can be noted and identified in warped crystals where large local strains have developed through plastic bending (see appendix II), but the procedures used are time consuming, and seldom yield unambiguous identification of the operative translation gliding systems. Using Equation 18 we can estimate how much internal rotation of a given lamella is to be expected for any value of \underline{s} . The maximum amount of strain in twinning observed in some of the rocks studied here is 0.05 (see p.163), and it is not unreasonable to expect that at least this amount of translation gliding strain exists undetected in the aggregates. For the case of an \underline{e}_1 lamella, rotated by glide on \underline{r}_1 , with \underline{s} equal to 0.05, $(\alpha - \beta)$ is equal to 2.5° . For negative glide on \underline{r}_1 , $\underline{c} \wedge \underline{e}_1$ would equal approximately 24° , and for positive glide 29° . The smaller angle is just within the limits of measurement, while the larger angle lies in a region where a true effect is difficult to separate from one involving constant discrepancies for the angle $\underline{c} \wedge \underline{e}$, which may arise through cumulative error involved in locating \underline{c} -axes and \underline{e} -lamellae (Borg and Turner, 1953). For the above reasons translation gliding strain has generally not been included in any of the strain calculations presented below.

Accuracy of the strain calculations

There are two ways in which inaccuracies can enter into the calculation of the observable part of the strain in an aggregate using the above method. The first comprises errors due to the assumption that the strains are infinitesimal so that Equations 5 apply. The second kind of errors are those of observation including measuring errors with the universal stage, errors in visually estimating the amount of twinned material in a grain, and especially in establishing which part of a crystal represents twin and which host. To the extent possible, these questions are considered below.

The validity of applying infinitesimal-strain transformation formulae to actual observations representing finite strain cannot be investigated thoroughly without entering into the mathematically cumbersome subject of finite strain. However, it can be expected on general grounds that the errors and uncertainties introduced in this way will be of the order of the squares of the observed strain components, because terms of this order are of the lowest order omitted in all calculations that assume infinitesimal strain. The nature of these errors can be illustrated in the following way. In a deformed body the rotation components ω_{ij} are in general of the same order of magnitude as the strain components e_{ij} . When a body that has been strained by amounts e_{ij} is rotated by components ω_{ij} , the strains with respect to axes fixed in space change by amounts (Kamb, 1961, p. 264),

$$\Delta e_{ij} = e_{ik} \omega_{kj} - e_{kj} \omega_{ik} ,$$

where the tensor summation convention has been used. Thus since the external rotations ω_{ij} remain always unobservable in the individual crystals of naturally deformed specimens, the calculated components of strain e_{ij} are always uncertain to the order e^2 , no matter what strain transformation formulae are used. Since the maximum observable strain component in a calcite crystal deformed 50% in twinning is normally 0.17, the maximum errors introduced by assuming infinitesimal strain and by neglecting the ω_{ij} 's are about 20% of the strain components themselves. Such errors, in view of the general uncertainty of observational fabric data are not intolerable.

Observational errors are quantitatively about as important as those introduced by the mathematical approximations discussed above. For example the adopted practice for determining the degree of twinning in a grain is to estimate visually this quantity while making the other normal petrofabric measurements. With visibly twinned lamellae it is unlikely that any such estimate is accurate to any better than 10%. This means that the principal strains given by Equation 14 are uncertain to about 3%, or for a grain that is 50% twinned about 20% of the strain components themselves. A special problem is presented by deformation lamellae in calcite commonly termed nontwinned by most investigators. For reasons developed later (p.199) these are here renamed microtwinned lamellae. They have been taken into account in the strain calculations by assuming that the crystal is on the average

0.1% twinned by each set of microtwinned lamellae it possesses regardless of the spacing index* of the set. In practice it has been found that the contribution of the microtwinned lamellae to the total strain is usually dwarfed by that of the more prominently twinned sets in a grain.

The most serious observational difficulty arising in determining the visible strains is as follows. It has been indicated that a distinction must always be made for each partially twinned grain as to which part is twin and which host (or original) crystal. In effect changing the choice reverses the principal axes of strain for the crystal, and this will in turn alter its contribution to the computed bulk strain components E_{ij} because of the summation process in the weighting of strains from individual crystals. Commonly it is rather loosely assumed that the twinned part of a grain is that represented by the smaller volume of crystal. If this criterion is rigidly adhered to it will set an upper limit to the observable amount of strain due to twinning in the aggregate, for it then becomes apparent that distinction of host and twin in a crystal 50% twinned is not possible unless some independent means is available for establishing one of these orientations. In an aggregate containing randomly oriented crystals each 50% twinned, the

*The spacing index for a lamellae set is defined as the number of lamellae per millimeter encountered in a traverse normal to the set. (Turner and Ch'ih, 1951, p. 896.)

maximum strain per crystal is, from Equation 14 roughly $\frac{1}{2} \times \frac{1}{2} \times 0.69 \times (1/3)$, or 0.06, where a weighting factor of 1/3 enters to take account of the supposed random orientation on the strain. If the rock is equigranular and the strain homogeneous from grain to grain, the maximum observable strain in the aggregate is also approximately 0.06. In the event a random choice is made between host and twin in grains that are 50% twinned, then on the average, the contributions to the total strain from these grains should cancel. Errors will enter the calculated magnitudes of the principal strains if the wrong choice for the host (or twin) is made. In all of the rocks examined in the present work, the number of crystals showing greater than 40% twinning is always less than 10% of the total number of grains examined. The errors likely to enter the calculations because of faulty assumptions as to the deformation in this many crystals can be estimated as follows. If 100 grains are measured in a section of equigranular rock with random c-axis fabric, and 10% are 50% twinned, then the calculated components of strain will be in error by $\pm 0.1 \times 0.06$ or 0.6%. The minus sign applies when choices between host and twin are random so that contributions of these grains cancel, and the plus sign applies if all wrong choices have been made. Thus for a rock where the $E_{i,j}$ are 0.04, the errors due to this observational difficulty are about 15% of strains themselves.

Unfortunately it is not possible to cite general criteria which will enable a clear distinction to be made be-

tween host and twin orientation in a twinned crystal. In rocks showing a good preferred orientation before deformation, this problem is not so serious because the original fabric of the rock can sometimes be used as a guide to the behavior of material that has undergone deformation. This is an important reason for examining fabrics of specimens from both limb and axial regions of folds that have undergone large deformations. In selected situations it is sometimes possible to distinguish host from twin, particularly where the host contains two sets of twins. If an early formed set of twin lamellae is disrupted by twinning on a later set, the appearance of the early twins changes, and they become thicker, darker, and serrated in appearance in the twin, while remaining sharp and straight in the host. A distinction between the two orientations can thus be made relatively easily. It is clear that very careful observations will be necessary if calculations like those described above are to be carried out on highly deformed material.

The combined effects of all the different kinds of errors enumerated above are difficult to assess. This could be done if the strains could be measured in an experimentally deformed aggregate in which the bulk strains are known, but this calculation has not been made in the present work. It is however certain that the estimates of visible strain derived by this procedure are no better than the errors introduced at any step, i.e., roughly 20% of the strain components themselves.

For geological situations, particularly where no other measure of the strains are possible, such errors are perhaps acceptable.

A convenient numerical check is available for some parts of the computations used in obtaining the bulk strain components. The sum of the principal strains for each grain is $e'_x + e'_y + e'_z = 0$. This sum forms the first invariant of the strain tensor e_{ij} , so that $e_{xx} + e_{yy} + e_{zz}$ and $E_{xx} + E_{yy} + E_{zz}$ are zero as well, and this fact may be used to partially check the numerical work. No very convenient means such as this is available for checking the off-diagonal components of strain.

Relation between the strain calculations and dynamic analysis

Results of strain calculation for a particular fold which allow comparison with a dynamic analysis of the associated twin lamellae fabric are given in Figure 12 (p. 102). The principal axes of strain and values of the principal strains have been obtained using most of the available twin lamella data for the rock, but the associated diagram giving the distribution of C and T axes has been modified from the original data (fig. 14) by simply striking out closely spaced pairs of C and T axes ($< 5^\circ$ apart). In this particular example 17 pairs of axes were removed from a total of 100, and in doing so more distinct maxima have been generated in the diagram. It can be noted that an alteration of the data of this type does not change the general nature of the result, at least for this

particular case, but does serve to clarify somewhat the picture presented by the dynamic analysis. In essence a comparison of the strains and dynamic analysis data shown that groupings of C-axes (in both the complete and reduced data) are associated with a direction of shortening and T-axes with a direction of extension for the rock. An unlimited cancellation of the sort suggested here cannot be made however, for clusterings obtained in this manner are probably not significant in view of the likely possibility that some grouping could occur just through superposition of random patterns of C and T axes (B. Kamb, oral communication). Lacking a statistical study of this problem it is not possible to place precise limits on the degree of cancellation permissible.

Petrofabric method for determining the bulk rheological properties of limestone under deformation in nature

The strain analysis procedure described above in practice turns out to be relatively sensitive in detecting small changes in strain throughout a body if these strains are near zero (p.119, this thesis). This indicates that the method may be used to investigate the detailed distribution of strain in a fold, given suitable specimens with which to work. Knowing the strain distribution, it is in principle possible to distinguish between broadly different kinds of mechanical behaviour in calcite aggregates deformed under natural conditions, viz., Newtonian viscosity and perfect plasticity obeying the Mises or Tresca yield condition for

plane strain. In order to illustrate this idea, a very simple example is considered. Imagine again the flexure fold of circular cross-section which is deformed in plane strain by pure couples applied in the limbs, the fold axis being the axis of bending. Let all other surfaces of the layer be stress-free. For an incremental increase in the angle of bending, the strain distribution will vary throughout the body in a way which depends upon the rheological nature of the material. In particular the position of the neutral surface will be different for the two types of bodies mentioned above, and if the deformation proceeds from an initially annealed state of the material, the difference in position could be detected by sufficiently refined measurements of the strain. As a numerical example, if the outer radius of the fold is twice the inner radius, the difference amounts to approximately 3% of the inner radius, the smaller value being associated with plastic behaviour. This result can be obtained by comparing results for circular beams given by Hill (1956, p. 289), and Timoshenko (1951, p. 64).

Numerous difficulties make it difficult to apply this method to natural folds. Even if a numerical method could be used to deal with complicated boundary shapes and stress and displacement boundary conditions, the strain history of any element would have to be known. For the critical region of the body, particularly just inside the neutral surface, elements first undergo compression followed by extension for

an increase in the deformation in bending, and the neutral surface moves toward the inner boundary (Hill, 1956, p. 289). It is hard to imagine the precise effects on individual crystals which would be produced when the neutral surface moves through a given part of the aggregate, but the result would probably complicate exact location of the surface. The problem is partly circumvented by the specification of small deformations from an initially annealed state of the material, but this demand is contradictory to the requirement that the folded structures have small radii of curvature. Another difficulty in applying the method is that in "real" folds pressures on transverse cross-sections of the beds will also tend to displace the neutral surface, and perhaps remove it from the layer.

Though the method described above is probably inapplicable to most folds in practice it does illustrate in principle an approach by which petrofabric data can be used on a detailed basis to obtain geological information about the rheological properties of limestone. It turns out to be inapplicable to the folds studied here, because in the single example which approaches some of the necessary requirements (p. 119), the difference in position of the neutral surface between the cases of viscosity and perfect plasticity is only 0.1 inches. Furthermore, it is not certain that the neutral surface has not been considerably disturbed by compression throughout the fold.

In reality one would perhaps not need to carry through the complicated procedure described above, because a simple examination of thin sections from all parts of a fold could reveal variations in amount of strain due to twinning, which would qualitatively accomplish the same purpose as the strain analysis. Folds containing oolites would also be especially valuable for this purpose.

Petrographic Techniques Employed

Petrofabric analysis procedure

Petrofabric observations for this study were made using a Leitz P.III M petrographic microscope equipped with a Leitz four-axis universal stage. Universal stage measurements were made using hemispheres of index 1.649 and mounting oil of index 1.638. Universal stage techniques described by Turner (1949) have been used throughout this investigation except as described below.

Where possible, two mutually perpendicular thin sections were examined in the various parts of each of the folds studied. In all cases orientation data from at least 100 grains were taken from thin sections from each position in the fold. In linearly traversing a thin section, all grains along the line of the traverse were measured rather than at equally spaced intervals. Orientation data taken in highly warped crystals were measured as close as possible to the same spot in a given crystal. These data were plotted on

the lower hemisphere of a Schmidt equal area projection net of 20 cm diameter. Interfacial and zonal measurements were made on this net and the values obtained were recorded for future reference along with net coordinates of individual grains. Descriptive data such as amount of twinning, lamella warping, grain boundary structures, and special or anomalous features (internally rotated lamellae, evidence of recrystallization) were also recorded. Positions of grains were located on photomicrographs of the thin sections. Orientation data are presented as scatter diagrams rather than as conventionally contoured orientation density diagrams. This is advantageous because the irregular detail in conventionally contoured diagrams has no statistical significance (Kamb, 1959, p. 1909) and further serves to obscure the picture presented by the original data.

For reference purposes in describing orientation data, a system of orthogonal coordinate axes fixed with respect to a particular fold has been adopted as follows: facing the outcrop, the (+) b-coordinate axis is into the outcrop along the fold axis: (+) a is along the normal to the fold axial plane directed to the right if the flexure is convex upward (anticline) and to the left if convex downward (syncline); (+) c is normal to the ab-plane directed outward in the convex direction of the flexure. These directions are noted on each fabric diagram presented in subsequent sections. Positive directions are specified along the axes to allow

comparison of diagrams of different orientation. The fold coordinate axes are not generally coincident with the arbitrary reference axes of the strain analysis procedure. They coincide for cases in which a thin section is cut exactly parallel to the fold coordinate plane with edges parallel to the coordinate axes. Orientation of thin sections relative to the fold axes are known to approximately $\pm 3^\circ$. The accuracy of orientation data from individual crystals, as established through repeated measurements are: for c-axes on the average $\pm 3^\circ$; for e-lamellae $\pm 1^\circ$.

New developments in carbonate petrofabric study

Twinning lamellae in calcite and dolomite present certain problems in microscopic fabric analysis. The first of these is an interpretational one concerned with the deformational significance of the so-called "nontwinned" lamellae parallel to e in calcite, structures often observed in rocks used in this investigation as well as in both experimentally and naturally deformed marbles (Borg and Turner, 1953). Nontwinned lamellae are described as being so narrow that when tilted into the vertical plane they appear as hair-sharp lines, rather than as lamellae, but are distinguished from cleavage parallel to r by the tendency to remain clearly visible between crossed nicols even when tilted at large angles to the vertical. They are further distinguished by the fact that when in the vertical position twinned material cannot be recognized within them through symmetrical

extinction about the lamella plane with the host crystal (Turner, 1949; Borg and Turner, 1953). Actually, such lamellae can be shown to contain optically recognizable twinned material and to average a few microns in thickness (p.203, this thesis). Methods are also developed below in detail for determining optically the thicknesses of twinned material in these lamellae both individually and when several are superimposed through orientation of the grain in thin section. As a result of the studies described below, it seems appropriate to redesignate these structures as microtwinned lamellae, a term which more correctly describes their nature. They will henceforth be referred to by this name.

Another problem presented by deformation lamellae in carbonate minerals is that of obtaining orientation data on these lamellae when they are inclined at angles of less than 35° to the plane of the thin section. Such lamellae are normally inaccessible to measurement using conventional universal stage orientation methods, and this fact accounts for the central "blind-spot" in e and f lamellae pole diagrams, and necessitates examination of two perpendicular thin sections in a carbonate rock to obtain an accurate picture of the distribution of lamellae (Turner, 1949). The study of microtwinned lamellae has led to discovery of an optical technique for obtaining orientation data on shallowly inclined lamellae of both the visibly twinned and microtwinned varieties. The technique turns out to be more readily ap-

plicable to dolomite than to calcite. Since the three $\underline{f} \{02\bar{2}1\}$ twin planes in dolomite are oriented at approximately 80° to one another and this determines that one set of these lamellae will be inaccessible in most grains (Christie, 1958, p. 162). The method developed here utilizes the optical properties of the twins and is described later in detail (p.196). Its discovery came rather late in these investigations and it consequently was not used during the fabric studies.

FABRIC STUDIES OF FOLDED LIMESTONES

Introduction

Fabric data from two geographically widely separated folds are presented in this section. The first fold to be discussed was found in western Maryland, and the second was obtained from Darwin wash in Inyo county, California. The fold from Darwin was originally collected by Kamb (personal communication) who also measured a preliminary fabric in the structure. When fabric analysis of the fold was completed by this writer in other portions of the structure, it became clear that no simple relation existed between the fabrics and the megascopically observable deformation in the fold. A new search was then instigated for other examples of simply folded carbonate rocks, and this search ultimately led to the folds in western Maryland. A number of other attempts were made to find deformed rocks suitable for the purposes here. Studies of folds visited in the field during these searches (folds which were rejected for various reasons) are summarized below.

In general we have found that although there are numerous examples of folded limestones, any of a combination of factors can limit the usefulness of a particular structure or eliminate it completely as a desirable object of study.

Many folds are located in undesirably complicated geologic environments. Others examined contained strong axial plane cleavage, and still others were highly fractured or contained vein-like or irregular masses of secondary calcite. Where cleavage, veining, or fracturing were subordinate, the rocks were sometimes too finely crystalline to permit microscopic determination of c-axis fabrics. Another sort of development has emerged from one example (see "Mule canyon" below). In this case no deformation fabrics were observed in a fold in coarse grained limestone in which well developed fabrics, for the observed large strain, could have been expected. This indicates that either recrystallization intervened to destroy the fabric or that a fabric never developed in the rock as a result of the deformation. The conclusion derived from these searches is that simple flexure folds ("simple" here being used in the context of the requirements laid down in the Introduction) suitable for this study are rather hard to find. This by no means weakens the case for using such folds in these investigations, because under the special considerations here invoked, these structures still present the most straightforward examples of bodies where local variations and amount of strain can be independently estimated and fabric changes compared with those expected in theory.

As will be discussed in detail below, the examples of folds actually studied have not yielded deformation fabrics resulting from large strain which can be simply related to

the observed deformation. As a result of this it is not possible to draw any certain conclusions as to the relevancy of past experimental studies in describing the detailed behavior of carbonate rocks during natural deformation. Where appropriate, some comparisons are made below.

Before giving the results of the fabric studies, the other fold localities visited and examined in the field are treated in summary form.

Localities Examined

A search for deformed limestones suitable for purposes of the present investigation has been carried out in a number of areas. These are given below, and pertinent information as to location, geologic setting, descriptions of the folds examined, and petrographic characteristics of the rocks are also included. The two folds which are reported on in detail in following sections are not included here.

- I. Fold from the Talc City Hills, Inyo County, California.
 - A. Location - The fold occurs on hillside just northeast of road connecting California State Highway 190 with the Sierra Talc mines, $3/8$ miles southwest of the Talc City mine.
 - B. Geologic Setting - The fold is developed in limestone of the Pogonip group (Gay and Wright, 1954) in a position roughly 200 feet vertically below a large thrust fault which has placed Ordovician and Silurian sediments over those of Carboniferous age. The thrust fault is itself

warped (?) into a gentle syncline about an axis trending N. 50° W. The minor fold is perhaps related to the thrusting. Cretaceous intrusives crop out 1/4 mile to the SW.

- C. Details of the Structure - The fold occurs in light gray, finely crystalline, slabby bedded, calcareous limestone which is highly veined with secondary white calcite. In outcrop its plan is asymmetrical. The axial plane strikes N. 16° W., dips 61° E., and the fold axis plunges 18° to the northwest. At the axial plane the radius of curvature is about one foot. Cleavage parallel to the axial plane is well developed in the structure.
- D. Petrography - In thin section the limestone appears considerably deformed, with abundant visible twinning and warped lamellae.
- E. Remarks - Although the rocks appear highly deformed in outcrop and thin section, the presence of axial plane cleavage in the fold, its complicated geologic setting below a large thrust fault, and position immediately adjacent to plutonic intrusive rocks render it undesirable for the purposes intended here.

II. Bullfrog District, Bull Frog Hills, Nevada.

- A. Location - Approximately two miles south of Beatty, Nevada.
- B. Geologic Setting - A section of predominantly quartz biotite schist of pre-Silurian (?) age (Ransome, 1910) contains thin lenses of calcite schist and calcite marble. The calcareous bands are flat lying or dip gently south, and range in thickness from 5-40 feet. Foliation within the marble units is parallel to layering in the enclosing schists.

- C. Folded Structures - Small microfolds and irregular wavy foliation are well developed in the marbles. No consistent trend was noted in the structures. The marble is gray to brown, and consists almost completely of calcite, but locally contains a few percent muscovite. The rock is equigranular with grainsize of about one millimeter.
- D. Petrographic Data - none
- E. Remarks - Original intent here was to find some well developed flexure folds in this homogeneous coarsely crystalline material. The small microfolds as such probably reflect a complicated deformation pattern and are not useful in terms of the type of folds sought. The observed folds were not considered further.

III. Grapevine Mountains, lower Titus Canyon.

- A. Location - Approximately 1.5 miles from the mouth of Titus canyon, along the canyon bottom, north side.
- B. Geologic Setting - General geologic relation of small folds developed in Pogonip (?) limestone (Ball, 1907) to larger structures in the Grapevine mountains is unknown. Ball describes isoclinally appressed folds with horizontal axes which trend parallel to the axis of the range, and which are associated with a large anticlinorium that forms the backbone of the range.
- C. Description of the Fold - Fold (anticline) located low on north wall of Titus canyon. The fold axis trends about N. 30° W. and is nearly horizontal. The axial plane dips 30° SW. The radius of curvature is about 3 feet. The rocks consist of massive to slabby bedded, fine grained, dark gray limestone. In hand specimen a few coarse crystals (~ 1mm) are visible. The lower limb is covered by alluvium filling the canyon bottom.

- D. Petrography - Coarsely crystalline material composes roughly 10% of the rock and displays only incipient twinning (microtwinning lamellae). The rest consists of finely crystalline calcite (0.01 mm), which shows no evidence of deformation.
- E. Remarks - Though the fold has good geometry, relatively good exposure it shows no appreciable evidence of deformation and is too fine grained to permit study with the universal stage.
- IV. Alexander Hills, Inyo and San Bernardino counties, California.
- A. Location - The areas of concern are in the Alexander Hills which form a southern extension of the Nopah range, about 5 miles east of Tecopa, California. (See Wright, 1954.)
- B. Geologic Setting - A reconnaissance was made of outcrops of the Lower Cambrian Johnnie formation in search of folds in a 5-10' layer of brown weathering oolitic dolomite. The Johnnie formation in the Alexander Hills generally strikes N. 30° W. and dips 45-55° east. It is offset by a number of small both right and left hand strike slip faults. Dragging of the oolite bed along these breaks was searched for but not found.
- C. Petrography - The oolitic dolomite is cream colored on fresh surfaces weathers to a brown, oolitic texture. The rock consists almost completely of nearly spherical oolites 0.5 mm in average diameter. The rock is well cemented, breaks across individual oolites on fresh surfaces. Each oolite is concentrically layered, contains a nucleus of finely crystalline material (dolomite (?)).
- D. Remarks - Though no folds were found in the Johnnie in this region, it would be interesting to observe such structures for study of strain throughout a fold much as has been carried

through by Cloos (1947). Subsequent searches have been made by this writer for folds in a dolomitic layer of the Johnnie (?) formation in the Bare Mountains and Grapevine Mountains near Daylight Pass, but no folds in the oolitic dolomite layer have yet been discovered.

V. Mule Canyon, Calico Mountains, San Bernardino County, California.

A. Location - One mile above the mouth of Mule canyon, in the NW 1/4 sec. 25, T. 10 N., R. 1 E. and SW 1/2 sec. 24, T. 10 N., R. 1 E.

B. Geologic Setting - The Calico Mountains consist of Miocene (?) volcanic and sedimentary rocks resting on a basement of Paleozoic sedimentary and Mesozoic intrusives and are intruded by Pliocene (?) andesites and rhyolites. In Mule canyon a sequence of these Miocene (?) lake beds (Erwin and Gardner, 1940) including shale, sandstone, tuff and limestone members, is thrown into a series of folds trending N. 70 E. which are overturned slightly to the north. The folds have amplitudes between 50-100'; a few are broken in the crests and troughs. Folds in the limestone member are rounded, but zig-zag folds are almost always developed in the clastic sediments.

C. Description of the Fold - Fabric studies were made (see Remarks) on rocks from the inner part of the bend in a broken, over-turned (45° N) syncline in the limestone member. The layer examined, part of a 3 to 5 00 section of dark brown limestone, is 4-4.5" thick and is surrounded by loosely consolidated sandstones and shales. The radius of curvature of the central section is approximately 5 inches indicating a maximum bending strain of roughly 40%.

D. Petrography - The rock consists primarily of calcite and a small amount of hematite. A number of bulbous algal-like structures are apparent in thin section and consist of hematite strained calcite crystals connected to one another by patches of clear calcite. Numerous 1-2 mm irregular cavities occur in the rock, occupy roughly a volume of 20%. All of the material is almost completely untwinned but some grains give an anomalous undulatory-like extinction. Grainsize about 0.01 mm.

E. Remarks - Kamb (personal communication) has made fabric studies of this material and has found that no c-axis preferred orientations whatsoever can be seen. The results are definitely negative, in that there is no suggestion of a reorientation of the c-axis fabric around the a-axis of the fold, as could be expected from material in the part of the fold studied.

VI. Johnny Lyon Hills, Cochise County, Arizona.

A. Location - NE 1/4, sec. 22, T. 15 S., R. 21 E., between Tres Alamos Wash and Javelina Hill.

B. Geologic Setting - Southeast of Javelina Hill a major fold is developed in the upper plate of a large thrust fault (Silver, 1955, p. 315-316). The fold involves beds of upper Paleozoic age, the Horquilla and Earp formations. A north-striking limb of beds in the Horquilla formation dips east and steepens southward until the beds overturn and strike southeastward. The inverted limb dips 45° SW. In the core of this large fold thin shales and limestones of the Earp formation are tightly folded. Axial planes of the minor folds strike S. 85° E., dip 45° S. Axes plunge 30° SE. Axial plane cleavage is well developed in the rock. Right lateral faults with large strike slip displacement offset the core of the fold

and displace the overturned limb westward relative to its original position. The folded parts of the Earp formation consist mainly of shale with subordinate thin bedded siltstones and sandstones, a conglomerate and a number of thin to medium bedded light green, yellow, and pink limestones.

C. Petrography - These limestones consist for the most part of calcite, are inequigranular, containing large rounded calcite grains up to 3 mm in diameter to small angular fragments 0.01 mm in diameter. The rock is rich in fossil debris (*Triticites* (?) and other fauna) (Silver, 1955). All of the rock appears to have a cataclastic texture, although this may represent the original depositional texture of the material. Local patches of untwinned (recrystallized (?)) calcite are present.

D. Remarks - Folds in the Earp formation are from a very complicated structure and contain well developed cleavage. The rocks are also relatively poorly exposed on low slopes adjacent to Tres Alamos wash, and are partly obscured by thin alluvial and colluvial deposits. The strong axial plane cleavage has also allowed cobbly poorly constituted outcrops to form which make difficult the problem of sampling. Oriented specimens were not collected from these structures.

VII. Washington County, Maryland.

A. Location - Eight large folds were examined in various parts of Washington county, as listed below:

- (1) 1 1/2 miles north of Spickler--anticline in the Conococheague limestone axial plane strikes N. 35 E., fold axis plunges 5° (?) north.
- (2) 2 miles southeast of Williamsport Station--syncline in Beekmantown and Stones River formations, strikes N. 30° E., plunges 5° north.

- (3) Pinesburg Station--series of drag folds (?) along a vertical fault trending N. 20 E. Folds in Chambersburg limestone strike roughly parallel to the fault dip north approximately 5° .
- (4) $1/4$ mile east of Downs ville--two anticlines with intervening syncline in Conococheague limestone, strike N. 26 E., plunge 5° north.
- (5) 2 miles northeast of Funkstown--anticline in the Conococheague limestone, strikes N. 20 E., plunges 5° N.
- (6) 2 miles southeast of Funkstown--syncline in Conococheague limestone strikes N. 20 E., plunges 5° N.
- (7) 1 mile southwest of Beaver Creek--anticline in Waynesboro formation, strikes N. 30 E., plunges 10° (?) north.
- (8) 1 mile east of Chewsville--anticline in Tomstown dolomite and Waynesboro formation, strikes N. 41° E., plunges south 5° .

B. Geologic Setting - The geology of Washington County has been discussed in detail by Cloos (1951). Folds in the Paleozoic rocks throughout the county trend N. 20-30° E. and plunge between 5° N. and 5° S. They are generally asymmetrical with axial planes consistently overturned to the west. The degree of overturning increases to the east. Thus at South Mountain, the axial plane of the South Mountain fold dips 30° E., while near Hancock the axial planes of folds dip roughly 80° E. Either axial plane or fan cleavage is present in almost all folds listed in (A) above except those at Pinesburg Station, where the Chambersburg limestone is very fine grained to sublithographic. Cleavage generally dips to the east and becomes more prominent in that direction.

- C. Description of the Folds - Most of the folds (except at Pinesburg Station) are sharply bent in the axial region with strata standing vertical along the axial plane. Cloos (1947) has shown from an analysis of the oolite deformation in most of the folds given above where oolites are present, that individual ooids are consistently flattened in the plane of cleavage and usually are elongated normal to the fold axis. The folds are of large dimensions, having wavelengths of $1/4 - 1\ 1/2$ miles and amplitudes of $1/4$ mile or greater.
- D. Petrography - Petrography of the Paleozoic carbonate rocks east of South Mountain has been discussed in great detail by Cloos (1947). The major petrographic features are only summarized below. Oolites are found in the Conococheague, Stones River, Chambersburg, Beekmantown, Elbrook, Waynesboro, and Tomstown formations. Individual ooids are spherical or deformed into ellipsoidal shapes which develop ragged ends with "elongation" of approximately 60% or greater. Oolites are often concentrically layered or show radial structure, but may also consist of single crystals or rounded groups of small crystals. They may contain shale pellets, shell fragments, quartz or other grains as nucleae. Secondary growths of coarsely crystalline calcite and quartz and finely crystalline calcite form the matrix of the rocks.

Cloos (1947) gives the following sequence of events in the growth and deformation of the oolites: (1) ooid growth around nucleus, (2) sedimentation, (3) deformation before induration of the rock and before the growth of secondary "aprons" of calcite around the ooids, (4) growth of new crystals in the de-

formed rock, (5) deformation of the interstitial calcite, formation of cleavage, fracturing, (6) healing and annealing.

- E. Remarks - Although the deformed oolites form a ready index of the strain throughout these structures, the oolite deformation is indicated to be earlier than crystallization of the matrix calcite. Thus the deformation recorded as twinning in the matrix calcite may not be related to that indicated by the oolites. (Fabric studies like those pursued here could perhaps shed light on the relation if one exists). Since the purpose here has been to study folds where large variations in strain throughout small portions of the structure could be observed, and which are not cut by cleavage (whose mechanical significance and effects are uncertain), these folds were bypassed in favor of other structures discovered in western Maryland which are discussed below.

Folds from the Cacapon Mountain Anticlinorium

Geologic setting

Small folds occur on the limbs and in the axial region of the large Cacapon Mountain anticlinorium which traverses western Washington County, Maryland, in a northeast direction. Figure 8 is a geologic map and cross-section (after Stose and Swartz, 1921) of the area adjacent to and including the so-called Cacapon section of the anticlinorium. The location of the fold studied here is also shown. The index map of Figure 7 shows the position of the map area in western Maryland.

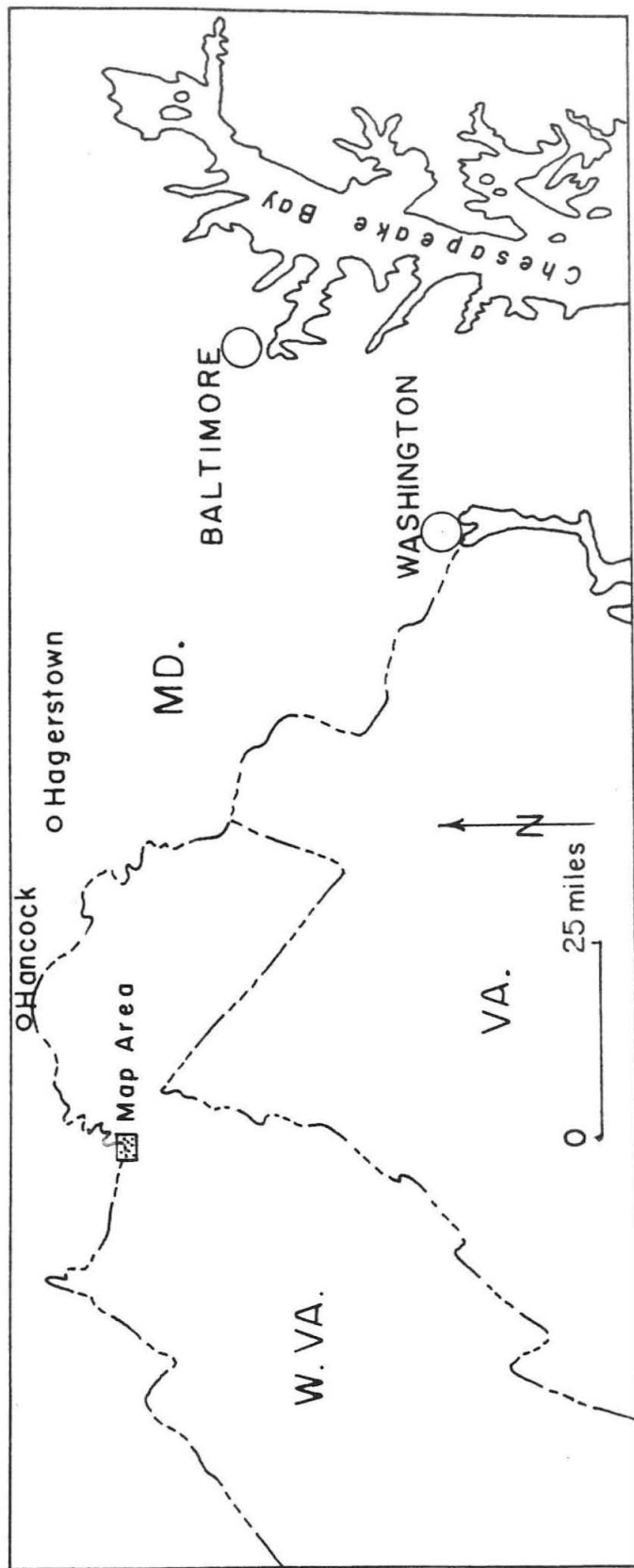


Figure 7. Index map showing location of part of the Cacapon Mountain anticlinorium in western Maryland. Geologic map of the hachured area is given in Figure 8.

EXPLANATION

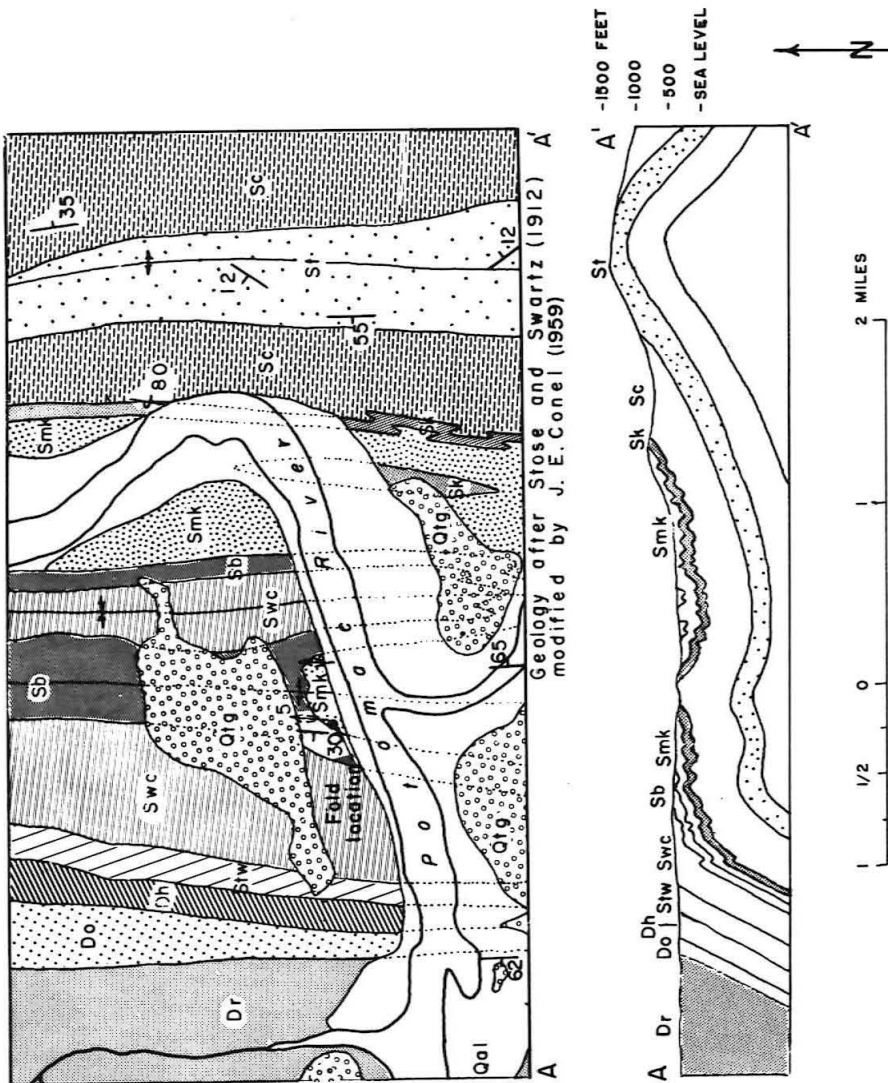
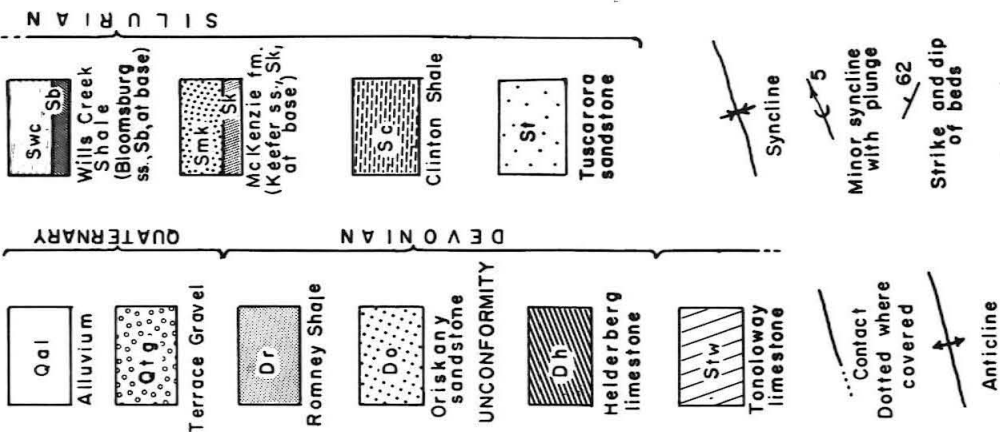


Figure 8. GEOLOGIC MAP OF PART OF THE CACAPON MOUNTAIN ANTICLINORIUM

Like most folds of the Appalachian Valley of this region the major anticlinorium and the minor folds it embraces are overturned toward the west by 20° . Beds in the western limb of the major structure dip 55° west and those of the eastern limb $35-45^{\circ}$ east. The cross-section in Figure 8 is drawn along a line forming the lower boundary of the geologic map given above it. Schematically depicted are the minor even wave length crenulations which occur in thinly bedded Silurian strata of the McKenzie, Tonoloway, and Wills Creek formations. The actual fold studied is not shown because its position is north of the line of the cross-section. However its relationship to the larger fold is similar to that of the structures shown in the drawing. These minor folds appear to have arisen through a simple squeezing of sediments in the core of the large Cacapon anticlinorium.

Detailed description

Figure 9 shows the fold studied here (designated hereafter as fold PC) which occurs in the McKenzie Creek formation about 10 feet below the upper contact of this unit with the overlying massive Bloomsburg sandstone. Figure 10a is a drawing from the above photograph of the particular limestone layer studied in this investigation (for convenience this horizon is designated layer A). The medial plane of the layer is deformed into a nearly circular curve whose radius



Figure 9. Fold in thinly bedded limestones and shales of the Silurian McKenzie Creek formation, approximately 10 feet below contact with the overlying Bloomsburg sandstone. The particular horizon investigated here is labeled "A." At place marked "B" other layer in the fold is broken by radial tension fractures that are filled with secondary white calcite. These white veinlets at "C" show right differential offset by slip along the bedding planes. The position of this structure is approximately shown on the geologic map in Figure 8. Layer A is approximately 4 inches thick.

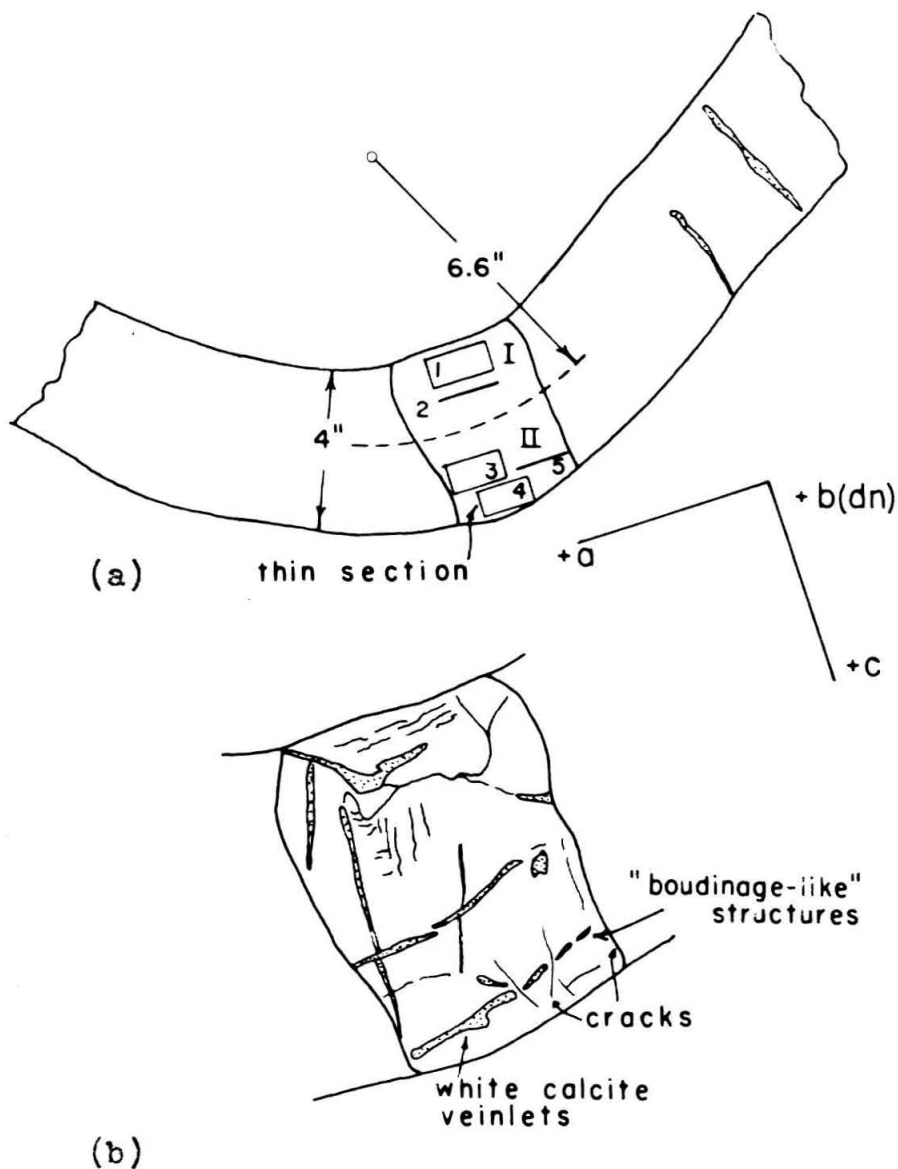


Figure 10. Sketch of the fold in Figure 10, layer A, axial portion. (a) Dimensions of the layer, positions and orientations of thin sections approximately to scale. Region I lies inside the circular dashed line (which marks approximately the medial plane of the layer) and Region II outside. Stippled areas are white calcite filled veinlets. (b) Fracture and veinlet pattern in the axial portion of the fold. The composite fracture and veinlet trending diagonally across the layer at the top of the drawing makes an angle of approximately 30° with the ab-plane of the fold. Stippled areas are white calcite veinlets. Reference axes with positive directions are as shown.

of curvature is 6.6 inches (16.8 cm). Both the upper and lower boundaries of the layer are nearly circular as well, and have a common center of curvature with the medial plane. Figure 10b shows the details of the veining and fracture patterns in the axial region. The rock is laced by two sets of calcite filled veinlets, with the veinlets in each set being about one millimeter in width. One set lies parallel to bedding in the layer and the other is tilted at a small angle to the axial plane. The veinlets parallel to bedding are offset by and are therefore later than veinlets of the other set. In addition to the veinlets, three mutually perpendicular sets of fine fractures have been superposed upon the rock. These fractures are oriented parallel to the planes defined by the coordinate axes in the fold (see p. 75). Bedding is mainly manifested in the rock by ostracod and other broken shell debris. Within the stratigraphic column, layer A is sandwiched between thin one-half inch thick layers of dark gray, fissile shale above and shaly limestone below. The rocks stratigraphically above the layer are broken and crumpled in the axial region (fig. 9), but below the layer they are unbroken and maintain continuity around the bent region. The limbs of the fold are broken by fractures which are filled with secondary calcite, but some fractures of this type are apparently later and are not mineralized.

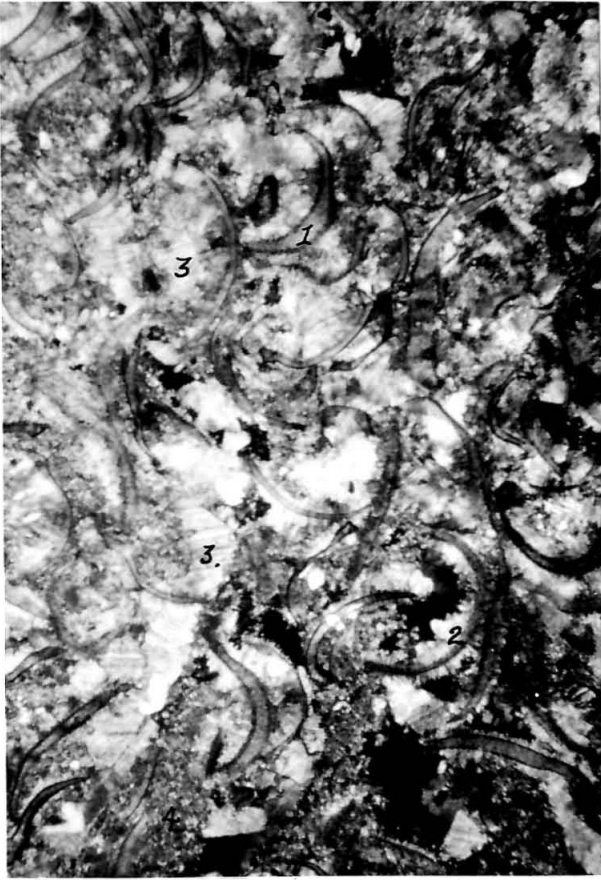
Axial plane cleavage is not developed in this fold. However, both flexural and shear (?) folds have supposedly

been described from the Cacapon section (Cloos, 1951, p. 153). The following points indicate that the fold studied here is at least partially flexural. (1) There is no development of axial plane cleavage or fan cleavage in the fold, (2) radial fractures are developed in other beds beneath layer A (fig. 9, area labeled "B"), (3) white veinlets (fig. 9, area "C") show differential offset of individual beds in the proper sense for the folding. (4) There is no significant thickening of the strata near the axial plane as is common in shear (?) folds of this area (Cloos, 1951, p. 153).

Petrographic character of the rock

Figure 11 gives a photomicrograph of the material from layer A. The rock consists of variable amounts of partly recrystallized shell detritus (5-30% flattened and deformed ostracod shells 0.5-5 mm in length), accessory amounts of rounded quartz, and large (up to 3 mm) subhedral dolomite grains which appear rust brown in plane light. Finely divided sericite and a small amount of opaque material (carbon ?) have also been noted. From the standpoint of this study, there are texturally five types of calcite visible in thin section: (1) ostracod and other shells made of exceedingly fine (ca. 1μ) equant crystals which show some preferred optical orientation within individual shell fragments, the c-axes of most crystals lying perpendicular to the margins of the shells. This material is not discernibly twinned. Quartz appears to replace some shells

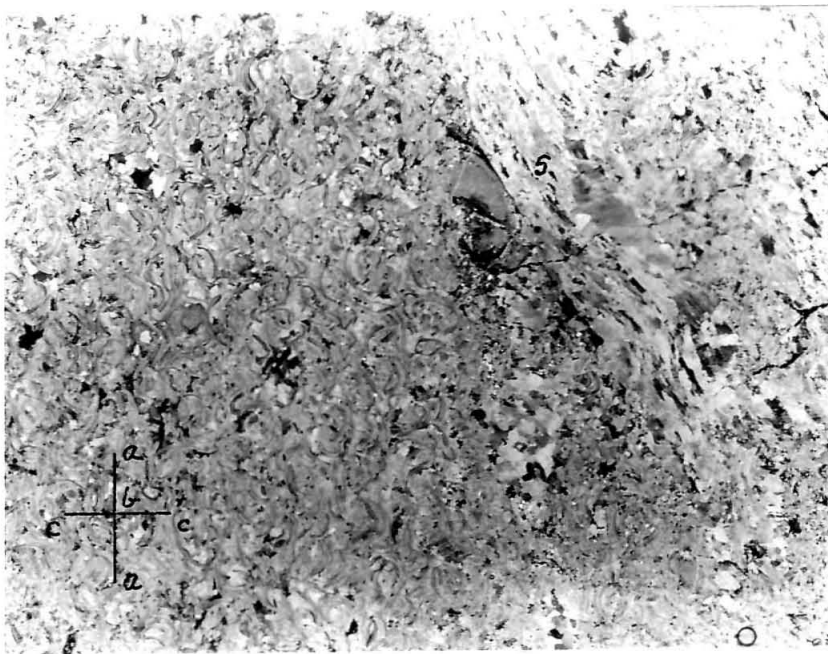
Figure 11. Photomicrographs. Material from layer A (region I). The rock consists of variable amounts of shell material (1), coarse and finely crystalline calcite (2) through (4). See text page 97 for further description. The wavy structure containing elongate crystals marked (5) on the right side of the photograph in (c) is part of the diagonal veinlet near the inner boundary of the layer in region I, Figure 10a. Several dark fractures traverse the veinlet. Crystals marked (3) in (a) and (b) are twinned variable amounts. A dark grain near the left margin of (b), center, contains thinly twinned (monotwinned) lamellae showing type I (?) interference fringes (see page 179, this thesis). All pictures taken with crossed nicols. Scales as shown.



(a) (x 50)



(b) (x 138)



(c) (x 8)

Figure 11

and a few consist of coarse calcite. (2) Surrounding many shells are radiating saw-tooth-like groups of elongate crystals and clusters of equant crystals 0.05-0.1 mm in size. Most grains of this type are twinned. (3) The third type of material consists of individual equant crystals 1-2 mm in diameter scattered through the rock embedded in a coarse matrix of crystals of types 1 and 2. Type 3 are distinguished from these latter groups by their larger size and by having no apparent association with these groups (as, for example, type (1) and type (2) appear to be associated). (4) Often enclosed within complete outlines of shells and forming an interstitial matrix for all of the above groups of crystals are small (0.01 mm) equant crystals which are not discernibly twinned. (5) Included within the fifth category are all ages of veinlet material. Specifically two ages of veinlets are present as noted previously. These are easily distinguished from one another in thin section by the fact that the later (radial) set contains undeformed calcite crystals. Crystals of the earlier set (parallel to bedding) locally appear highly sheared out (fig. 15). Profuse twinning (micro-twinned lamellae), undulose extinction, development of extremely elongate crystals are common. Fabric studies reported here utilized crystals of groups (2) and (3), but a special study of material from a deformed veinlet is also presented.

Fabrics from the fold

Fabrics from fold PC are presented in Figures 12, 13, and 14. Separate parts of the fold are distinguished in discussing the data. "Region I" is designated as occupying the part of the axial plane region toward the center of curvature from the medial plane: "region II" lies outside the medial plane.

(1) c-axis fabrics: Scatter diagrams of c-axes from regions I and II are shown in Figures 12a and 13a. Neither of these diagrams discloses a tendency for preferred orientation in the specimens analysed, and there is no symmetrical distribution of c-axes with respect to the coordinate axes in the fold (these axes are defined on p. 75).

(2) e-lamellae preferred orientation: The distribution of poles to all e-lamellae in grains from regions I and II are given in Figures 12b and 13b. In both figures solid dots represent positions of poles to the most prominently twinned lamellae set in each grain (designated e_1) and open circles represent subordinate or incipient lamellae sets (designated e_2). In region I, 76% of grains measured showed only one set of lamellae per grain, while 7% showed two lamellae sets with one set incipient and poorly developed (microtwinned). In region II, 70% of the grains measured showed only one set of lamellae, 20% two sets and 5% no twinning at all. One percent of the grains in region II showed recognizable twinning, with the remainder of the lamellae being microtwinned.

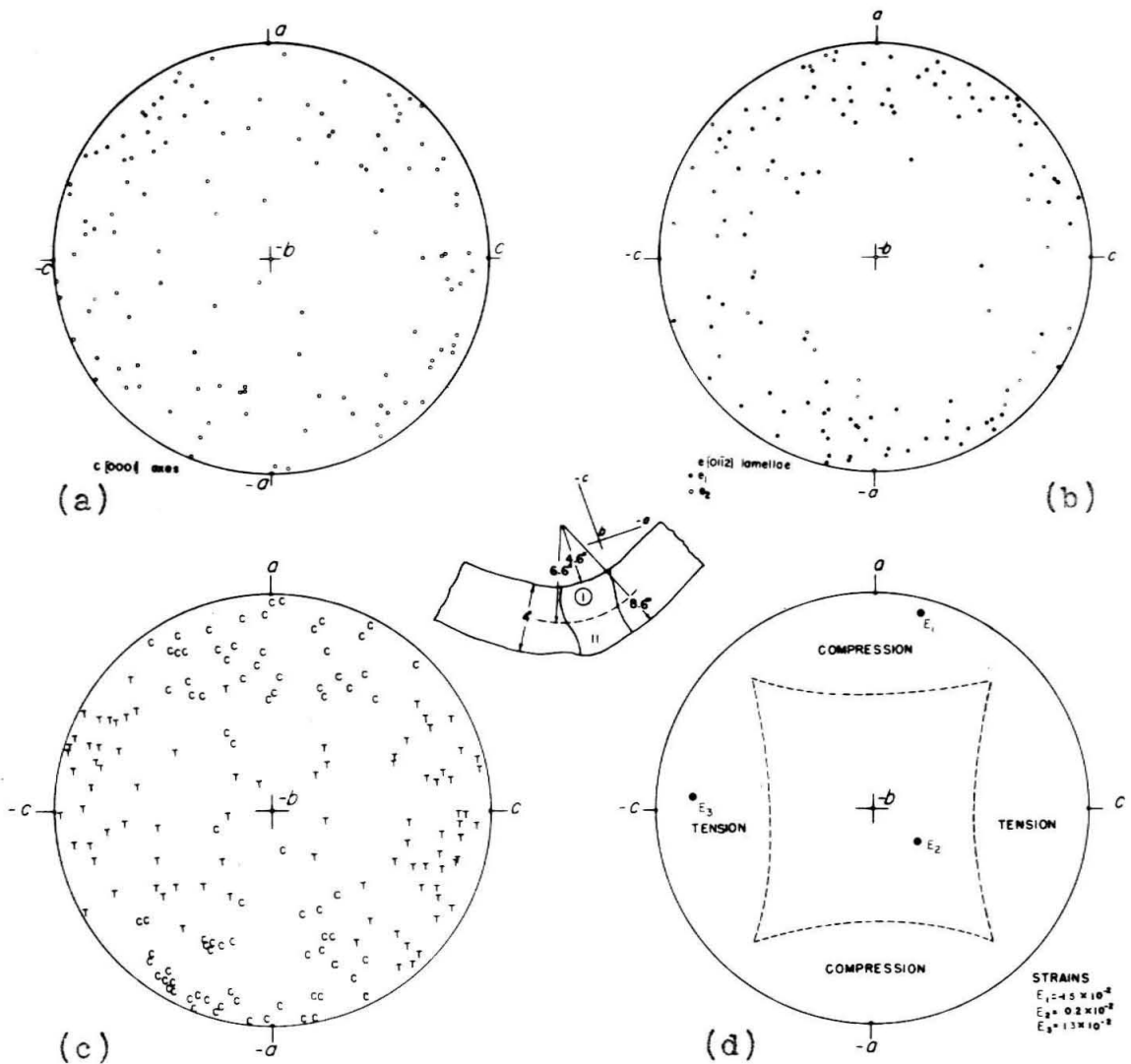


Figure 12. Fabric and strain data from Region I. (a) c -axes; (b) e -lamellae data. Closed circles represent positions of poles to most prominently twinned set of lamellae in a grain (e_1), open circles less well developed sets (e_2, e_3); (c) dynamic analysis (reduced diagram) of twin lamella fabric. C = axes of compression, T = axes of tension; (d) orientation of the principal axes of twinning strain, magnitudes and senses of the principal strains. $E_1, E_2,$ and E_3 refer to the algebraically least, intermediate, and greatest strains (negative values compressive), the magnitudes of which are given below the diagram. The dashed lines outline areas of concentration of C and T axes from the dynamic analysis. All diagrams equal area projections, lower hemisphere. Position in the fold from which these data were obtained is given by the circled number in the drawing at the center of the figure. As the coordinate system is drawn, the (+) b-axis is down in this figure.

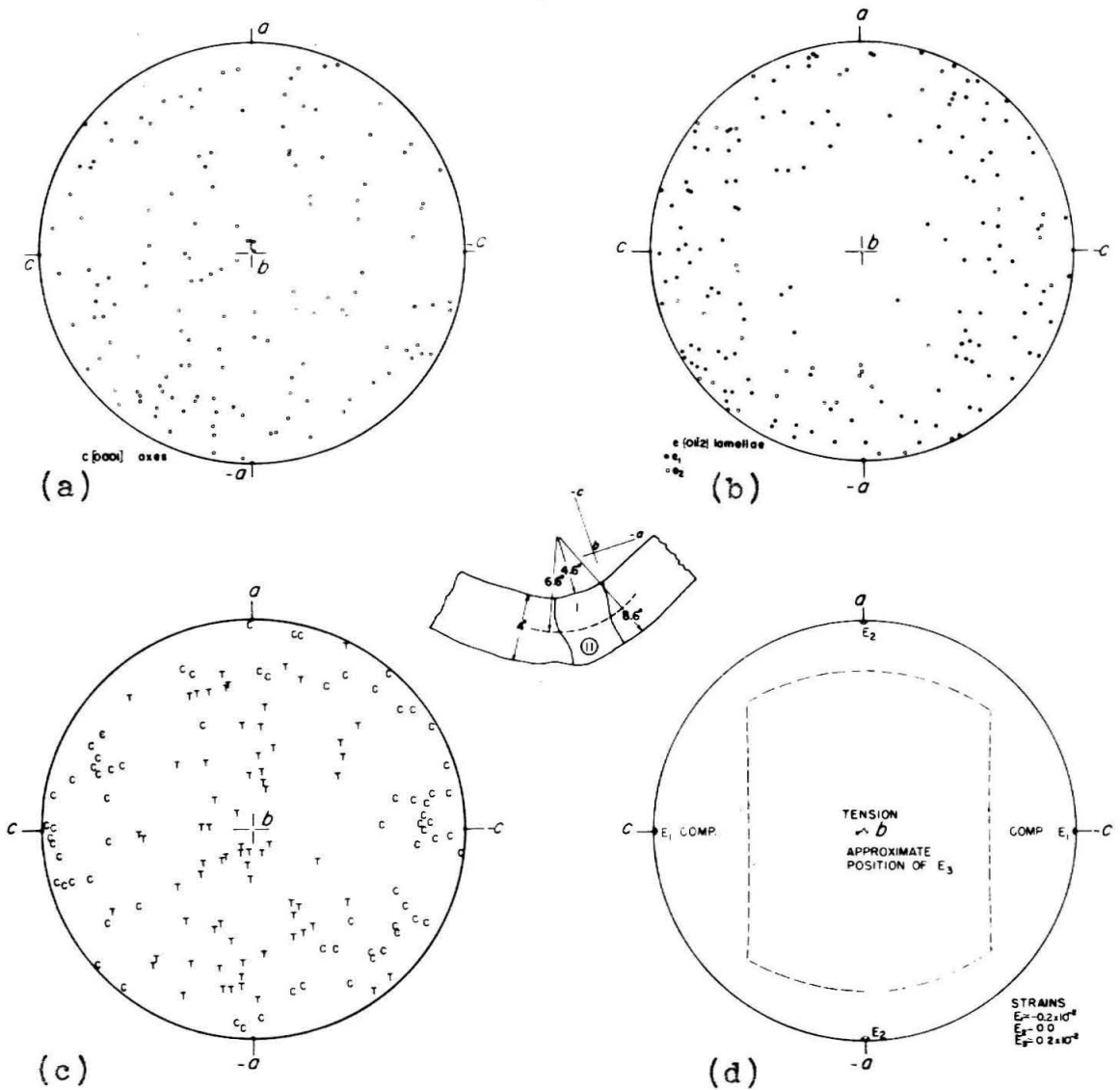


Figure 13. Fabric data from Region II. (a) c-axes; (b) e-lamellae data. Closed circles represent positions of poles to the most prominently twinned set in a grain (e_1), open circles less well developed sets (e_2, e_3); (c) dynamic analysis (reduced diagram) of the twin lamella fabric. C = axes of compression, T = axes of tension; (d) orientation of the principal axes of twinning strain, magnitudes and senses of the principal strains. $E_1, E_2,$ and E_3 refer to the algebraically least, intermediate, and greatest strains (negative values compressive), the magnitudes of which are given below the diagram. The dashed lines outline areas of concentration of C and T axes from the dynamic analysis. All diagrams equal area projections, lower hemisphere. Positions in the fold from which these data were obtained is given by the circled number in the drawing at the center of the figure.

Scatter diagrams of e-lamellae poles deserve some special comment. In both regions I and II there is a tendency for these poles to lie in a broad girdle about the b-axis of the fold, the girdle being somewhat stronger in region II. This distribution of points for each region must partly result from the optical inaccessibility of e-lamellae lying parallel to the ac-plane of the fold. In preparing each of these diagrams mutually perpendicular thin sections were examined from each region, but more grains were measured in the ac-sections than in sections cut from the parallel to the ab-plane. In particular, in region II, 70% of the data were obtained from ac-sections, and in region I 75% of the points were measured in thin sections of this orientation. The e-lamellae data are thus somewhat biased by this weighting. In both regions practically all of the visible lamellae measured in ab-sections were incipient in development (microtwinned, showing very low 1st order interference colors (see p. 199)) and were widely spaced, so that they do not contribute significantly to the strain in twinning. In region I the degree of twinning is much greater in section (1) (see fig. 10a) than in section (2). In region II, sections (3), (4), and (5) show on the average the same amount of twinning per grain (most grains contain only microtwinned lamellae). It appears that the girdle fabric in each region is to some extent due to observation. This will be taken into account in later discussions of results given by the dynamic analysis of these lamellae fabrics.

When these diagrams are examined in detail, openings in the girdle pattern may be noted in region I around the c-axis of the fold. No such distinct opening can be seen in the diagram from region II. In region I there is a marked tendency for \underline{e}_1 -lamellae to be distributed around the a-axis of the fold, with \underline{e}_2 -lamellae scattered throughout the rest of the girdle pattern. In region II the pattern is not as straightforward, \underline{e}_1 -lamellae are generally distributed about the c-axis of the fold. \underline{e}_2 -lamellae appear to be more numerous around the a-axis, but this density variation may not be significant statistically.

(3) Dynamic Analysis Results: Figures 12c and 13c also show results of a dynamic analysis of the twinning lamellae in regions I and II respectively. These particular figures are "reduced" diagrams, prepared by the method suggested on p. 70. The composite scatter diagrams of compression and tension axes obtained from all sets of \underline{e} -lamellae in all grains for each region are given in Figure 14a,b. Referring to the reduced diagrams the major features of the pattern in region I are maxima of compression axes around the a-axis of the fold, and tension axes around the c-direction. These latter points tend to form a girdle in the bc-plane of the fold. The situation in region II is that broad clusterings of C-axes occur around the c-axis of the fold, and a very broad T-axis maximum is situated about the b-axis. In the composite diagrams (fig. 14) the situation

described above for region I is again portrayed, while the patterns for region II consist roughly of a T-axis girdle in the ab-plane and a C-axis girdle in the ac-plane which overlap in a portion of the diagram corresponding to the direction of the a-axis.

As far as the dynamic interpretation is concerned, the above results indicate the following points: in region I compression of the rock along the a-axis, tension along a direction normal to this axis, or a combination of such stresses could account for the twinning observed. In region II the analysis indicates compression parallel to the c-direction in the fold, a tension along the b-axis, or some combination of these could produce the observed twinning. These results are to be compared with those derived above (p. 52) for an aggregate obeying the maximum resolved shear stress law. The simple model for the fold chosen there consisted of an unconfined circular beam deforming in plane strain and loaded elastically by forces applied at the ends of the beam perpendicular to the axial plane. A comparison will show that qualitatively there is reasonable agreement between the model and the observed natural fabrics, and this indicates that a stress system like that in the axial region of the model could account for the observed twinning in the natural fold.

Concerning the major concentrations of axes in each diagram, the dynamic analysis indicates a reorientation of

the principal axes of stress as one passes from region I to region II, such that the axis of compression lies parallel to the a-axis in region I and parallel to the c-axis of the fold in region II.

We can estimate the effect produced on the dynamic analysis results by the observational "blind-spot" problem mentioned above (p. 104), by considering what pairs of C and T axes are omitted from the C-T diagrams which correspond to lamella pole positions at the center of a lamella pole scatter diagram. For a pole exactly at the center of a diagram, the associated c-axis of the crystal could lie anywhere on a small circle $26\frac{1}{4}^{\circ}$ about this pole. The C and T axes would then occupy positions on a small circle of half angle 45° about this pole. The exact positions of a pair of C and T axes will naturally depend on the orientation of the c-axis and the applied stresses, but qualitatively if polar e-lamellae are not measured, then associated points on the C and T diagrams are omitted which fall in a zone about the small circle with half angle 45° which has its center on the pole to the plane of the C-T diagram and about the pole to the diagram. In the complete fabric diagrams shown in Figures 14a and 14b, a low density of T-axes about the pole in the diagram may result from this difficulty.

The above dynamic analysis results were obtained from an original isotropic distribution of c-axes in each region of the natural fold. Thus the data are not restricted

Figure 14. Complete dynamic analysis data for the fold.
(a) Region I; (b) Region II. Previous diagrams (fig. 12c, 13c) were prepared using data given here by striking out closely spaced pairs of C and T axes (see text, p. 70).

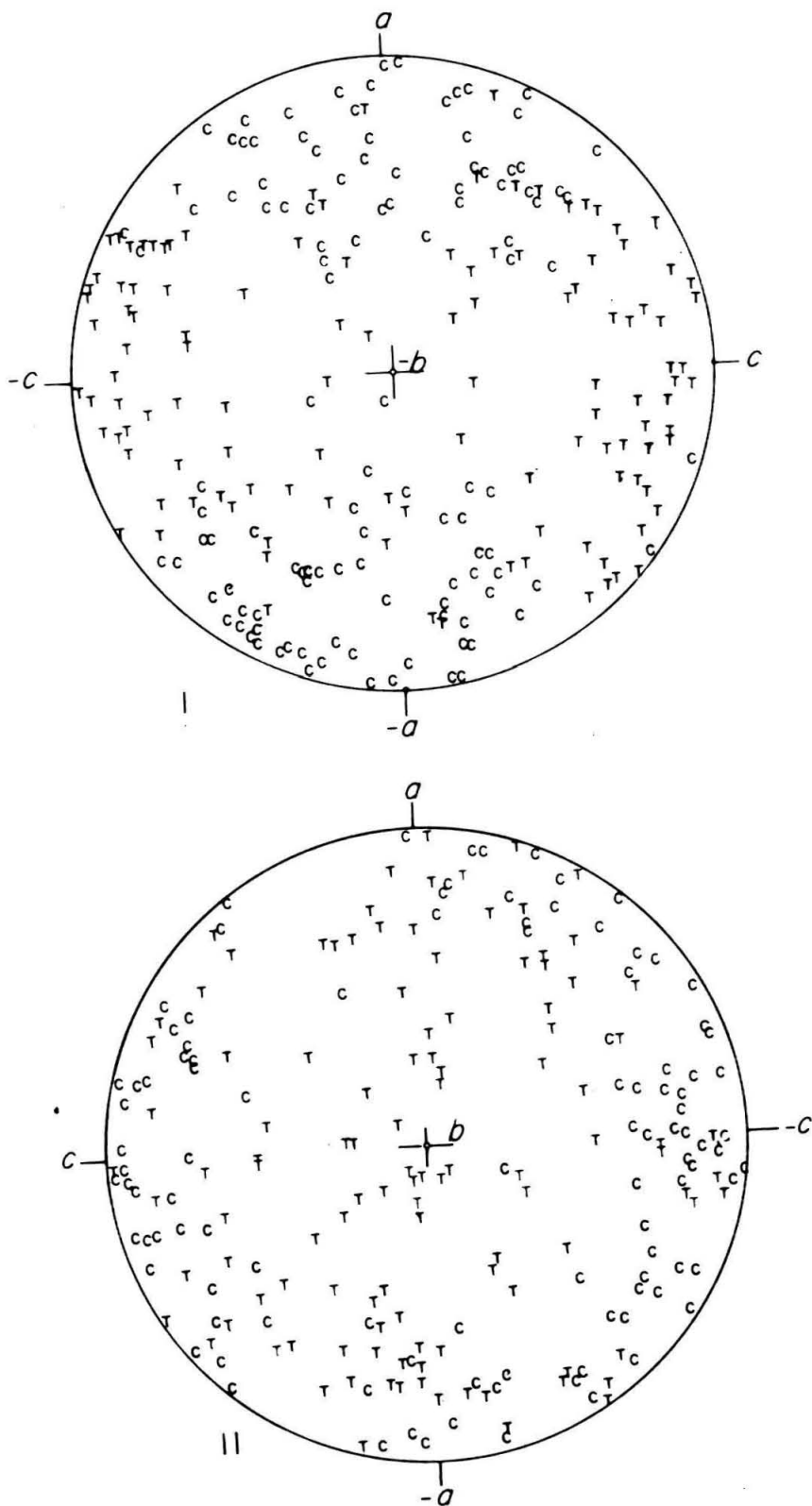


Figure 14

by the considerations which have been mentioned for aggregates showing highly preferred \underline{c} -axis orientations.

(4) \underline{c}' -axis orientations: The distribution of \underline{c}' -axes (that is orientations of the optic axes of the twinned parts of each crystal) have not been plotted directly for the fold but an idea of the distributions resulting from the deformation can be gained from results of the dynamic analysis. These distributions will represent a first approximation to the resulting deformation fabric. For calcite the \underline{c}' -axis lies $52\frac{1}{2}^{\circ}$ from the \underline{c} -axis of the host crystal and is symmetrically related to the host \underline{c} -axis position about the pole to the operative twin plane. From the geometry of the twin plane in calcite the compression axis of the dynamic analysis lies 71° from the \underline{c} -axis of the host crystal along the great circle containing \underline{c} and \underline{c}' , and the difference in position between the compression axis and the \underline{c}' -axis is only 19° . Clusterings of compression axes thus roughly approximate new \underline{c} -axis positions developed in a calcite aggregate through twinning. By referring to Figures 12c and 13c the new optic axis orientations due to twinning will be around the a-axis of the fold in region I and about the b-axis in region II. As pointed out earlier these are approximately the new orientations to be expected from twinning on the approximate model of the flexural fold given on page 47 .

(5) Calculation of Strains due to Twinning:

the calculation of visible strain due to mechanical twinning has been carried through for the fold using the procedure presented earlier (p. 56). In region I, 85 sets of lamellae have been used to determine the amounts of strain and orientation of the principal axes of strain. Orientation of the principal strain axes with respect to the fold coordinate axes are given in Figure 12d. The strain tensor matrix referred to these axes (\underline{x} = a-axis; \underline{y} = b-axis; \underline{z} = c-axis) is:

$$\begin{bmatrix} -1.43 & 0.03 & 0.21 \\ 0.03 & 0.15 & 0.36 \\ 0.21 & 0.36 & 1.29 \end{bmatrix} \times 10^{-2}$$

Referred to principal axes the strain components become

$$\begin{bmatrix} -1.5 & 0 & 0 \\ 0 & 0.2 & 0 \\ 0 & 0 & 1.3 \end{bmatrix} \times 10^{-2}$$

In the figure the areas enclosed by dashed lines correspond roughly to the areas of concentration of C and T axes in the dynamic analysis. The general agreement between the dynamic analysis result and the calculated strain reflects the fact that the C and T axes for each grain are the principal axes of strain associated with twinning for a particular grain. Since the final calculated strains represent weighted averages of the individual contributions, the agreement is inherent.

Two important points emerge from these results. (1) The calculated principal strains agree with the type of strain to be expected in the folded layer in region I if the deformation increment represented by the twinning lamellae has been such as to more tightly fold the layer. That is, there has been shortening parallel to the a-axis, extension parallel to the c-axis and only a slight deformation along the b-axis. The region has therefore deformed approximately in plane strain ($|E_{zz}| \ll |E_{xx}|, |E_{yy}|$). (2) These calculated values of strain are significantly less than the geometrically indicated total strain near the boundaries of the fold of 0.25, which is calculated from Equations 2 using the dimensions of the fold shown in Figure 10.

Instead of carrying through the lengthy strain computations for region II an estimate can be made of the strains for this region using the agreement between the calculated directions of the principal axes of strain and results of the dynamic analysis, as has emerged from the analysis in region I. By this analogy, the c-axis of the fold in region II is the axis of greatest shortening, and the b-axis is a direction of extension. The magnitudes of the principal strains are estimated in the following way. The average spacing index (number of lamellae per millimeter traversed normal to the twin set) of microtwinning lamellae measured in 170 grains throughout region II is about 7. Microtwinning lamellae in these rocks are, on the average about one micron

in thickness, i.e., they show gray to dark gray interference colors when oriented with the pole to the twin set nearly parallel to the microscope axis (see p. 199). The average strain in the direction of the c-axis of the fold can thus be approximately deduced from Equations 14, p. 57 and is

$$E_1 = -(7 \cdot 10^{-3} \cdot 0.69)/2 = -0.0024$$

or about -0.24%. The deformation along the b-axis of the fold (E_3) is then also 0.24% because of the fact that in this calculation the sum of the principal strains must equal zero. In detail the strain distribution is probably not this simple, for in arriving at the above results, C and T axes lying near the a-axis of the fold have been neglected. The magnitudes of these principal strains are also probably too high because there is considerable dispersion of the principal axes of strain (the C and T axes) in region II.

The important features of the strain distribution that has been approximately derived for region II are: (1) the principal axis of greatest compressive strain is oriented differently than that in region I by 90° . (2) The axis of greatest extension is along the b-axis of the fold rather than along the c-axis as in region I, showing that the fold is not deforming in plane strain in region II. (3) The average strain in region II is much smaller than the geometrically indicated maximum strain of about 25%, and is an order of magnitude less than that computed for region I.

On the basis of the above discussion it seems that twinning lamellae in both regions I and II represent either a minor deformation (essentially bending) of the material, and record only a final increment of the deformation or else they indicate that most of the permanent deformation of the rock has been accomplished by crushing and development of displacements along fractures such as are visible in the drawing of figure 10, and not by plastic deformation. The possible strains to be accounted for by fracturing are discussed next.

The fracture systems in fold PC which are filled with secondary white calcite may record several different kinds of accommodation to the bending strain. In region I a calcite filled fracture traverses this part of the fold at an angle of 30° to the bedding. In thin section crystals of the filling are highly elongate parallel to the walls of the fracture (see photomicrograph, fig. 15). These crystals show considerable microtwinning and undulatory extinction which is indicative of high deformation. In region II and near the medial plane of the fold, thin calcite filled fractures cut the layer parallel or at a small angle to the bedding. The lowest of these veinlets appears to be intensely stretched out into a number of boudinage-like segments (lowest veinlet, fig. 10b; also fig. 15). In thin section, crystals in these veinlets are also highly elongate and show abundant microtwinning. On the other hand, calcite crystals which

fill cracks running perpendicular to the plane of bedding are almost completely undeformed. The highly deformed nature of the fracture fillings could indicate localized deformation along these discontinuities. This is considered likely because crystals immediately adjacent to the veinlets in the host rock are relatively undeformed compared to those in the fractures. The diagonal fracture in region I is properly oriented (near 30° to an axis of compression as measured in the plane containing the axes of greatest and least principal stresses) for Coulomb type fracture of the material in this region. Crystals within the fracture appear to be bent over in a manner indicating a left hand displacement across the fracture in the ac-plane of the fold looking along the positive direction of the b-axis. However slickensides observed on the planar surface of the fracture make an angle of 18° in the ab-plane with the a-axis (62° with the (-) b-axis). Fractures parallel to bedding in region II could represent planes along which the rock has slipped during flexural folding. This is indicated by slight right hand offsets (fig. 10b) of nearly vertical veinlets in several planes. Part of region II does lie slightly to one side of the axial plane, so that some slipping of this type might be expected, although from symmetry it should vanish at the axial plane of the fold. The amount of strain in bending in the axial region could be considerably reduced depending on the closeness of these slip planes in the layer and upon

the amount of slip along each. A rough calculation using Equation 1 shows that if slip has always occurred along the lowest fracture parallel to bedding in region II so that only the small layer of bed between the fracture and the boundary deformed in bending, the maximum strain to be expected at the outer boundary (radius equal to 8.6 inches) is only about 4%. This type of strain accommodation might well account for a significant part of the discrepancy between observed and geometrical strain in the fold. There appears to be little or no displacement on most of the unmineralized fractures which lace the rock. These often cut through shell fragments, which are not offset by the fractures. The amount of displacement along the various sets of mineralized fractures is difficult to assess. The elongate nature of many crystals in the central parts of the veinlets could certainly be a feature partly inherited from the crystal habit of the undeformed vein material, so that the extreme elongation of the crystals would not be totally due to deformation. The diagonal fracture in region I does not produce offset of the stratigraphic lower boundary of layer A so that deformation along it must be absorbed within the layer, but at any rate outside the area designated region II in Figure 10a. Therefore the strain in region II cannot be influenced by this discontinuity. The amount of strain to be accounted for along the diagonal fracture in region I can be approximately estimated as follows. As-

suming that crystals in a portion of the veinlet (now 2 mm in width) originally were elongate perpendicular to its plane, they can be observed to have been sheared through an angle of approximately 40° . This amount of shear would indicate relative displacement of opposite walls of the filling (assuming further that no change in thickness normal to its plane has occurred) of roughly 2 mm. The associated displacement parallel to the a-axis of the fold is $2 \times \cos(30^\circ)$ or 1.7 mm. Since the distance parallel to the a-axis over which the fracture runs is not known, we approximate this by taking the distance which can be observed in hand specimen of 80 mm. The presently determinable "strain" accommodated by this fracturing is thus of the order of $-1.7/80$ or -0.02 in region I. By a similar calculation, the amount of strain due to filling of fractures parallel to the bc-plane of the fold in both regions i.e., extension parallel to the a-axis, is estimated at 0.01. The net effect of fracturing is then shortening of about 1% in region I, and extension of 1% in region II.

The possibility that significant amounts of strain (relative to the strain actually observed due to twinning) have developed by translation gliding on \underline{r} $\{10\bar{1}1\}$ should be considered. Theoretically it can be expected that this strain will be of the same order as the twinning strain. From Equation 18 the maximum expected internal rotation of an \underline{e}_1 lamella by glide on \underline{r}_1 for a shear of this amount is

less than one degree, and this difference is almost always undetectable in practice. It is therefore not surprising that unequivocal evidence of internal rotation was not noted in the examination of these rocks.

In addition to the question of the low amount of strain recorded in twinning, there is also the discrepancy between the amounts and senses of twinning strain recorded in regions I and II. If deformation in the fold were in pure bending and plane strain, then it would be natural to expect strains from these two regions to be of approximately equal magnitude though reversed in sense except along the b-axis if the fold has deformed in plane strain. Equations 9 and 10 indicate that for the points in the fold where these equations apply and under the assumption of the model, the ratio of the elastic strain parallel to the a-axis (x - direction in the calculation at the axial plane) in regions I and II is $E_{xx}^{II}/E_{xx}^I = -1.25$. However the observed ratio in this fold is zero (see p. 111 and 113). Aside from the possible peculiarities introduced into the strain picture by the fracturing discussed above, the strain distribution calculated for the fold in the axial region might represent a combination of different types of deformation, (1) bending, with the strain distribution reflecting stresses like those given in Equations 9 and 10, and (2) uniform shortening parallel to the a-axis of the fold. Thus bending would extend elements of the layer in region II while uniform shortening

would tend to cancel out the bending strain. Both deformations would act together in region I to accentuate the strain there.

The foregoing analysis illustrates that the dynamic analysis and the strain interpretation based thereon can be quite sensitive in detecting minor changes in strain in a deformed carbonate rock. There is thus a possibility of applying such calculations in finding the position of the "neutral surface" in a flexure fold and therefore of carrying through an analysis like that suggested on p. 71 . Applying these earlier considerations to the present fold it can be calculated that for its dimensions (inner radius 12.15 cm, outer radius 22.7 cm) the difference in position of the neutral surface for a Newtonian viscous material and one showing perfectly plastic behavior is about 0.25 cm with the neutral section in the viscous body lying nearer the center of curvature. However, the computed result that the strain in the direction of the a-axis in region II is small or zero makes it unclear that a neutral surface still exists in the layer. Furthermore the fold has not deformed in plane strain parallel to the fold axis, and above all has probably not deformed in pure bending. Nor is it possible that its surfaces were stress-free, though orientation of the principal axes of strain (stress also) normal to the boundaries of the layer in both regions of the fold suggest that the boundaries were in fact free of shearing stress in



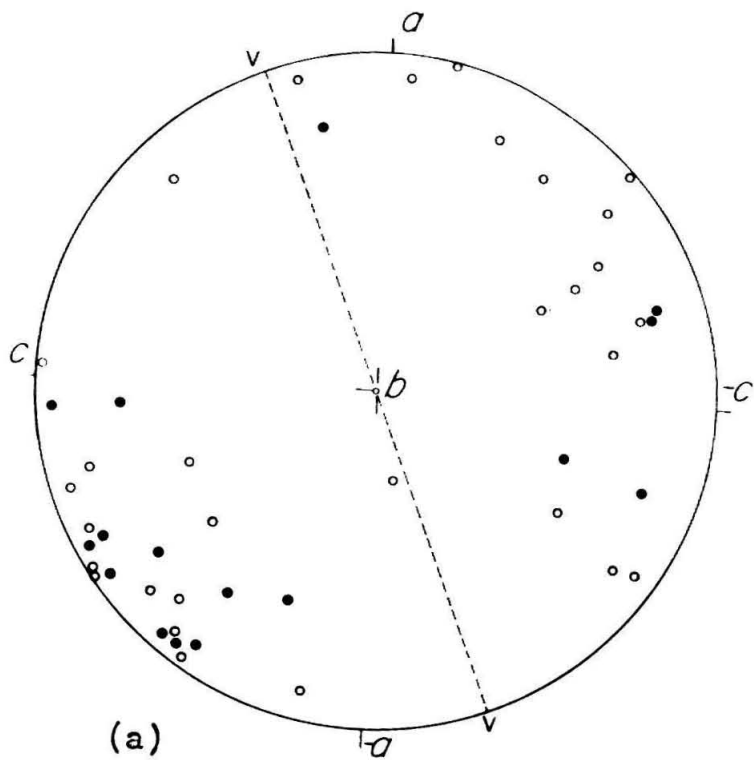
Figure 15. Photomicrograph. Stretched out vein material from region II, lowest veinlet shown in sketch in Figure 10b. Note elongate nature of the crystals. Dark bands in individual grains are $\{01\bar{1}2\}$ lamellae. A small crack (dark line) runs irregularly with sub-horizontal attitude just below the center of the picture. Partly crossed nicols (x 200).

the axial region (which is required by the symmetry of the deformation). These difficulties preclude the possibility of applying the method of page 71 for discriminating plastic from viscous behavior in this fold.

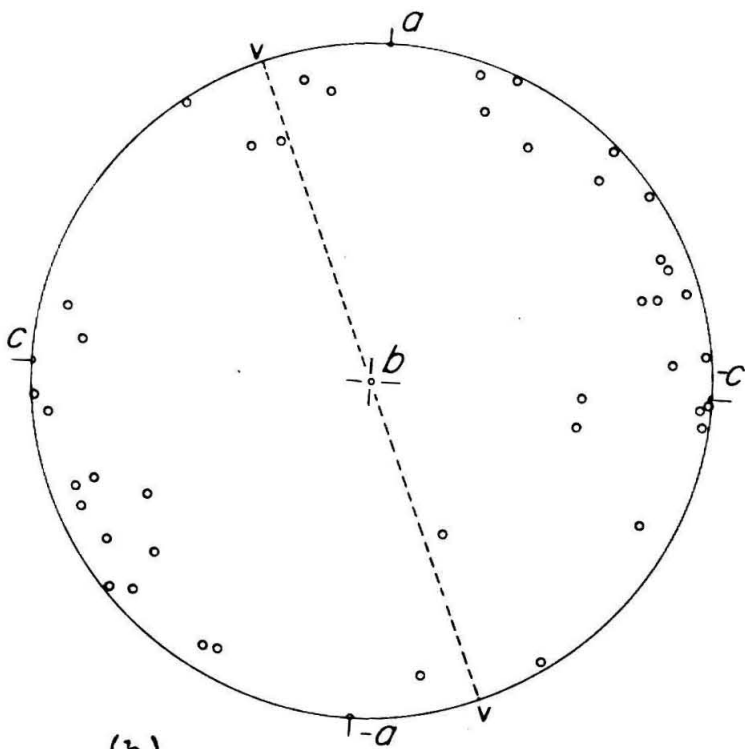
Fabrics of highly deformed vein material

Crystals in a mineralized fracture in region II that appear to have been highly deformed have been studied in some detail (fig. 15). The vein material greatly resembles highly deformed Yule Marble (Turner, et al., 1956, plate 5) in that in both individual crystals are stretched out into lensoid shaped grains with ragged boundaries and both show considerable evidence of development of microtwinned lamellae. Figure 16a is a scatter diagram of 50 c-axes for calcite from the veinlet shown in Figure 15. In this diagram solid dots represent positions of c-axes of what appear to be exceptionally highly deformed, elongate grains which show undulatory extinction, and numerous twinning lamellae. The main c-axis pattern of the relatively few grains accessible to measurement is approximately normal to the trace of the veinlet in thin section and normal to the direction of elongation of the crystals. Part of this pattern is perhaps remnant from the original fabric of the vein. Highly deformed individual grains were too nearly destroyed optically to permit detailed work to be done with them. However their distribution generally coincides with the main pattern. The

Figure 16. Petrofabric data from highly deformed vein material in Region II. (a) c-axis fabric. Solid dots are positions of c-axes of highly deformed, elongate grains showing undulatory or wavy extinction. (b) e-lamellae fabric. VV marks trace of veinlet in plane of the thin section and also the approximate direction of elongation of the grains. Equal area projection, lower hemisphere.



(a)



(b)

Figure 16

distribution of e-lamellae poles is shown in Figure 16b. The relatively few measured show a tendency to cluster around the same direction as the c-axes. Earlier it was suggested that these fractures represent places where the rock has sheared during flexure. With this in mind it is interesting to compare these orientation data (inconclusive though they are statistically) with marble experimentally deformed in shear (Turner, et al., 1953, p. 1341). The experiment referred to consisted of 37% compression of a cylinder of Yule marble (cut normal to the foliation) at 300° C. A shear zone developed in the barrel shaped cylinder at an angle of 40° to the axis of compression because of eccentric loading of the specimen during deformation. Individual grains within the deformed zone are flattened parallel to a plane which makes an angle of 70° to the axis of compression. The resulting fabrics consist of maxima of both c-axes and e-lamellae about the normal to this plane. Thus there is some similarity between the fabric resulting from experimentally imposed shear of a marble aggregate and the fabric from what is thought to represent an example of a naturally sheared aggregate.

Application of the law of maximum resolved shear stress

As previously discussed, several different theories have been proposed to account for the development of deformation fabrics in metals (Taylor, 1938; Bishop, 1954) and in

carbonate rocks (Handin and Griggs, 1951; Turner et al., 1956) and the applicability of each of these treatments to the present work has been pointed out. During deformation of a polycrystalline aggregate, the Bishop theory states that within a single crystal the strain takes place in accordance with the principle of maximum plastic work (Bishop, 1954). According to the principle (Bishop and Hill, 1951a) the work done in a given plastic strain increment by any stress physically capable of producing it is greater than or equal to the work done by any other stress not violating the critical shear stress law on the active glide planes in the crystal. The maximum resolved shear stress "law" used by Turner et al. (1956) (see p. 8, this thesis) can be interpreted a special case of this principle modified to account for deformation on a single slip plane. As applied to an aggregate, this "law" as used would strictly apply only in situations where individual crystals could accommodate themselves to the macroscopic strain and to strains in surrounding grains by glide on a single glide system. Otherwise five independent glide systems would generally be required to operate in each grain for the aggregate to remain cohesive after straining. A consideration of this type can naturally account for the observation that crystals in the rocks studied here (especially throughout region I) do contain more than one set of twins per crystal, which is a clear violation of the maximum resolved shear stress

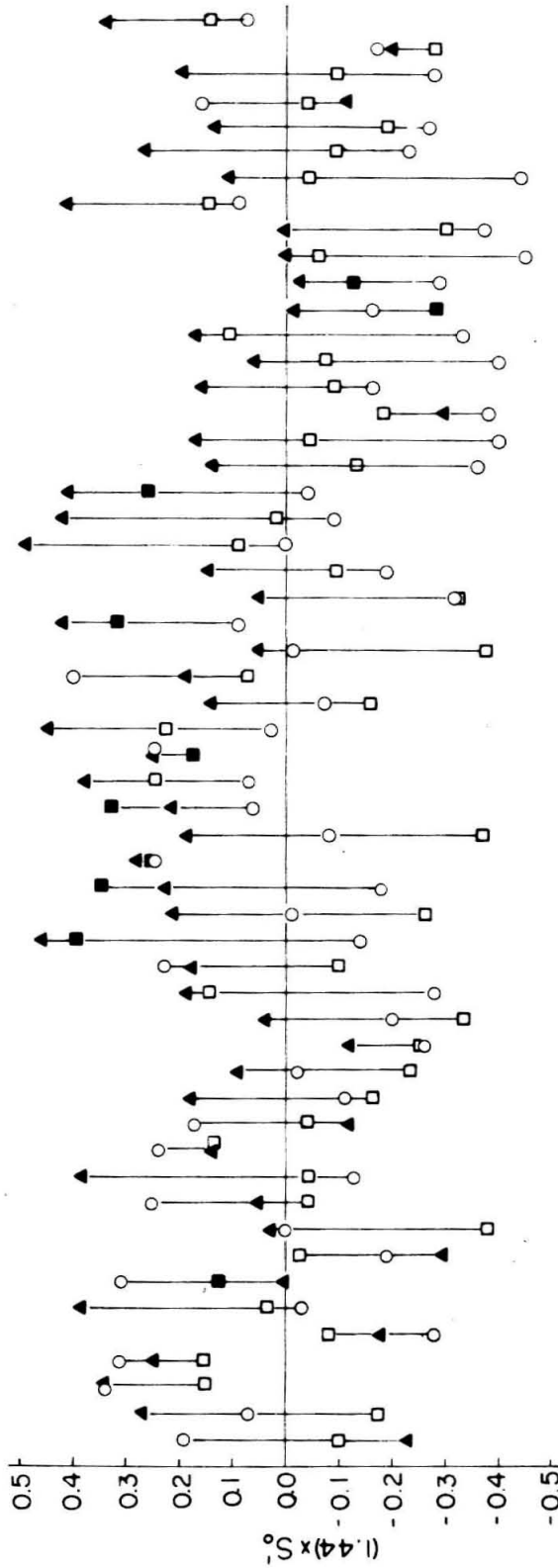


Figure 17. Resolved shear stress data, from region I. Each vertical grouping of three points refers to a single crystal. S_0 given by the first of equations 12 is plotted along the vertical axis. To get the actual value of S_0 for any particular twin set in a crystal, divide value along the ordinate by 1.44. For each grain a solid point represents a twin set actually developed: Triangles = e_1 , squares = e_2 , circles = e_3 .

"law." However, it is still required that for slip to take place in a crystal the critical shear stress must be reached on each active system. It is shown below that the "law" does apply as an approximation.

A comparison of the results predicted theoretically for the dynamic analysis assuming operation of the maximum resolved shear stress law and those actually observed for a natural fold, qualitatively suggests the applicability of this law in the present case. A more detailed comparison has been made in Figure 17. Since it is not possible to speak in terms of the magnitudes of the stresses responsible for the observed deformation in fold PC, the resolved shear stress coefficient S'_0 , defined by Equation 12 is computed instead. In Figure 17, S'_0 for the three twin sets in each of 54 randomly selected crystals from region I are shown. The vertical axis gives the value of S'_0 computed from the first of Equations 12. Above the horizontal axis ($S'_0 = 0$), S'_0 is favorable for twinning and below unfavorable. For each grain the data are plotted along a single vertical line, each point representing the value of S'_0 for a particular twin set in the grain. Solid points represent twin sets actually developed in a grain and open ones sets that are undeveloped. Triangles represent the most prominent twin set in a particular grain (designated as e_1), squares the next best developed set (e_2), and circles the remaining

set (\underline{e}_3). Obviously this designation between \underline{e}_2 and \underline{e}_3 is arbitrary from an observational standpoint when only one set of twins is developed in a grain and is only made in the interests of organizing the data during actual calculation. When two sets of twins are equally developed (each microtwinned for example) the designation between \underline{e}_1 and \underline{e}_2 is also arbitrary observationally. Figure 17 shows that deformation in about 75% of the grains examined in this analysis of the aggregate in region I conforms to expectation on the hypothesis that the maximum resolved shear stress law applies if it is assumed that Equations 9 and 10 describe the stress situation in the fold. In 80% of the grains showing two sets of lamellae, twinning is in accordance with the law under the assumed stresses in that the most prominent set has the highest value of S'_0 and the next most prominent set the next greatest value of S'_0 . In an earlier attempt at this kind of analysis it was assumed that the observed deformation was in uniaxial stress (an assumption approximately equivalent to plane stress deformation in the fold) i.e., all stresses zero except along the a-axis of the fold and the x-axis in Equation 12. For this assumption the agreement between observation and theory for 37 randomly selected grains from region I (not necessarily the same grains as used above) was only slightly poorer, in that in only 70% of the grains measured was the set with best developed twinning also that with the highest value of S'_0 . Furthermore in

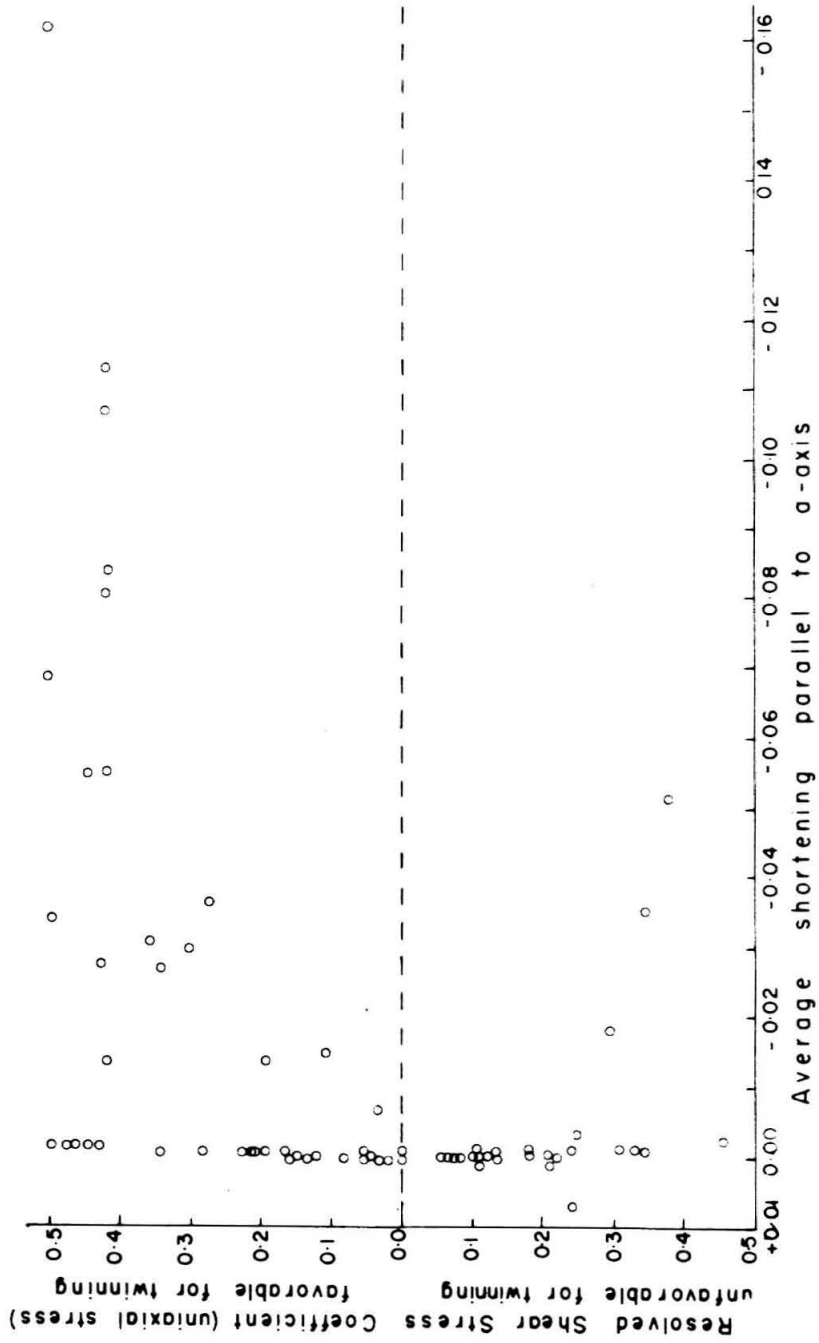


Figure 18. Twinning strain along a-axis (x-axis) of the fold in individual grains from region I as a function of resolved shear stress coefficient (S_0), for uniaxial stress, i.e., all stresses assumed zero except τ_{xx} in Equation 11.

about 70% of the grains with two sets of lamellae, \underline{e}_2 was associated with the next highest value of S'_0 .

Figure 18 illustrates the relation between the amount of strain individual crystals have undergone along the a-axis of the fold, and their orientation with respect to the applied stress (uniaxial case). Each point in the figure describes a single crystal. The indication from the apparent relationship is that for the strain increment recorded as twinning throughout the portion of region I covered by the present petrofabric analysis, the deformation is nonhomogeneous from grain to grain, and is dependent on orientation of the grain in the stress field. Considering the texturally nonhomogeneous and fractured state of the material in this fold it is perhaps surprising that such qualitative good agreement between theory and observation is actually possible.

It is concluded that under the plausible assumption that the stress distribution in region I is given by the first of Equations 12, twinning deformation in the aggregate appears to follow reasonably well the law of maximum resolved shear stress. Agreement is only slightly poorer, however, when a uniaxial stress situation is assumed.

Fold from the Darwin Hills, Inyo County, California

Geologic setting

The Darwin Hills are located in the south-central part of the Darwin quadrangle in central Inyo County, California, 35 miles southeast of Mt. Whitney, and 40 miles west of Death Valley (see index map, fig. 19). The most recent geologic report concerning this area is by Hall and MacKevett (1958). Hopper's (1947) excellent regional study also includes considerable information on the Darwin quadrangle. In the present study geologic mapping has been done in only a small area in upper Darwin Wash, the area of principal concern in the present work. General information concerning the regional stratigraphy and geologic history is drawn from the publications given above.

The Darwin Hills and adjacent areas in Darwin Wash consist of folded and faulted Pennsylvania and Permian sediments which have been intruded by gabbroic to granitic rocks, considered to be of similar age to the lower Cretaceous intrusives of the adjacent Sierra Nevada batholith. The sediments consist of thinly bedded gray and brown, locally crinoidal and nodular limestone, shale, quartzite, and bedded chert whose combined thickness is somewhat in excess of 8000 feet. In upper Darwin Wash these sediments have been warped into several north-south trending gently north-plunging folds of moderate size, which are terminated at the Darwin tear fault, near the head of the wash. This fault, which is pre-

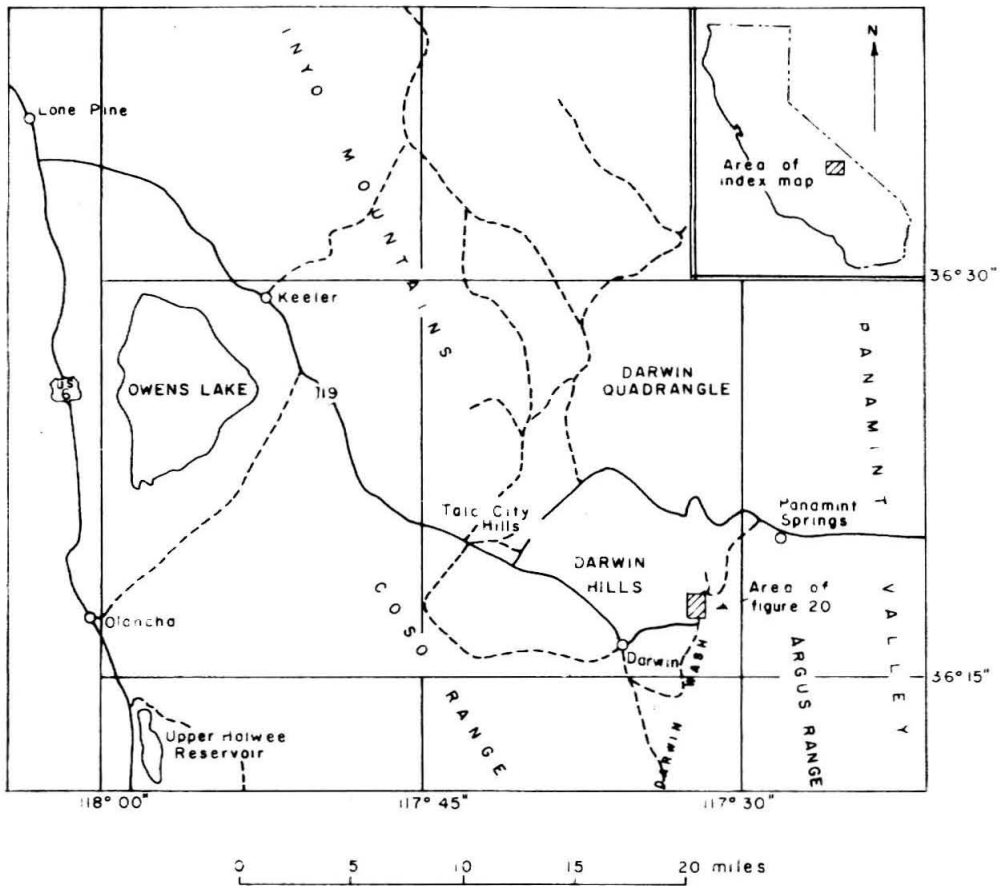
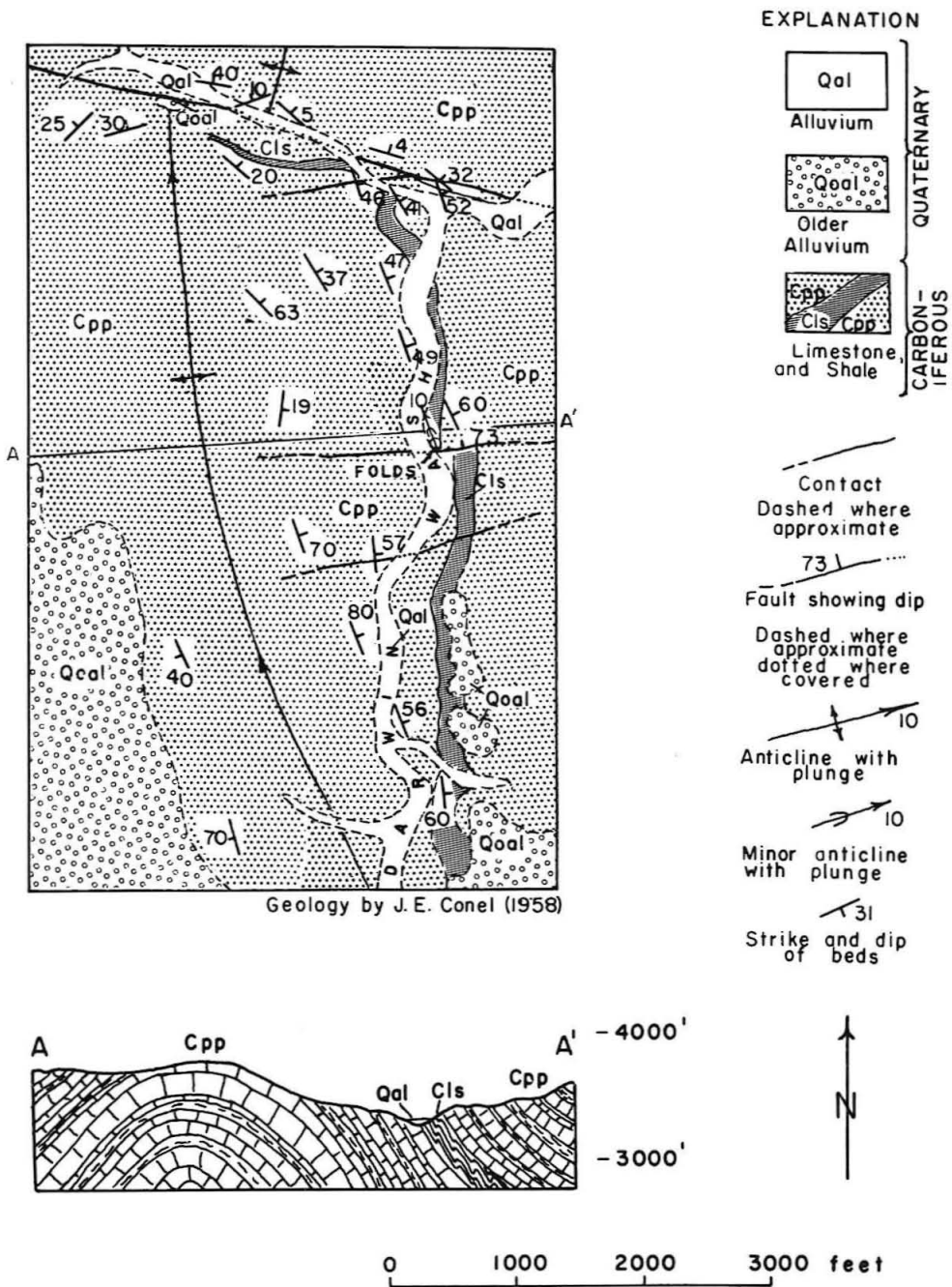


Figure 19. Index map of the area in the geologic map of Figure 20, Darwin Hills, Inyo county, California.



GEOLOGIC MAP OF PART OF UPPER DARWIN WASH
Figure 20.

Cenozoic in age (Hopper, 1947, p. 421) dips south 80° , trends east-west, and has about 2200 feet of predominantly left lateral and some dip-slip displacement, with the north side moving westward and up with respect to the south side.

Figure 20 is a geologic map of part of upper Darwin Wash south of China Garden spring. The principal structural feature of this area is a large north-plunging anticline, the axis of which follows the western margin of the map area and veers southeastward near the southern boundary. The fold includes sediments of Pennsylvania and Permian age which have not been differentiated by either Hopper, Hall and MacKevett or this writer. These sediments consist of several thousand feet of locally crinoidal and coral- and fusulinid-bearing limestones interbedded with thin units of black and red shale. The western limb of the fold is partly covered in the map area by Quaternary alluvium. The nose of the fold is transected by a nearly vertical, left lateral (?) strike slip fault which is perhaps subsidiary to the Darwin Tear fault. The amount of displacement across this structure is uncertain but is estimated from the offset anticlinal axis at 700' (?). Exposed along the eastern limb and in the nose of the anticline is a 20-50 foot section of interbedded slabby dark gray, fine grained limestone, compact red and yellow shale, and gray shaly limestone in which is developed a series of drag folds. This limestone-shale unit is designated C1s in Figure 20. Figure 21 shows how typical folds

in unit Cls are developed and is a photograph of the outcrop from which specimens for this study were taken. The attitudes of the minor folds are somewhat variable due to the fact that the drag folds themselves have been folded, but generally are nearly the same as that of the anticline with which they are associated, with plunge 10° N. and strike N. 30° W. At this particular outcrop, designated on the geologic map as "folds," strata on the limb of the larger anticline dip 60° west and strike N. 30° E. Stratigraphically above Cls are massively bedded, nodular, shaly limestones of yellowish color. Below it the rocks consist of massively to slabby bedded finely crystalline, dark gray limestone. The intensity of drag folding varies from place to place on the exposed limb of the major anticline. A few hundred feet south of the locality shown in Figure 21a, the axial planes of individual folds are considerably folded. At the nose of the anticline, the rocks are essentially unfolded. The degree of folding appears to be dependent upon the amount of shale in the unit. Where layers of limestone and shale are of approximately equal thickness, folding is most intense, but as the amount of shale decreases, the folding deformation also decreases.

Strata on the limb of the large anticline are cut and displaced in a left lateral sense 250 feet by an east-west trending, north-dipping fault whose trace passes a few feet south of the outcrop pictured in Figure 21a.

Figure 21. Drag folds in limestone-shale unit (Cls) in upper Darwin wash. (a) General view (facing north) of the folds as they appear at the position marked "FOLDS" on the geologic map, Figure 20. The folds strike $N.20^{\circ} W.$, plunge $10^{\circ} N.$ Enclosing strata strike $N.20^{\circ} W.$, dip $60^{\circ} E.$ Three white calcite filled veins (approximate width 2 inches) cut across the folded strata and enclosing rocks. The large veins strike parallel to the bedding, dip $35^{\circ} W.$ (b) Closeup view of the folds studied. Plastic rule (six inch) gives scale. Note change in attitude of axial plane from top to bottom of photograph. Fabrics obtained from layer marked "X" in the photograph. Slabby beds are limestone, recessed strata shale. Area outlined in the figure is sketched in Figure 22.



(a)



(b)

Figure 21

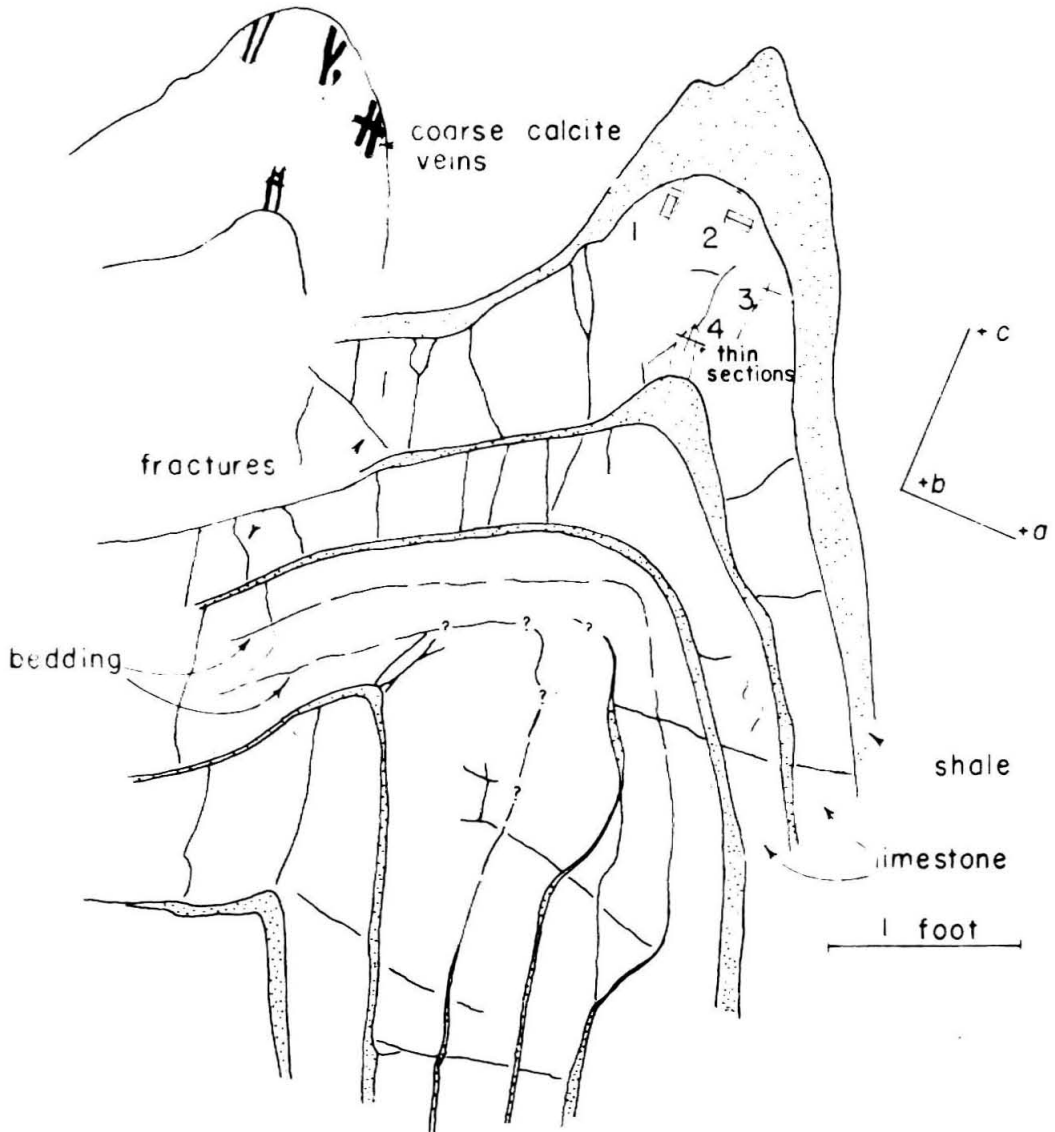


Figure 22. Sketch of the fold. Main drawing shows locations of specimens (outlined by dashed lines) and positions of thin sections cut in each position in the fold. The individual locations are designated 1, 2, 3, 4. Offset drawing shows traces of coarsely crystalline calcite veinlets. The coordinate system to the right designates positive directions of the axes.

Description of the fold studied

Figure 21b is a close-up of the fold studied and Figure 22 is a sketch of the area outlined by a dashed line in Figure 21b. The folded rocks pictured in the sketch consist of six inch to one foot beds of dark gray, finely crystalline limestone, with irregular tabular portions of very coarsely crystalline dark gray calcite. Separating the limestone beds are thin red and yellow compact shale units of variable thickness. There has been marked thickening of both limestone and shale units in the axial region of the fold. Individual limestone beds within the fold are broken by a number of fractures which run approximately normal to the boundaries of the individual layers. Displacements were not noted along these breaks. Axial plane cleavage is not present in the particular structure studied, although a series of thin (~ 1 mm) veinlets filled with white calcite do cut individual layers within the fold parallel to the axial plane (these features are now shown in fig. 22). At other places in the outcrop cleavage is well developed, especially where the folds are extremely tight. This cleavage is manifested on weathered surfaces by sharp V-shaped grooves which trend irregularly parallel to the axial planes of the folds. On fresh surfaces there is no visible trace of the weathered surface pattern except where individual flutes are developed along thin calcite filled veinlets.

The uppermost folded layer sketched in Figure 22, the particular stratum studied here in detail, is slightly greater than one foot (30.5 cm) thick in the axial region. The limbs are from six inches (15.2 cm) to ten inches (25.4 cm) thick. The radius of curvature of the upper surface is about 5.5 inches (14 cm), and the lower boundary has a radius of curvature of about three inches (7.6 cm). Their respective centers of curvature are about nine inches (23 cm) apart.

From the geometry of the upper limestone layer, this layer has not been deformed simply by bending alone, because such deformation cannot account for the observed variations in thickness in the limbs and crest. The numerous radial fractures which cut across this bed, as well as other beds below it in the fold, suggest that there has been some flexural folding. However it is perhaps very doubtful that such fractures could remain preserved from a time when the rock was obviously in a very plastic condition. The dissimilar shapes of the various layers comprising the fold and the fact that boundaries between the upper limestone layer and shale strata surrounding it do not show significant irregularity or offset parallel to the axial plane of the fold suggest that the structure is not a 'shear' fold.

In order to account for the present geometry of the fold in a simple manner, it seems necessary that in addition to bending, the upper strata have undergone shortening perpendicular to the axial plane as well, so as to thicken the

bed. Thus in attempting to unravel the strains imposed upon the rock it is necessary to reconstruct a possible strain history involving each of these deformations. In order to accomplish this it is assumed that the original thickness of the layer was about eight inches, the present average thickness of the limbs. Undoubtedly the present limb thicknesses or their average cannot represent the original thickness very accurately, because both have probably been deformed as well. However, there is no basis for assuming another figure. Now assuming that uniform compression was superposed on the bent layer of this thickness a widening of the bed in the axial region to the present dimension of one foot corresponds to a shortening perpendicular to the axial plane of about 30%. To obtain an idea of the bending strains, the 30% shortening along the axis of the fold must be removed. It is further assumed that this was uniformly imposed over the cross section of the layer in the bc-plane of the fold (definitions of coordinates as on p. 75). Removing this strain and assuming the resultant fold to be circular in shape, the dimensions obtained are approximately:

Inner radius of curvature	5 inches	(13 cm)
Outer radius of curvature	13 inches	(33 cm)

Using Equations 2a and 2b, the resultant extension and compression at the outer and inner boundaries respectively are both about 45%. Superposing the shortening and bending

strains indicates that the outer layers of the fold have undergone a net extension of 15% while material near the opposite boundary has been shortened 75%. This picture of the strain is undoubtedly oversimplified as is discussed below in greater detail.

Macroscopically, rocks from this fold are very non-homogeneous. In the axial region of the flexure, the material consists of approximately 70% finely crystalline dense dark gray limestone, with patchy limonite stained areas, and roughly 30% very coarsely crystalline dark gray calcite, with individual crystals as large as one cm in diameter. The coarse material is distributed in three approximately mutually perpendicular sets of irregularly tabular-shaped masses one millimeter to six or seven millimeters in thickness, which are oriented throughout the entire axial portion of the bend nearly parallel to the fold coordinate planes. In general, veins of this material parallel to the coordinate plane are thicker and more numerous than those of the other two sets. These coarsely crystalline masses are confined to the limestone strata in the fold, and do not extend into shaly layers separating individual beds. No unequivocal evidence has been found which established precisely the age of development of this coarsely crystalline material with respect to the folding of the rocks. In nearby layers of this fold thin veinlets of the dark calcite follow around the bend of the fold parallel to bedding within the rock. In other folds

found elsewhere along Darwin wash in the unit C1s (fig. 20) megascopically similar dark colored coarsely crystalline calcite masses have been contorted along with enclosing bedding in the limestone, but post-deformational preferential recrystallization or replacement along bedding surfaces cannot be ruled out in either of these cases. In fact, fractures parallel to the minor fault adjacent to the fold location, and which must post-date the folding, are also filled with dark calcite. Microscopic evidence presented below suggests however that this vein filling material has participated to a considerable extent in the deformation.

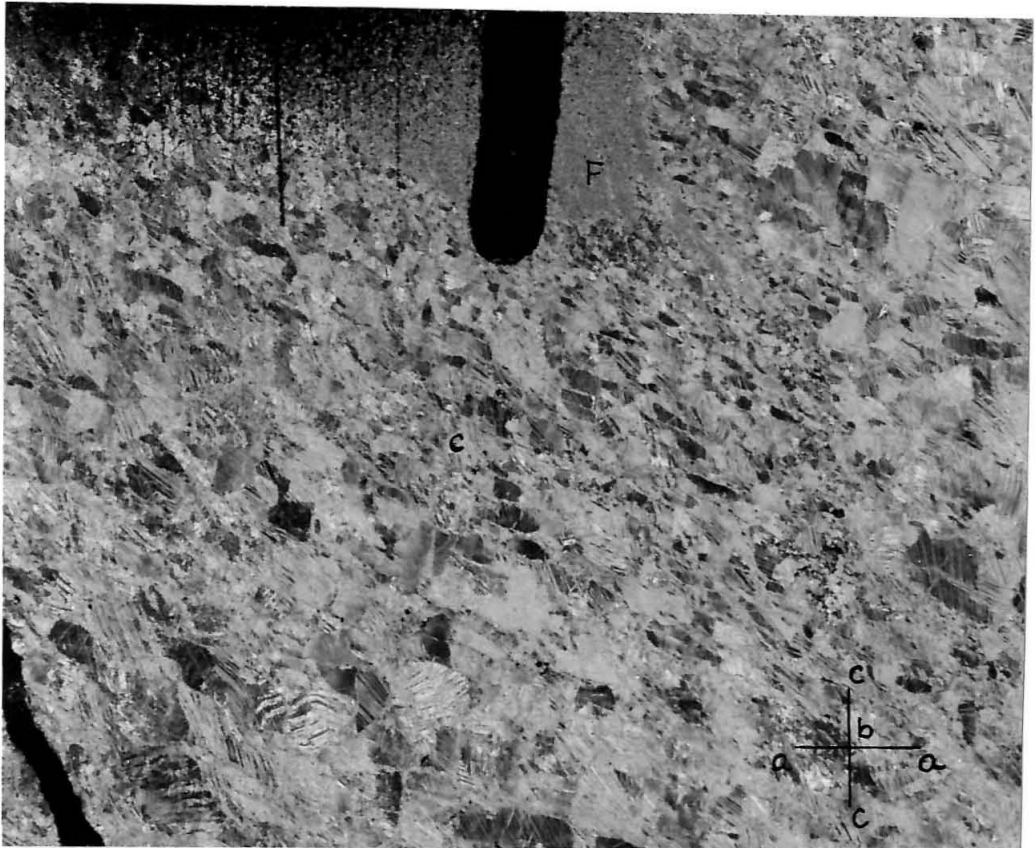
Two other minor, nearly perpendicular sets of veinlets mentioned earlier cut the rocks of this small fold. The veinlets are about one millimeter in average width, and consist of coarsely crystalline white calcite. The veinlets lie in the ac- and ab-planes of the fold. They offset (by dilatation) veins of the dark gray calcite where the two intersect, and often persist through shale units separating individual limestone beds in the fold.

Petrographic character of the rock

The general petrographic character of the rock comprising the small fold is shown in the photomicrographs of Figure 23. The rock is composed of 95% calcite, up to 5% 0.05 - 0.1 mm subangular, strained quartz grains, and a small amount of red hematite in streaks and as grains about

Figure 23. Photomicrographs. Coarse and finely crystalline material from the fold. (a) Material at location 2 in thin section cut in the ac-plane of the fold, nearly parallel to the plane of a vein of coarse material. Crystals in plane of the photograph are elongate in a skew direction with respect to the coordinate axes. In portions of the field there is a suggestion of cataclastic texture ("C"). Vertical scratches near the top of the photograph are due to grinding of the thin section. The vertical U-shaped groove is an orientation reference notch and the black streak in one corner a place of separation in the rock slice. (b) Material from location 4. Note veined nature of the rock and elongation of crystals perpendicular to the trace of the veinlets in thin section. Dark streaks near the top of the picture are quartz-rich layers in the rock. All coarse crystals in these and other locations in the fold contain at least one and often two or three sets of lamellae, and many of the lamellae are bent and twisted. In general there are no noticeable fractures or other discontinuities (other than grain size) between patches of coarse and fine calcite (marked "F"). Crossed nicols (x 10).

(a)



(b)



Figure 23

0.05 mm in size. Two distinct types of calcite are noted in thin sections: (1) large 0.5-10 mm elongate, highly twinned clear calcite crystals compose about 25% of the volume of the rock. Most large crystals contain two sets of twin lamellae and some contain three. Specifically, 18% of the grains measured contain three sets, 60% two, 20% one, and 2% no lamellae. About 25% of the grains containing two sets of lamellae have one set microtwinned, and 40% of those with three sets have one or two sets microtwinned. Twinning lamellae are often bent and twisted and many given anomalous values for the angle $c \wedge e$. Bending of these lamellae is discussed in Appendix II, where the observed warping is used as a clue to establish glide mechanisms within individual crystals using the method of Turner et al. (1954). Curiously, the smaller twinned set in many grains is consistently offset by twinning in the major sets, and is therefore considered to be earlier in origin. Grain boundaries are both straight and sutured, and there is often a breccia-like zone of finely crystalline material between adjacent grains that are highly twinned. (2) The second type of material distinguished in thin section consists of finely crystalline calcite (average crystal size about 0.01 mm) which comprises the bulk of the rock. Individual crystals are large enough to be easily resolvable under high power. These crystals are generally equant, but are locally elongate except as noted in the fabric diagram in a similar manner to ad-

jacent coarsely crystalline material. Twinning is not present in the fine grained material of crystal size less than about 0.1 mm. Both of the above types of calcite may be noted in Figure 23. A patch of fine calcite in the top central part of the figure is labeled "F". Only the coarsely crystalline material was studied in this investigation, as the finer calcite was too small to permit measurement of c-axis orientations.

Results of the fabric studies

Fabrics have been measured in a number of specimens from the upper layer sketched in the figure, and individual locations of specimens are designated 1, 2, 3, and 4. Orientation data from the fold are given in Figures 24, 25, 27, and 28.

(1) c-axis fabrics: The distribution of host c-axes at locations 1-4 are given in Figure 24. In each diagram the fold coordinates are shown as well as the trace of bedding in the specimen (BB), shown as a dashed line when projected on the lower hemisphere of the net. EE marks the direction of elongation of grains in the plane of the thin section for sections where a consistent elongation can be noted, and VW are attitudes of veined structures on the rock. At locations 1 and 3, the distributions are characterized by broad concentrations of c-axes around the a-axis of the fold. In location 2, c-axes are distributed in a

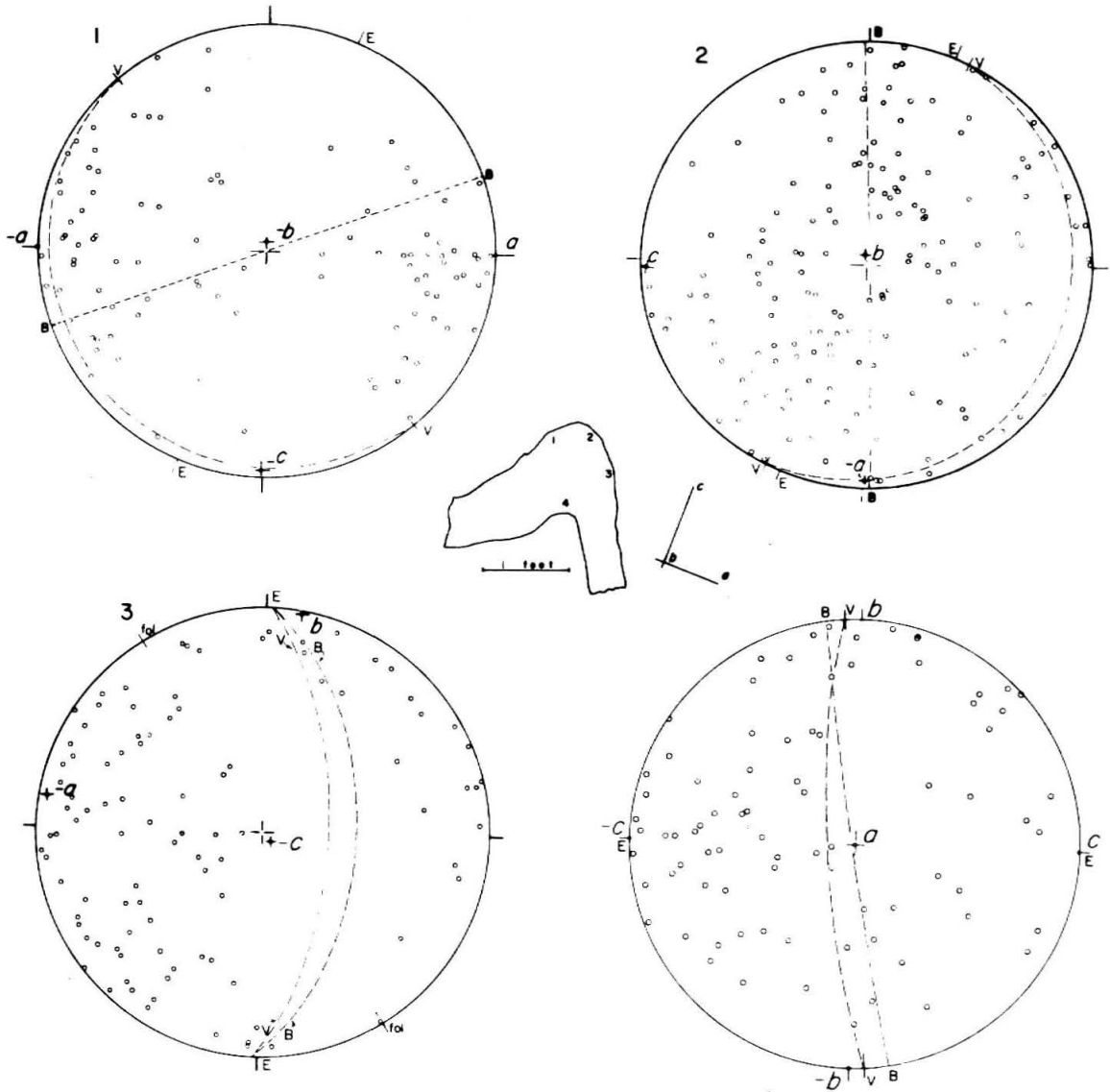


Figure 24. c -axes from the Darwin fold. Orientation data from each location indicated by numbers. The dashed great circles marked BB, and VV denote planes of bedding and veined structure respectively projected onto the horizontal plane. EE is the direction of elongation of grains in the plane of the thin section. At location 3, "fol" marks direction of prominent foliation in finely crystalline material. In all diagrams only the minus directions of coordinate axes are so designated, and the point of emergence of a particular axis on the projection is designated (\ominus). The cross in the center of each diagram is the pole to the thin-section plane and straight reference marks lying 90° apart in the equatorial plane denote directions parallel to the edges of the thin section. All diagrams equal area, lower hemisphere. (Fabric at location 4 by Kamb).

broad girdle in the ab-plane, and tend to cluster around the b-axis (fold axis). In location 4, the c-axis of the fold is the center of a diffuse maximum of optic axes.

(2) c'-axis fabrics: Figure 25 shows positions of optic axes for the most prominently twinned set of e-lamellae in each grain for each position. Closed triangles designate measured points, and open ones positions constructed from host c-axis and e-lamellae data in each grain. In many cases a twin set was observed to be visibly twinned, but the c'-axis position could be measured because of the thinness of the twins. Common to all of the diagrams is the tendency for these axes to form distinct maxima, which are broader and less well defined in some of the figures. As presented, these differ in orientation. In order to compare orientations from the different positions in the fold, the approximate positions of maxima are plotted on a single diagram which is given in Figure 26. This projection is oriented so that the (+) b-axis of the fold is the pole to the equatorial plane, (+) a is to the right, and (+) c at the top. Orientation of these axes with respect to the fold itself is shown in the small figure at the center of the diagram. The numbered crosses which are enclosed by dashed small circles on the net are positions of the approximate geometric centers of c'-axis concentrations for the diagrams in Figure 25, with the small circles representing the approximate limits of each maxima. As far as individual positions in the fold

Figure 25. c' -axis data from the Darwin fold. Orientation data from each location indicated by numbers. At location 4 data gathered from sections in the ab-plane (location 4-A) and ac-plane (location 4-B) are presented separately to illustrate difference in fabrics obtained from adjacent sections (see text, p. 154). In each diagram solid triangles represent positions of measured c' -axes, and open triangles constructed c' -axis positions. The dashed great circles marked BB and VV denote planes of bedding and veined structure respectively projected onto the horizontal plane. EE is the direction of elongation of grains in the plane of the thin section. At location 3, "fol" marks direction of prominent foliation in finely crystalline material. Equal area projections, lower hemisphere. (Fabrics 4-A and 4-B by Kamb and Conel.)

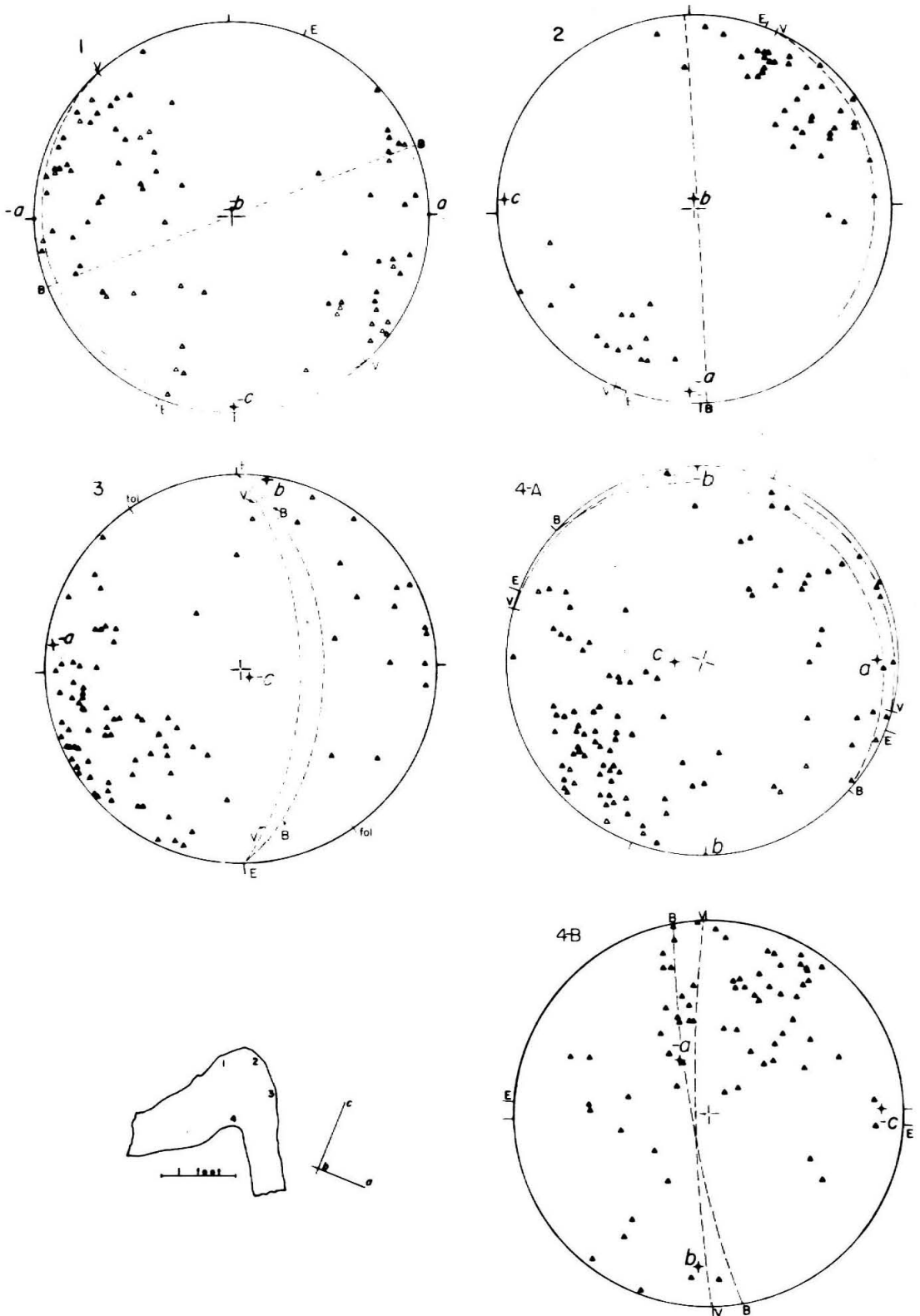


Figure 25

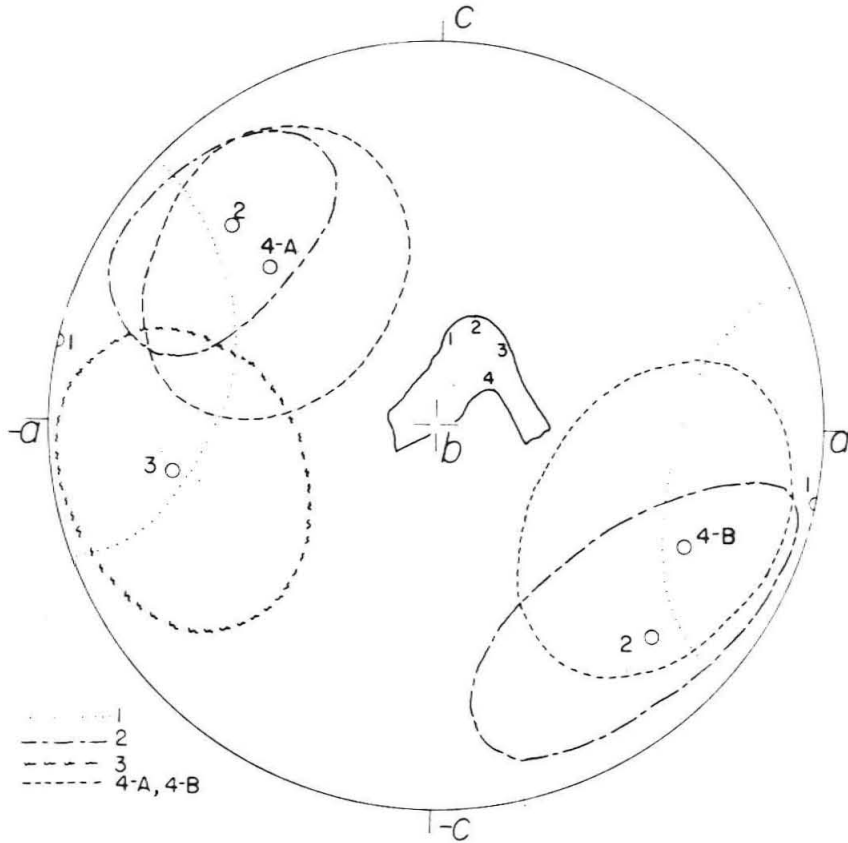


Figure 26. c' -axis data from locations 1-4 compared in one diagram. The approximate geometric center of each clustering of axes given in Figure 25 are located at the small circles and are identified by the appropriate number. The approximate extent of each maximum is indicated by dashed lines. The small drawing at the center of the diagram gives the position of the fold with respect to the axes in the drawing. Note how maxima from the two positions 4-A and 4-B do not coincide, and also how there is a general tendency for all maxima to fall about the a-axis of the fold or to lie in portions of the diagram defined by the -a,b,c, and a,b,-c axes. Equal area projection, lower hemisphere.

are concerned, there is considerable variation in the location of these maxima with respect to the fold coordinate axes.

(3) \underline{e} $\{01\bar{1}2\}$ orientation data: \underline{e} -lamellae orientation diagrams for locations 1-4 are presented in Figure 27. In each diagram, solid circles represent the positions of poles to the most prominently twinned \underline{e} -lamellae set in each crystal (\underline{e}_1 -lamellae), and open circles the less prominently twinned sets (\underline{e}_2 or \underline{e}_3 -lamellae) in each location with the exception of 4, only one thin section was used in obtaining orientation data from the aggregates. This restriction weakens the results of the \underline{e} -lamellae studies statistically, and is responsible for the "blind-spots" in the lamella pole diagrams. The initial studies on this fold consisted of measuring fabrics from a single thin section at each location to obtain some idea of the possible consistency of the observed fabrics in relation to the supposed deformation in the structure. When the result emerged, as will be discussed more fully below, that these fabrics were not simply related to the geometry of the structure, further studies to simply improve statistics seemed pointless. Furthermore it is likely that merely examining more thin sections would not measurably improve the statistical picture at each location. As has already been described, the material in all locations studied is very nonhomogeneous well below the scale of a single thin section, and the associated deformation is probably nonhomogeneous on as fine a scale. Hence sampling other sections

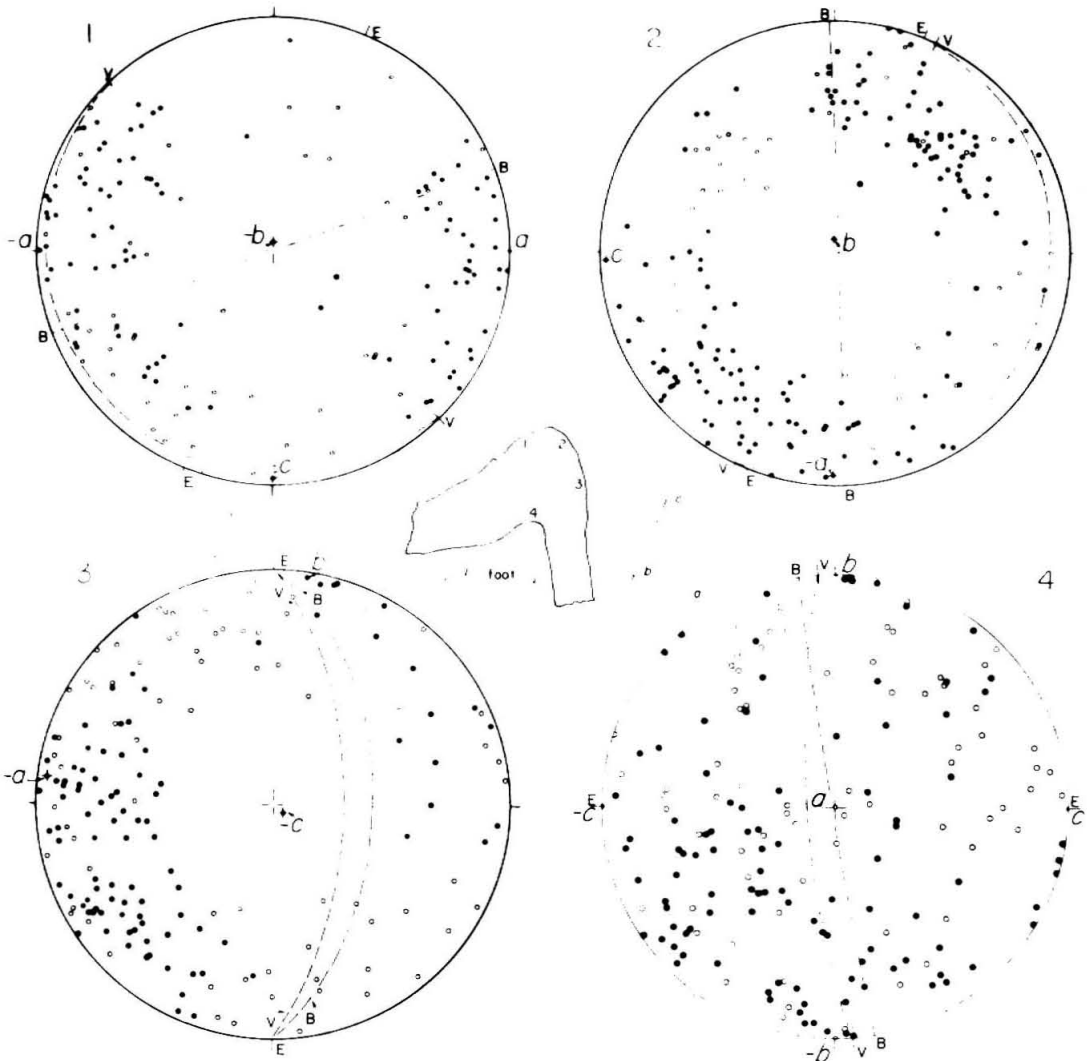


Figure 27. $e\{01\bar{1}2\}$ lamellae data. Solid circles mark positions of poles to most prominently twinned set of lamellae in each grain (e_1), open circles other sets (e_2 and e_3). BB and VV are planes of bedding and veins projected onto the horizontal plane. EE is the direction of elongation of grains and at location 3 "fol" marks the trace of foliation in the finely crystalline material (fabric at location 4 by Kamb).

would only effectively amount to measuring fabrics from other points in the fold, not improving statistics for any single location.

In these \underline{e} -lamellae fabrics, there is a general tendency for maxima in the diagrams to correspond to the \underline{c} -axis maxima from the same location. This is, no doubt a reflection of the control of the possible lamellae orientations by the preferred orientation of \underline{c} -axes. A more exact comparison may be made between the \underline{e} -lamellae diagrams and those for \underline{c}' -axes. In each case the maxima of \underline{e}_1 -lamellae correspond to those in the \underline{c}' -axis diagrams.

(4) Dynamic analysis of \underline{e} -lamellae: Data from a dynamic analysis of the twinning lamellae from locations 1-4 are presented in Figure 28. The analysis of \underline{e}_1 -lamellae is given in these figures, in order to simplify interpretation of the diagrams. Only at location (2) "strong" patterns of C and T axes observed, and this mostly reflects the preferred orientation of host \underline{c} -axes in this particular place.

The primary result of the analysis is that, though there is considerable dispersion in most of the data, a nearly common direction of compression is indicated from the several locations, and this direction coincides roughly with positions of concentration of \underline{c}' -axes. Like these \underline{c}' -axis maxima, the C-axis maxima are not generally symmetrically disposed with respect to the fold coordinate axes.

Figure 28. Dynamic analysis of the most prominently twinned set of \underline{e} -lamellae in each crystal (\underline{e}_1). C = axes of compression, T = axes of tension. Diagrams from each location as numbered. Data from location 4 are presented in two diagrams, in the ab- and ac-planes of the fold. In each diagram BB marks the plane of bedding, VV plane of vein structure, EE the direction of elongation of grains. "fol" at location 3 is the trace of foliation in finely crystalline material. All diagrams equal area projections, lower hemisphere.

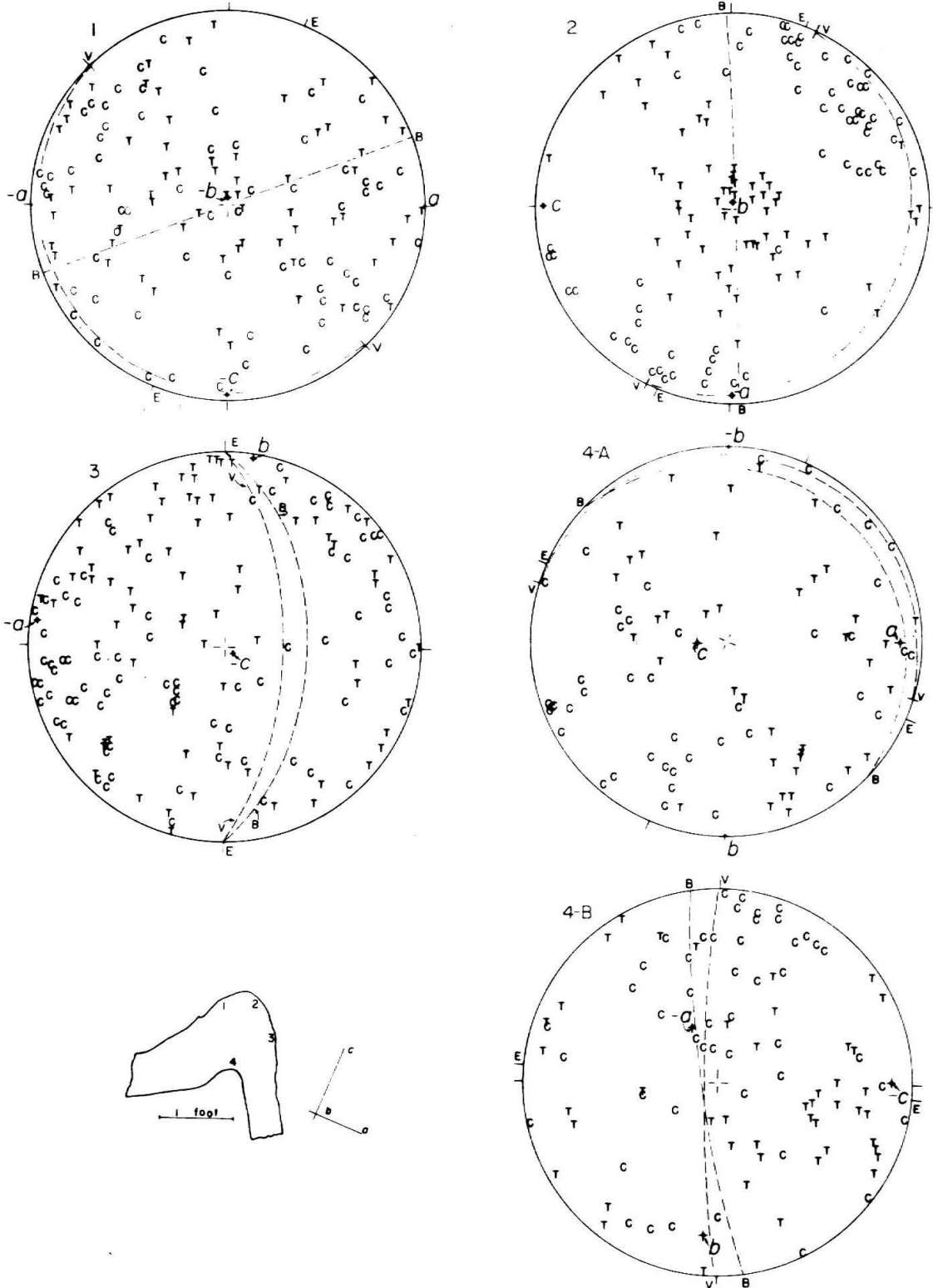


Figure 28.

(5) Calculation of Strain due to Mechanical Twinning: The great textural non-homogeneity of the rock comprising this fold, and the associated statistical uncertainties in orientation data for twinning lamellae preclude the possibility of obtaining any very accurate picture of the strains throughout the fold. However to obtain some idea of the orientation of the principal axes of strain and magnitude of strains due to twinning for some places in the fold, the available data have been used to compute strains at locations (3) and (4) by the exact method (p. 55), and at locations (1) and (2) by an approximate method.

Values of the components of the strain tensor resulting from the exact calculation for position 3 are:

$$\begin{bmatrix} -0.7 & 0.9 & 0.4 \\ 0.9 & 1.4 & 0.5 \\ 0.4 & 0.5 & -0.7 \end{bmatrix} \times 10^{-2} .$$

This matrix, as well as that for position 4, is referred to a coordinate system which is fixed with respect to the thin section from which the data for the calculations were taken. The axes are approximately: \underline{x} = a-axis of the fold, \underline{y} = b-axis, and \underline{z} = c-axis. Referred to principal axes the matrix becomes

$$\begin{bmatrix} -1.8 & 0 & 0 \\ 0 & -1.1 & 0 \\ 0 & 0 & -0.7 \end{bmatrix} \times 10^{-2},$$

where the positions of the principal axes of strain are given in Figure 29.

For position 4 components of the strain tensor are:

$$\begin{bmatrix} -2.2 & -2.7 & 3.2 \\ -2.7 & -1.1 & -0.6 \\ 3.2 & -0.6 & 3.3 \end{bmatrix} \times 10^{-2},$$

and referred to principal axes,

$$\begin{bmatrix} -5.0 & 0 & 0 \\ 0 & -0.2 & 0 \\ 0 & 0 & 5.2 \end{bmatrix} \times 10^{-2}$$

where the directions of the principal axes are shown in Figure 30.

The strains at locations 1 and 2 have been calculated by the approximation method suggested on page 112. This requires using the results of the dynamic analysis data (or alternatively and more approximately the c' -axis fabric data). It has been noted that relatively distinct groupings of the C and T axes data are evident at location 2, but are dispersed and uncertain at 1. For location 2, assuming as before that the mean direction of each grouping of axes represents the position of the corresponding principal axis of

Figure 29. Orientation of the principal axes of twinning strain and values of the principal strains at location 3. Negative values indicate compression, positive, extension. Calculations carried out using procedures given on p. 56. Equal area projection (dn) indicates + b-direction is downward.

Figure 30. Orientation of the principal axes of twinning strain and values of the principal strains at location 4. Negative values indicate compression, positive, extension. Calculations carried out using procedure given on p. 56. Equal area projection (dn) indicates + b-direction is downward.

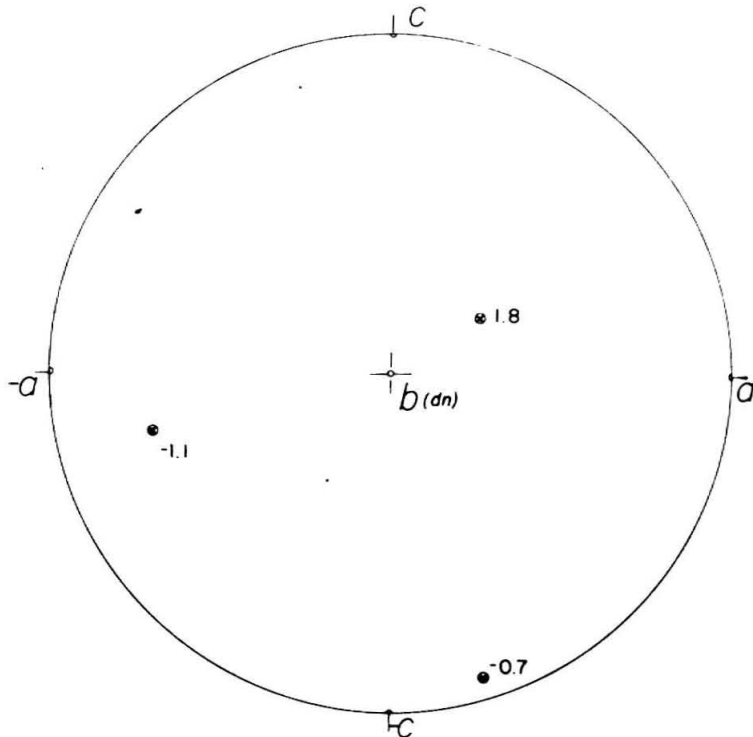


Figure 29

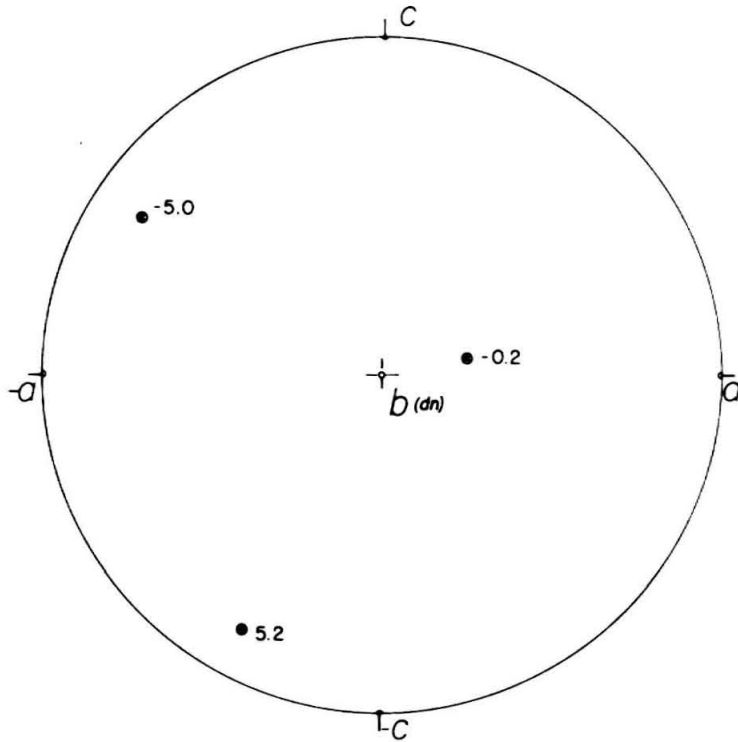


Figure 30

strain, the amounts of strain along these axes can be obtained from the average degree of twinning. The average amount of twinning in 100 grains from location 2 is 13%. This degree of twinning corresponds to principal strains of 0.045 by Equations 14. The principal strains written in matrix form are:

$$\begin{bmatrix} -4.5 & 0 & 0 \\ 0 & 4.5 & 0 \\ 0 & 0 & 0 \end{bmatrix} \times 10^{-2},$$

where this matrix is referred to Cartesian axes oriented so that the x-axis makes an angle of approximately 50° with the a-axis, and the y-axis is along the b-axis of the fold. When referred to the fold coordinate axes the above strains become

$$\begin{bmatrix} -1.9 & 0 & 2.2 \\ 0 & 4.5 & 0 \\ 2.2 & 0 & -2.6 \end{bmatrix} \times 10^{-2},$$

where the axes are as previously chosen (p. 75). It may be seen that according to this approximate calculation the fold has been shortened (though relatively slightly) parallel to the a-axis at location 2.

At location 1 the dynamic analysis data are very unclear, but nevertheless the same approximate calculation has been made here, assuming that the principal axis of

shortening now coincides with the geometric center of the \underline{c}' -axis maximum. (In any given crystal the position of \underline{c}' is 20° from the principal axis of shortening in twinning.) The dynamic analysis results show a clustering of T-axes about the b-axis of the fold (fig. 28). The principal axes of strain are thus taken to be: (1) axis of extension along the b-axis of the fold, (2) axis of compression approximately 25° from the +a-axis toward -c-axis in the ac-plane of the fold (this is the position of the geometric center of the \underline{c}' -axis fabric at location 1). The average amount of twinning in 100 grains from location 1 is 15% which, using equations 14, indicates principal strains of ± 0.05 . In matrix form for these strains are

$$\begin{bmatrix} -5 & 0 & 0 \\ 0 & 5 & 0 \\ 0 & 0 & 0 \end{bmatrix} \times 10^{-2},$$

and referred to the fold coordinate axes,

$$\begin{bmatrix} -4 & 0 & 2 \\ 0 & 5 & 0 \\ 2 & 0 & -1 \end{bmatrix} \times 10^{-2}.$$

The data presented above from all positions in the fold, in spite of their approximate nature, show that the strain recorded as twinning throughout the fold is not compatible with a simple deformation such as bending of

the layer nor simple uniform compression parallel to the a-axis of the fold. In fact, in a component for component examination of the strains from the various positions in the layer the deformation is very complicated. However two consistent features can be noted about the strains everywhere, (a) compression parallel to the a-axis of the fold, i.e. the strain $E_{\underline{xx}}$ is negative, (b) the strain $E_{\underline{xz}}$ is positive, which geometrically indicates that sides of a unit cube of material in the unstrained state originally parallel to the \underline{x} and \underline{z} -axes now make an acute angle with one another, which is given by $\pi/2 - 2E_{\underline{xz}}$ (Nye, 1957, p. 97). Some other features of the strains throughout the layer are: (c) at no position is the fold deforming in plane strain ($E_{\underline{yy}} = 0$) parallel to the b-axis, (d) the principal axes of strain at locations 2 and 4 are not parallel to one another as might be expected on a hypothesis of simple bending or shortening in the layer, (e) at positions 1, 2, and 3, the rock has been extended parallel to the fold axis and compressed along the c-axis, while the reverse has occurred at position 4.

It is almost impossible to account for these observed irregular variations in strain. The nonhomogeneity of the deformation may, in part, reflect the nonuniform grain size and the distribution of coarse and fine material in the rock. However there is no indication that the coarsely crystalline material has been more highly deformed than the fine even though one is tempted to assume this because of the high

degree of twinning in the large crystals. Fractures, shear zones, or other discontinuities between areas of coarse and fine calcite, such as might be expected if one type of material had preferentially deformed have not been noted (note for example contacts between coarse and fine material in fig. 23).

The strain recorded as twinning throughout the fold is also considerably less than that calculated approximately from fold geometry. General reasons why such discrepancies can always arise in calculating the strains due to twinning in aggregates that have undergone large deformation, have already been discussed with particular reference to the present fold (p.67). Aside from the neglect of translation gliding strain, which could increase the computed visible strains by a factor of two, deformation could have been accomodated in the aggregate through grain boundary slip and brecciation within the coarser material. Cataclastic textures can be noted in the Darwin rocks (see fig. 23), and such texture perhaps indicate regions of very great (though local) strain. It is not possible to estimate this strain with any certainty, so that its relative magnitude must remain unknown. The simplest (but probably not the complete) explanation of the overall discrepancy between visible and geometrically indicated strain in the fold is that the coarsely crystalline material originated later than a significant part of the deformation indicated by the present shape of the beds.

Interpretation of the Darwin fabric results and comparisons with experimental studies

A common feature of nearly all fabric and dynamic analysis data presented from the Darwin specimens is the non-symmetrical distribution of orientation density maxima with respect to the coordinate axes of the fold. This indicates that these fabrics in general must reflect a complicated non-homogeneous deformation, and do not represent fabrics which are expected theoretically (fig. 3) on the hypothesis of simple deformation in predominantly bending in the body. Some of the results may perhaps be partially explained in the following manner. As previously indicated, the strain calculations show a small shortening everywhere in the body perpendicular to the axial plane as well as a small positive shear in the ac-plane of the fold. From the geometry of the fold a macroscopic shortening perpendicular to the axial plane is clearly indicated although to a much greater extent than is suggested by the calculated strains. A small positive shear in the ac-plane of the fold is also indicated and this type of shear is compatible with that expected in the whole series of drag folds as a result of deformation in the larger structure (anticline) with which they are associated. Referring to the c -axis data, broad groupings of data points about the a -axis in locations 1 and 3 are approximately normal to the direction of grain elongation in the plane of the thin sections and in the same direction as the indicated direction of shortening in

the fold. The c-axis fabric from location 2 does not agree with this picture, and measurements at location 4 are also not in agreement with simple shortening parallel to the a-axis. As for the c'-axis measurements (fig. 26), maxima in these diagrams tend to be confined to the portion of the projection defined by the (+) a and (-) c-axes (or -a and +c). The collective maxima diagram shows a very crude monoclinic symmetry.

Experimental deformation of Yule marble in compression produces maxima of c-axes and e-lamellae which coincide with the axis of compression in the deformed specimens (Griggs et al., 1951; fig. 7a; Turner et al., 1956, fig. 9c). c-axis from locations 1 and 3 may result from such compression. In experiments involving shear within the deformed specimen (see p. 114, this thesis), orientation density maxima show skew orientations with respect to the plane of shear. The c'-axis fabrics from Darwin, from their crude symmetry, might arise from shear of the type indicated by the calculated strains (orientation of the principal strain axes on c' data are not completely independent) and necessitated by the observed geometry of the drag folds as they are related to the larger anticline in Darwin wash.

In order to develop anything resembling a stable, well defined deformation fabric, wherein rotations of the crystal axes of individual grains relative to the principal axes of strain in the specimen cease with further deformation,

translation gliding must also occur (Turner et al., 1956). This kind of deformation mechanism can be observed in non-homogeneously deformed single crystals from these rocks (appendix II), and does, in some cases, account for development of a range of c - and c' -axis orientations within a single crystal of as much as 40° . But significant translation gliding leading to development of an unquestioned stable fabric, as in the experimental work, has not been found.

Though the purpose of this study has been to investigate the mechanical behavior of material texturally similar to Yule marble, a comment on the nature of the finely crystalline portions of the rock is appropriate. Lack of microscopic "evidence" for deformation of this material is an important point. This observation may be accounted for in at least three ways: (1) the finely crystalline material has not deformed. This is discounted by the fact already mentioned that discontinuities between coarse and fine material are not apparent. (2) The finely crystalline material has deformed by the same processes observed in larger crystals, but has undergone an annealing recrystallization which has removed all evidence of deformation. (3) Due to the large area of grain interfaces per unit volume in the fine material, the 'normal' deformation processes are inhibited, and the aggregate has essentially deformed through grain boundary slip and/or recrystallization. On the basis of available evidence, a choice between (2) and (3) cannot be made, and

a future investigation bearing on this problem would be of considerable interest.

Summary and Conclusions Drawn
from the Fabric Studies

The underlying purpose of the fabric investigations has been to quantitatively compare crystal fabrics of naturally deformed limestones with deformation fabrics produced experimentally in marble. To achieve this, simple examples of naturally deformed rocks, flexurally folded limestones, have been selected. Folds in limestone are relatively numerous, and more importantly, flexurally folded structures as such are ideally examples of nonhomogeneous deformation, the nature of which is to some extent determinable from geometrical considerations. With a knowledge of the strains, deformation fabrics can in principle be approximately predicted for any combination of glide mechanisms and the results compared with the naturally observed fabrics developed under these strains. In detail, the problem of theoretically predicting fabric changes in a homogeneous aggregate associated with even the simple deformation in an ideal flexure fold is difficult and can be computed only with a theory like that developed by Bishop (1954), which allows sufficiently arbitrary deformations to be specified in individual crystals so that the whole aggregate may undergo the prescribed strains and still maintain continuity after deformation. At present it is

in principle possible but not feasible to derive exactly the fabrics to be expected in folds. However, an implication of the Bishop theory is used to derive approximate stable fabrics to be expected with bending in a fold deforming approximately in plane strain, in a material which has an initial c-axis fabric identical with that of undeformed Yule marble. The utility of the result is thus definitely impaired, but does give some idea of the deformation fabrics which ideally would arise in folds under the special assumptions employed.

.To insure maximum success in either substantiating or disproving the applicability of the experimentally deduced behavior of marble aggregates to naturally deformed rocks, it is evidently advantageous to apply these results under the most favorable natural conditions where they could reasonably be expected to apply. This consideration together with the inherent time consuming nature of the fabric studies is the reason for making very careful choices of the actual materials investigated here. Neither of the folds studied meet in detail all of the various fundamental requirements presented in the Introduction, but from the standpoint of the strains indicated in these bodies, it would not be unreasonable to expect development of good deformation fabrics within them. The observed host and twin c-axis fabrics do not clearly reflect the observed macroscopic deformation in either structure. In the fold from Maryland

this is because the microscopic deformation of the material is slight, indicating either a recrystallization of the material just prior to the last increment of deformation experienced by the rock or bending with crushing and fracturing rather than plastic deformation of the material. In the second example from Darwin wash, the deformation in the fold and accompanying fabrics are also not clearly related, and if a gross relation between them is postulated, the fabric changes c'-axis orientations actually observed reflect relatively small strains of a rather uncertain kind.

The conclusion derived from these considerations is that, within the limitations posed by the small number of folds investigated, significant development of deformation fabrics in response to known large strain have not been observed and the intended comparisons with experimental studies are therefore not possible. The above investigations obviously do not exhaust the possibilities for using folds in the manner indicated here, and further work will most probably disclose other and better examples to be used in this kind of analysis.

Positive results of the fabric studies are the following: (1) the dynamic analysis when applied in detail to one of the folds studied (Maryland) yields results compatible with the expected deformation, and although complications in the actual deformation within the layer are evident, is sensitive in depicting changes in deformation due to twinning. (2) An analysis of the twinning deformation in this aggregate

carried through using a plausible simple model of an elastically deformed fold with circular geometry, shows that twinning in the aggregate follows the law of maximum resolved shear stress in a semi-quantitative manner. The implication of this result is that, to a first approximation, if the macroscopic stress distribution in an aggregate were known, then at least the first order fabric changes due to mechanical twinning alone could be computed. The converse of this is not true, i.e., if the c' -axis fabric (or a result of the dynamic analysis) is known a unique system of stresses causing the deformation is indicated. (3) For the small increment of deformation recorded in the rock as twinning, the strains vary from grain to grain and (from the rough data available) depend upon orientation of the crystal axes relative to the principal axes of strain in the rock. The twinning deformation is thus nonhomogeneous throughout the aggregate. (4) Unequivocal situations where "stable," fabrics have been achieved in response to large strain through twinning and translation gliding have not been observed.

A subjective conclusion is to be derived from these studies, and concerns the use of folds in the way attempted here. As mentioned before there is no other commonly occurring geologically deformed carbonate body wherein large strain from one place to another can be expected to occur in a somewhat predictable manner. However it is in a sense contradictory to expect a simple deformation and recrystallization history

to be associated with a homogeneous material coarsely crystalline enough (grain size > 0.1 mm) so that conventional microscopic methods can be brought to bear. A possible exception would be folded crinoidal limestones. Use of folds here has thus required the rocks to have undergone an incipient recrystallization, or alternatively to contain secondarily deposited calcite.

Future Studies

The limitation posed by grain size has greatly limited the number of examples of deformed limestone bodies which could be used in this investigation. This constraint on the method could be greatly eased by the use of X-ray techniques for determining fabrics of fine grained carbonate rocks (Higgs, et al., 1960). However the problems attacked in such a study would perhaps be quite different from those associated with plastic deformation and development of fabrics in coarsely crystalline aggregates (p. 168). Investigations of the deformation of finely crystalline rocks would thus form an interesting extension of the present work.

NATURE AND PROPERTIES OF $\underline{e} \{01\bar{1}2\}$ LAMELLAE IN
CALCITE AND $\underline{f} \{02\bar{2}1\}$ LAMELLAE IN DOLOMITE

Introduction

Without question the commonest planar features noted in the deformed calcite rocks used in this investigation are lamellae parallel to $\underline{e} \{01\bar{1}2\}$. In thin section features of this type are readily divided into two general categories twinned and nontwinned lamellae (Borg and Turner, 1953, p. 1345). Twinned lamellae are those wide enough to allow crystal in twinned position to be unambiguously identified by its symmetrical extinction with the host crystal about the vertically oriented interface between the two. The so-called nontwinned lamellae in contrast are so thin that when tilted into the vertical position they appear as sharp dark lines with no twinned material discernible. Knopf (1949b, p. 562-563) describes nontwinned lamellae from experimentally deformed Yule marble as possessing "color-banding" which "disappears when the lamellae are turned into a position where their bounding surfaces are parallel to the axis of the microscope" thus giving the whole surface of the grain a uniform interference color in polarized light. She attributes the "color-banding" to a "wedge effect caused by the diagonal position of the boundary surfaces of discontinuity" (p. 563).

The investigations described below involve a detailed examination of thin twin lamellae in calcite and dolomite rocks

which exhibit all of the features ascribed to nontwinned lamellae by Knopf (1949b). In fact it is possible to recognize five distinctly separate types of interference colors and fringes which arise through the presence of the lamellae. These interference phenomena may be used to investigate the properties and internal nature of the structures.

In particular it is shown below that nontwinned lamellae (lamellae exhibiting the properties described by Knopf (1949b)) are in fact exceedingly thin, but otherwise normal twin lamellae. A method is presented, which utilizes a standard optical technique, for obtaining the thicknesses of these twins and this information allows an estimate to be made of the strain recorded in an aggregate through deformation of this type. Calculations are also presented which show that only an average thickness (and hence only an estimate of the average strain per lamellae) may be obtained for a series of thin lamellae which are superposed under the microscope. The most important result of these studies is a new method for measuring the orientation of twins that are shallowly inclined to the plane of the thin section. This method allows a complete picture of the orientation-distribution of e-lamellae in a calcite rock (or f-lamellae in dolomite) to be obtained from one thin section rather than from two or more perpendicular sections as heretofore required.

Previous Studies

Nontwinned lamellae have been widely noted in both naturally and experimentally deformed marbles. In fact they are the most abundant deformation feature to be seen in many naturally deformed rocks (McIntyre and Turner, 1953; Gilmour and Carman, 1954; Turner, 1949). Knopf (1949a, 1949b) and Turner (1949) were perhaps the first to point up the peculiar nature of these features, but they had of course been noted much earlier by various workers (Adams and Nicolson, 1901) being termed "twin bands" and "lamellae" (Knopf and Ingerson, 1938) or "translation lamellae" (Sander, 1950, p. 232-235). Adams and Nicolson (1901, p. 375) indeed do mention that "fibrous" structure developed during their experiments on the deformation of marble appeared to consist of extremely minute polysynthetic twinning, but they present no evidence for this conclusion. In the exhaustive study of experimentally deformed calcite single crystals carried out by Turner et al. (1956), the suggestion is forwarded that these lamellae may be "stacking faults due to ultramicroscopic twinning or some other disturbance of the lattice." Garber (1947) has made extensive and interesting studies on the mechanism of twinning in calcite which appear to deal with structures resembling nontwinned lamellae. Garber did not use a universal stage in his investigations and so the features he discusses cannot be compared directly with those studied here. He describes interference phenomena similar to one of the five types

described here. Garber has recognized four distinct stages in the process of twinning in calcite: (1) elastic deformation of the crystal, (2) formation of "elastic" twins, twins which disappear when the load is removed, (3) formation of stable twin layers, (4) thickening of the twin layers. Elastic and stable twins supposedly show reflection (?) interference colors and fringes, which Garber describes as resembling Newton's rings. He computes the thicknesses of the elastic twins by assuming that the lamella and surrounding crystal are isotropic and that the interference colors observed are due to reflection (his unnumbered equation p. 63)* within the lamella. A further assumption is made in taking $n_{1-2} \cos r$ equal to unity, where r is the angle of refraction inside the lamella. This will not in general be true except for special arrangement of the specimen in his optical system, but such arrangements are not described in the text. Nevertheless, the thicknesses obtained are about 1μ , which are similar to those observed in the present studies.

The approach developed below is adapted to universal stage methods and depends upon measuring between crossed nicols, the phase difference produced in waves transmitted by the anisotropic crystal slice, when the lamella is in special orientation.

*The equation is $k = 2n_{1-2} d/\lambda$, where k is the order of an interference fringe, n_{1-2} is the average index of the lamella, d is the lamella thickness, and λ is the wave length of light.

Nontwinned lamellae are especially significant in the present investigation. For example, in fabric studies of the fold from Maryland, the dynamic analysis, strain calculations, and investigations concerned with the law of maximum resolved shear stress are all based on deformation features of this type.

It is suggested that the term nontwinned lamella be replaced by microtwinned lamella, which suggests the truly twinned nature of the lamellae as established in the present study, and suggests also in a qualitative way the thicknesses of these structures (usually from one to four microns).

Description of Microtwinned Lamellae

Microtwinned lamellae in calcite and dolomite show a variety of interesting optical features which do not appear to have been described in detail previously. These features consist of interference colors and several types of interference fringes. The same optical phenomena can also be noted with twinning lamellae which contain 'visibly twinned' crystal. The interference colors and fringes have practical importance because they can be used to indicate the horizontal orientation of microtwinned or visibly twinned lamellae. A technique for accomplishing this is described below. These interference phenomena are also used to determine the internal nature of the lamellae.

Interference colors and fringes

In general microtwinning lamellae are easily visible in thin section because they show overall low order (first to occasionally fourth) interference colors when viewed between crossed nicols with the host crystal at extinction (fig. 31) and when they are not in the vertical or edge-on position. They appear as broad, mostly uniform colored bands traversing a grain with a color spectrum at each tapered edge (fig. 31). Depending on their inclination to the plane of the thin section, the boundaries of the bands may be sharp, or they may be highly serrated owing to irregularities in the ground surface of the thin section. When tilted into the vertical position, the interference colors progressively disappear, and the lamellae assume their well known, sharp, dark, linear appearance, with the properties described previously. In plane polarized light, without crossed nicols and with reduced illumination, these lamellae display uniform colors of different character from those observed between crossed nicols. These colors are more faded in appearance and seem to be generally of a higher order than the colors seen under crossed nicols. The colors visible in plane polarized light are probably due to internal reflection within the lamellae. The origin of these particular colors has not been studied in the present work.

Distinct from the overall, more or less uniform interference colors of the lamellae are several types of interference

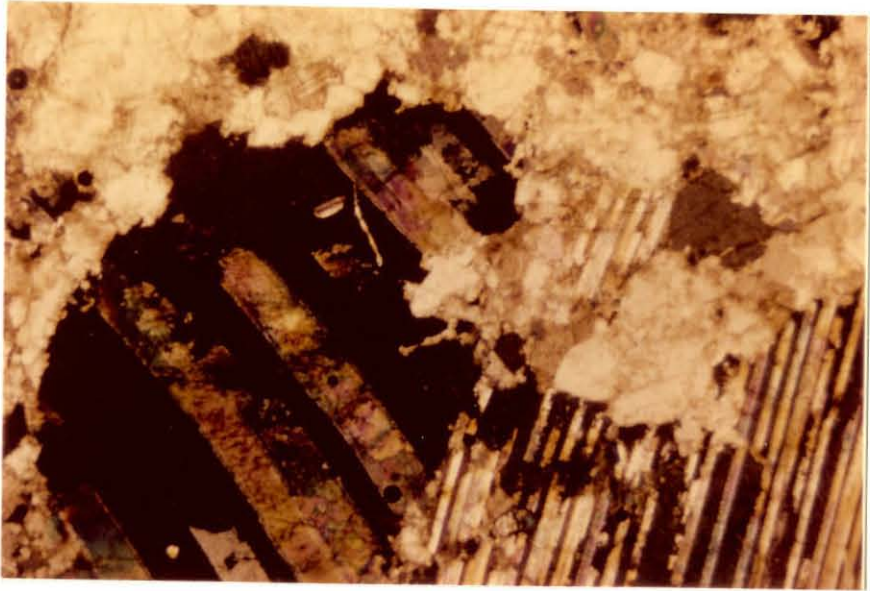


Figure 31. Photomicrograph. Uniform interference colors associated with shallowly inclined thin twin lamellae in dolomite parallel to $\{02\bar{2}1\}$ (darkened grains). These are best displayed in the wide lamellae, left grain, which are inclined at an angle of about 15° to the plane of the picture. Their thickness varies from zero to approximately 6μ . Near edges of each of the bright bands, for example one showing second order blue, green, and yellow interference colors (lower left hand corner) the color spectrum, produced by the tapered edge of the lamella where it intersects the surface of the thin section, is visible. Near the upper part of the left hand dark grain, four lamellae are disposed so that there is overlapping among them. In the most visible pair, each shows second order yellow and red and third order blue interference colors. The colors from the overlapping portion of the two lamellae are the same as those of the two lamellae separately, not the additive colors of the two lamellae. This effect is one predicted according to theory (see p. 215). Crossed nicols (x 35).

fringes which are superimposed upon the overall interference colors for some positions of the crystal between crossed nicols. Four types of fringes have been distinguished under the microscope, and these are designated types I, II, III and IV. All of the fringes are parallel to the trace of the lamellae in thin section. Types I and II may be observed in most lamellae, but observation of type III seems to depend to some degree upon the thickness and inclination of the lamellae, and upon the degree of development of the type II fringes. Type IV are not commonly observed. These fringe features are most easily seen under medium or high power in association with microtwinning lamellae that are inclined at a low angle to the plane of the thin section. They are also much more prominent in $f \{02\bar{2}1\}$ lamellae in dolomite than with $e \{01\bar{1}2\}$ lamellae in calcite, presumably because of the higher birefringence of dolomite. The observed properties of each of the fringe types are listed below, and the positions of the fringes as seen in a section which includes the normal to the lamella are shown in Figure 32. The characteristics of the fringes are as follows:

Type I: Visible when microscope is focussed on lower edge of lamella in both plane polarized light and under crossed nicols. Not visible when host is at extinction. Fringes begin at the inner edge of the color spectrum produced by the tapered edge of the lamella and the order of the fringes increases rapidly inward toward the center of the projected lamella width from the lower edge. As the host crystal passes through extinction, the fringe pattern shifts position corresponding to a

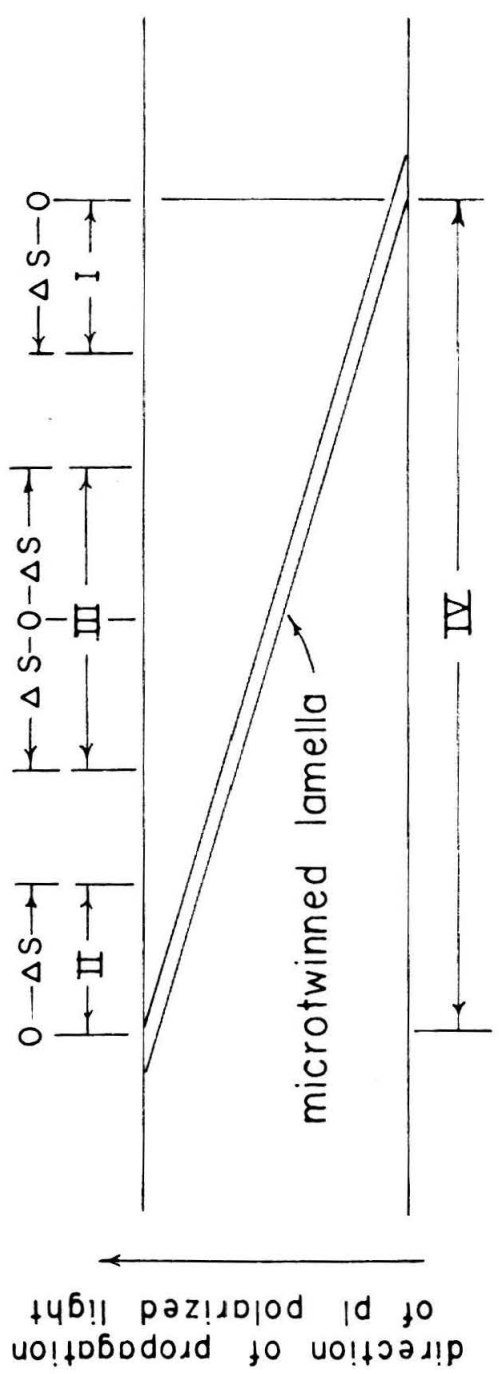


Figure 32. Location of fringe features in a shallowly inclined lamella. Arrows indicate direction of increasing retardation ΔS .

path difference of $\lambda/2$. Fringes are distorted by irregularities in the thin section surface, and where other twins or cleavage cut the lamella.

Type II: Visible when the microscope is focussed on upper edge of the lamella only under crossed nicols. Not visible when host is at extinction. Fringes begin at the inner edge of the color spectrum produced by the tapered edge of the lamella, and the order of the fringes increases rapidly inward toward the center of the projected lamella width from the upper edge. The fringe pattern shifts position corresponding to a path difference of $\lambda/2$ as the host crystal passes through extinction. They are generally not as prominent as fringes of type I. The fringes are distorted in a manner similar to that of type I.

Type III: These fringes may be sharply visible in a position of focus halfway between upper and lower edges of a lamella. They are visible between crossed nicols, and are most prominent when the host is in a position of maximum illumination. They are sometimes, but not generally, visible when the host is at extinction. Especially prominent fringes of this type may be visible in both plane polarized light and between crossed nicols. The fringe pattern shifts position corresponding to a path difference of $\lambda/2$ when the host crystal is rotated through extinction. The distribution of fringes is such that the zeroth order fringe is located exactly halfway between the edges of the types I and II fringe patterns, with the order of the fringes increasing rapidly outward in each direction from the center toward the edges of the lamella. Upon insertion of a quartz wedge (thin edge first) such that its fast direction is perpendicular to the trend of the fringe pattern, the fringes shift toward the lower edge of the lamella. The spacing of the type III fringes is approximately one-half that of types I and II. Type III fringes ultimately merge with those of the other types when both are persistent enough.

Type IV: Broad band-like variations in interference color across the projected width of the lamella. Zeroth order fringe in middle of the projected width, increasing in order outward from the center. Visible only between crossed nicols. Fringe spacing much wider than for types I-III, for lamellae with the same angles of tilt. Most plainly visible when host crystal is near extinction.

Figures 33-35 illustrate the optical features described above. In Figure 33, which show $f \{02\bar{2}1\}$ lamellae in dolomite, seven orders of type I fringes are visible across the lamellae shown. Type II fringe are not visible but greatly resemble those pictured. Type III fringes may be noted in Figure 34. Figure 35 illustrates type IV phenomena. All figures show these features as they appear in dolomite.

Origin of the fringe features and interference colors

Although a complete explanation of the causes of the fringe features described above cannot be given here, considerable light can be shed on their origin. The function of the lamella in producing the fringes of types I and II may be understood when the lamella is considered as a slice of crystal of different optical orientation than the host which, because of the difference in indices between the two, gives rise to preferential transmission of light vibrating in a plane perpendicular to the lamella. Thus with fringes of type I, the lamella can act, in a way owing to its different orientation, as an analysing nicol prism, and the fringes can be seen

Figure 33. Type I fringes associated with microtwinning $\{02\bar{2}1\}$ lamellae in dolomite. Fringes of lowest order are located at the intersection of the lamella plane with the lower surface of the thin section. Seven orders of these fringes are visible. The lamellae are inclined at an angle of approximately 15° to the plane of the thin section (and the photograph). A second set of nearly vertical microtwinning $\{02\bar{2}1\}$ lamellae cuts across the photo at a small angle to the horizontal. Crossed nicols (x 125).

Figure 34. Type III fringes along microtwinning $\{02\bar{2}1\}$ lamellae in dolomite. The fringes are closely spaced dark lines located in the center of the projected width of the lamellae. The zeroth order fringe occurs in the middle and fringes increase in order to either side. Fringes of both types I and II are also faintly visible. The fringes are distorted by other microscopic cracks crossing the lamellae and by irregularities (?) in the surface of the thin section. The lamellae dip toward the top of the photograph at an angle of about 20° . Another discontinuous set of steeply dipping $\{02\bar{2}1\}$ lamellae cut across the photograph in a northeast direction. Crossed nicols (x 125).

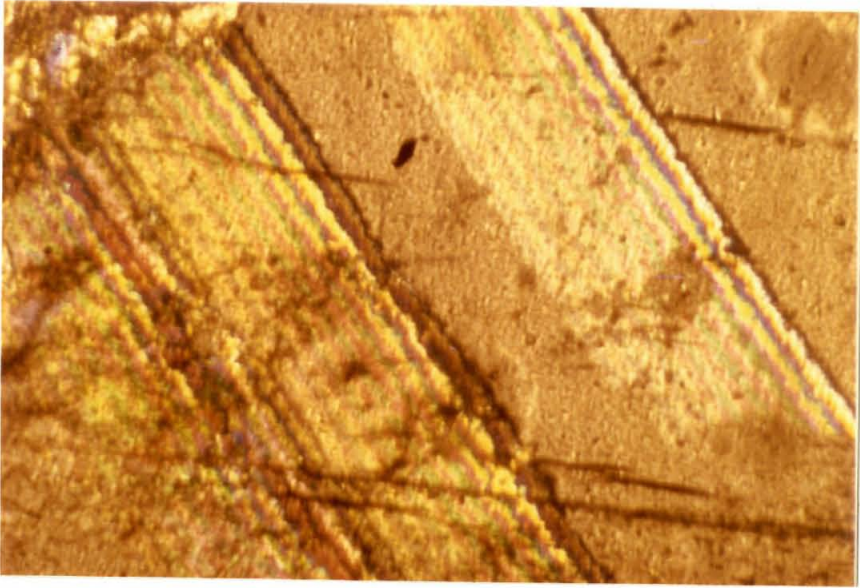


Figure 33

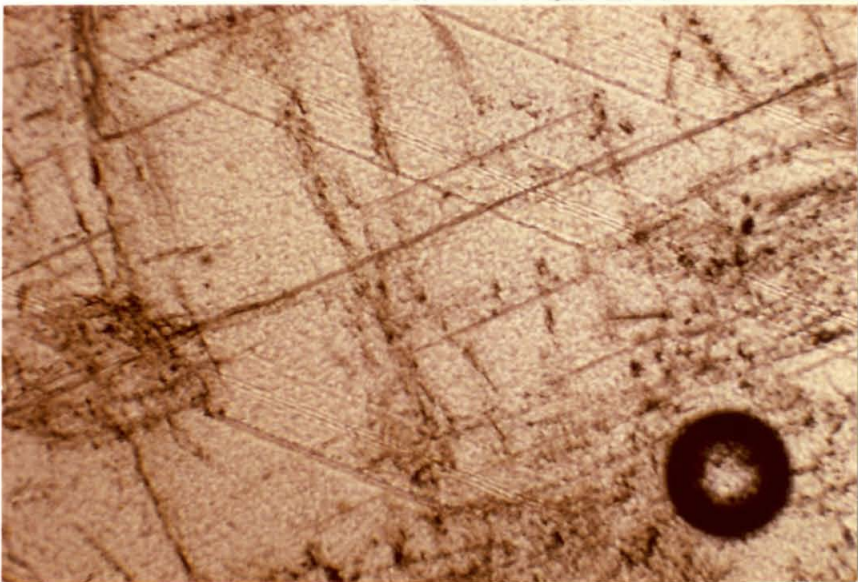


Figure 34

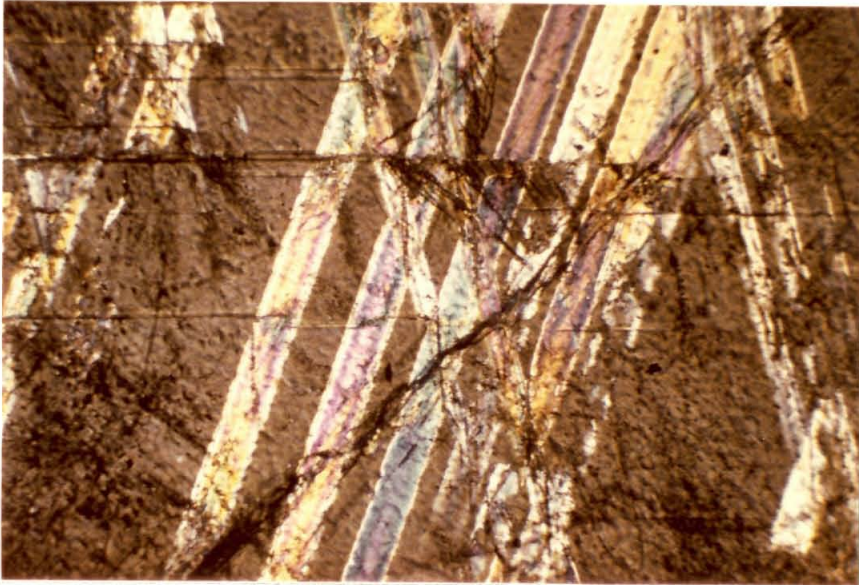


Figure 35. Type IV interference bands in $\{02\bar{2}1\}$ lamellae, dolomite (in broad colored lamellae). The other sharp, planar features trending horizontally across the field are also steeply dipping microtwinning lamellae parallel to $\{02\bar{2}1\}$. The irregular dark zone running diagonally across the field is a crack (irregularly) parallel to $\{10\bar{1}1\}$. The lamellae showing Type IV "fringes" dip 40° to the left. Crossed nicols (x 125).

without the aid of the microscope analyser. With type II fringes the lamella can act as the lower polarizer, and the fringes are visible with the microscope polarizer removed and the upper nicol prism inserted.

The relationships of the types I and II fringes to the edges of a lamella, with many orders of fringes visible and increasing in order toward the center of the projected width of the lamella, suggests that these fringes are related to the wedges of host crystal at the lower and upper edges of the lamella. If this is so, the spacing of the fringes will be simply related to the inclination of the lamella and the orientation of the host crystal. In monochromatic plane polarized light between crossed nicols, fringe minima (dark fringes) will occur when

$$\frac{\pi \Delta S}{\lambda} = k\pi \quad (k = 1, 2, 3, \dots) \quad (20)$$

where λ is the wave length of light, and where ΔS is written

$$\Delta S = \Delta n \cdot \underline{x} \cdot \tan \theta \quad (21)$$

In Equation 21, \underline{x} is the distance measured outward perpendicularly from the edge of a lamella toward the center, and θ is the angle between the plane of the section and the lamella.

Δn is the "effective" birefringence of the host crystal and depends on orientation of the crystal. Δn is equal to $\underline{n}_o - \underline{n}'_e$, where \underline{n}_o is the ordinary index of refraction of the host crystal, and \underline{n}'_e is its apparent extraordinary index which is given by

$$(\underline{n}'_e)^2 \left(\frac{\sin^2 \phi}{\underline{n}_o^2} + \frac{\cos^2 \phi}{\underline{n}_e^2} \right) = 1 . \quad (22)$$

In Equation 22, \underline{n}_e is the true extraordinary index of the host, and ϕ is the angle between the c-axis of the host and the plane of the section. Using Equations 20 and 21, the spacing $\Delta \underline{x}$ between fringes of order $\Delta \underline{k}$ apart is

$$\Delta \underline{x} = \Delta \underline{k} \cdot \lambda / (\Delta \underline{n} \cdot \tan \theta) . \quad (23)$$

Fringe spacings computed using Equation 23 may thus be compared with those measured with a micrometer ocular to test the concept suggested above. This is done in Table 2.

TABLE 2

Comparison of Computed and Measured
Fringe Spacings (White Light)

	$\Delta \underline{k}$	$\Delta \underline{n}$	$\tan \theta$	$\underline{x}_{\text{calc}}$	$\underline{x}_{\text{meas}}$	mineral
550 m μ	4	0.159	1.428	10 μ	10 μ	C*
550 m μ	4	0.157	0.900	16 μ	12 μ (?)	C
550 m μ	4	0.133	1.235	13 μ	14 μ	C
550 m μ	4	0.168	1.540	8 μ	9 μ	C
550 m μ	4	0.128	2.246	7 μ	7 μ	C
550 m μ	4	0.136	1.664	10 μ	9 μ	D*
550 m μ	4	0.180	0.900	14 μ	14 μ	D
550 m μ	4	0.100	0.287	77 μ	71 μ	D

*Data on calcite from the Darwin fold; the dolomite used was obtained from a series of dolomites and dolomitic limestones in San Antonio canyon, San Gabriel mountains, California.

The general agreement in these two results is surprisingly good in view of the difficulties in making many of the measurements involved in construction of the table. Measurements on both calcite (C) and dolomite (D) are included, and measurements on each of these minerals contain about the same discrepancies.

Type III fringes, which are generally invisible except when viewed between crossed nicols, are situated such that the zeroth order fringe is exactly halfway between the extremes of the projected width of a lamella. This relationship suggests that the upper wedge of crystal is in some manner compensating for the path difference produced in waves travelling through the lower wedge, with compensation occurring only where the path differences produced by the two wedges are equal.

The band-like variations in interference color referred to as type IV also have a zeroth order fringe located in the center of the projected width of the lamella, and this suggests that they, like type III arise through presence of both upper and lower wedges of host crystal. When type IV fringes are visible, they usually completely subdue effects of the other fringe types, and it is therefore difficult to discern a quantitative relationship between these and types I-III.

When a lamella is oriented horizontally under the microscope either between crossed nicols (horizontal orientation being such that the pole to the lamella is parallel to

the axis of the microscope) or in plane polarized light, the fringes are no longer visible. In this orientation, lamella and host are indistinguishable optically because of the symmetrical arrangement of their respective lattices with respect to the twin plane, and the lamella thus cannot make its influence apparent. Also, none of the fringe types described above may be seen on cleavage planes parallel to $\{10\bar{1}1\}$ in calcite or dolomite. This further illustrates the important role the lamellar material must play in producing these fringe patterns, for cleavage is thought to represent actual separation of adjacent parts of the crystal along the cleavage plane, not development of a crystallographically intact slice of material. Fringe phenomena are visible along grain boundaries between grains in different optical orientation, and especially when the grain contact is inclined at a small angle to the plane of the thin section. The fringes may be seen at each of the tapered edges of the grains. Fringes at the upper tapered edge are visible with either the polarizer or analyser removed or between crossed nicols when the grain below is in a position of extinction. Those at the lower edge may be seen between crossed nicols or with only the analyser removed when the grain above is in a position of extinction. Type III fringes are not visible. Although there is generally no regularly crystalline zone between grains along the grain boundary, as is true of the twin lamella, the situation is somewhat analogous, because there is a change in optical

properties at the interface which gives rise to a preferential reflection of light vibrating parallel to the interface.

The uniform interference colors produced by the micro-twinned lamellae, when the parent crystal is at extinction, arise in the following manner. When the host is at extinction, its permitted vibration directions are parallel to the analyser and polarizer directions in the microscope. In general this will not be true of the lamella. Thus in this setting the lamella acts simply like a thin anisotropic plate between crossed nicols which is not at extinction. These interference colors may be used to determine thicknesses of microtwinning lamellae, as will be demonstrated below (p.199).

A New Method for Measuring Orientations
of Twinning Lamellae

The "blind spot" problem

An inherent difficulty in studying carbonate rocks with the universal stage has been to obtain the spatial orientation of planar features such as twinning lamellae and cleavage which are inclined at angles less than about 35° to the plane of the thin section. The difficulty may arise either because of mechanical limitations of the stage or because of total reflection of light coming from the polarizer at the interface between the lower hemisphere and the glass stage plate. Thus, all orientation diagrams for poles to \underline{e} $\{01\bar{1}2\}$ lamellae, which are prepared from any one thin section, contain

a central "blind-spot," a region about the pole to the diagram of half-angle 35° , in which lamellae poles are not present. In order to obtain a complete picture of the distribution of lamellae throughout a given volume of rock, it has therefore always been necessary to examine two or more perpendicular thin sections from the rock. However in some situations, particularly those arising in small scale applications of the dynamic analysis or where the rock fabric is nonhomogeneous on the scale of a thin section, it is desirable and necessary to obtain a statistically complete picture from one section. The method described herein helps overcome the "blind-spot" problem. It uses the optical properties of twin lamellae (either micro-twinning or visibly twinned varieties) to place the lamellae in horizontal orientation, i.e., with the pole or a lamella parallel to the microscope axis. This technique has proved useful with calcite and is even better and easier to use with dolomite. Unfortunately its discovery came after completion of the major portion of the fabric studies reported on above, and it was therefore not available for use throughout this work.

Since the method utilizes an optical property arising from the twinned nature of material enclosed in the lamellae, it cannot be applied to cleavages or other planar partings which are physical separations of adjacent parts of the crystal lattice.

Physical principles of the method

The new method makes use of the interference colors visible in the projected width of a shallowly inclined lamella when the host crystal is at extinction. The object of the method is to bring the lamella to such a position that both it and the host crystal are in positions of darkness simultaneously, that is, with the permitted vibration directions in each parallel to one another (as seen in the microscope) and parallel to the nicol directions. In any given situation there are three positions of lamella and host where this may be achieved, as may be illustrated by reference to Figure 36. The diagram is a stereographic projection on the lower hemisphere of the projection sphere. The pole of the diagram is the microscope axis (MA). Let the cross labeled e represent the position of the pole to an arbitrarily chosen, but not too steeply inclined, e-lamella in calcite, the open circle marked C the position of the c-axis of the host crystal, and C' (solid circle) the position of the twin optic axis. With each optic axis position are shown the permitted vibration directions in host and lamella, and these are also projected onto the plane. If the trace of the lamella in thin section is brought parallel to the north-south (NS) stage axis, then its pole will lie along the great circle perpendicular to NS (which is shown in the figure as a dashed line labeled N-S). Tilting the stage about NS moves the plotted c-axes along small circles and e along a great circle, all three of which are shown as short dashed lines in

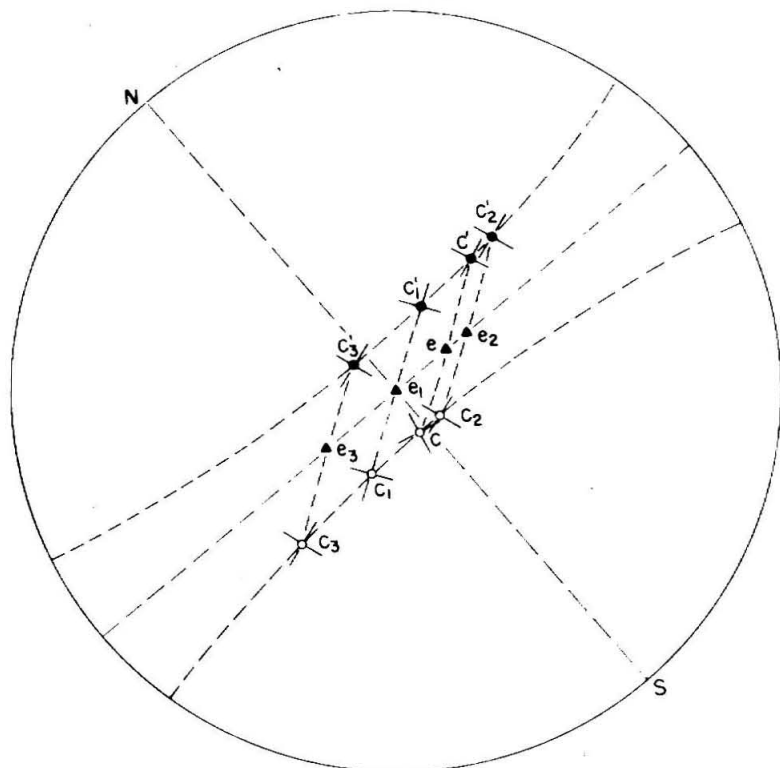


Figure 36. Stereographic projection used in illustrating method for orienting twinning lamellae horizontally with the universal stage (horizontal meaning with the plane of lamella parallel to the microscope stage). Solid triangles labeled "E" represent positions of the pole to the lamella, open circles marked "C" positions of the host optic axis, and solid circles "C'" positions of the optic axis in twin orientation. Through each optic axis position are also marked vibration directions in the crystal projected into the horizontal plane. The pole to the diagram is MA (down), and NS represents the north-south horizontal axis of the universal stage. As the drawing is constructed, for each of the positions of C and C' corresponding to lamella positions e_1 , e_2 , and e_3 , rotation on NS will produce extinction of host and twin simultaneously. e_1 as shown is the lamella pole position for true horizontal orientation.

the figure. As can be seen, there are three positions for the optic axes where their respective vibration directions are parallel to one another. These have been labeled C_1 , C_2 , and C_3 for the host positions, and C'_1 , C'_2 , and C'_3 for the twins. The corresponding positions for poles to the twin plane are e_1 , e_2 , and e_3 . One pole position, e_1 , is parallel to MA while the other two are symmetrically disposed about this point, one to either side on the great circle containing e and e_1 . The symmetrical distribution of these points is related to the fact that host and twin lattices are symmetrically disposed about the twin plane. With the stage tilted on NS to any of these configurations, rotation of the microscope stage (MS) will produce extinction of both host and twin together. The true horizontal position of the lamella can be distinguished from the two "false" positions by the fact that the fringes of types I-III disappear at the true horizontal setting (see discussion p. 191). The host c -axis and the measured lamella pole. If the true lamella position has been found, this angle should approximate 26° . In practice, both of the "false" positions have never been observed, but two positions are commonly obtained.

Method for measuring orientation of lamellae used in practice

In practice the following procedure can be used to place the lamella plane horizontal while simultaneously arranging the vibration directions in host and twin parallel to the vibration directions in the microscope:

- (1) With MS set at the zero reference mark, the trace of the lamella is brought parallel to the north-south cross hair in the microscope by rotation on the inner vertical stage axis (IV).
- (2) The host crystal is then rotated to extinction on MS so that the trace of the optic plane is east-west. Normally at this point the lamella will exhibit interference colors very different from those of the host crystal when the host is not at extinction.
- (3) The stage is now tilted about NS (which is of course no longer parallel to the north-south cross hair) in the proper direction to banish the interference colors of the lamella. Since the host is generally not now in a position of minimum light, a further adjustment on MS is necessary, and this may have to be followed by further rotation on NS to bring the lamella to darkness. The nicols are now uncrossed and the grain is checked to see if the fringes remain invisible during a rotation on MS.
- (4) For the special case when both the pole to the lamella and \underline{c} lie in a vertical plane, so that the lamella and host are simultaneously at extinction for any rotation on NS, the nicols may be uncrossed, and the disappearance of the fringes (type I) used to indicate that the lamella is horizontal.
- (5) The NS and IV stage settings are noted and the lamella pole is plotted on the stereographic (or equal area projection) using the same procedure as for polar oriented \underline{c} -axes (Faribairn, 1954, p. 279).

Difficulties in the method

In general this technique is not as easy to apply as the conventional one for obtaining the orientation of twinning lamellae with the universal stage (Turner, 1949). Difficulties are particularly apt to arise when working with grains on which more than one set of lamellae are present. This is because

when one set is dark, the others are not, and the first is then illuminated by the second. This makes it difficult to obtain the desired extinction in both host and twin simultaneously.

Principle use of the orientation method

The principle use to which this technique may be put is in obtaining the orientation of "inaccessible" twinning lamellae in carbonate rocks. These structures are termed "inaccessible" when they are inclined at a sufficiently small angle to the plane of the thin section so that they cannot be measured by tipping about NS into a vertical position (pole horizontal). A number of factors enter to set this upper limit of tilt. The relative indices of hemispheres and oils ($n = 1.649$) and glass stage plate ($n = 1.516$) set a maximum upper limit for total reflection of about 67° . However with the Leitz microscope and Leitz universal stage, the maximum tilt attainable is less than 55° because the upper hemisphere mounting screws hit the objective at this angle. In effect, a feature inclined at an angle of less than 35° to the plane of the thin section is thus not measurable. With the method described above tilts of $40-50^\circ$ can be measured, though only with difficulty at higher tilt angles, so that there is ideally effective coverage of the normal "blind-spot" region. The usual corrections for differences in refractive index between crystal and hemispheres must be applied for high tilt angles.

Another application of the present method is in obtaining the thicknesses of microtwinned lamellae, and this is discussed next.

Determination of Lamella Thickness

The question of determining the thicknesses of lamellae is important from at least two standpoints. First, if lamella thicknesses determined optically by making assumptions about the crystallographic nature of the lamella can be favorably compared with thicknesses determined by independent means, then this is evidence that the assumed nature of the lamella is correct. Secondly, insofar as microtwinned lamellae represent deformation by twinning, it is of interest to obtain some idea of the amount of strain they record. If thicknesses of individual lamellae or aggregate thicknesses of lamellae can be determined, then by Equation 13, the amount of strain recorded in twinning may be evaluated. In this section a standard optical technique for determining thicknesses using interference colors is applied to determination of lamella thicknesses. In the next section, the question of obtaining the aggregate thickness of a group of superimposed lamellae is discussed in detail.

If a twin lamella is oriented with its pole parallel to MA (horizontally) or nearly so, and the optic plane of the host crystal is east-west, then the c-axis positions of host and twin are symmetrically disposed about the lamella pole,

each lying $26\frac{1}{4}^{\circ}$ from MA in opposite directions along the great circle containing \underline{c} , \underline{e} , and \underline{c}' . Between crossed nicols both are at extinction. When the lamella pole is almost vertical, and the trace of the optic plane of the host is east-west, the ordinary wave vibrating north-south (parallel to the lower nicol vibration direction) is resolved into two waves of different velocity in the lamella. On passing through the lamella a path difference ΔS is produced between these two waves which is given by (Ditchburn, 1957, p. 370)

$$\Delta S = t \cdot \Delta \underline{n} \quad (24)$$

where all of the symbols have been defined on p.188. Δn is now defined by writing \underline{n}'_e , the "effective" extraordinary index of the lamella as

$$(\underline{n}'_e)^2 \left(\frac{\cos^2 \theta}{\underline{n}_o^2} + \frac{\sin^2 \theta}{\underline{n}_e^2} \right) = 1 ,$$

where, for example, θ is the angle $\underline{c} \wedge \underline{e}$ in calcite, equal to $26\frac{1}{4}^{\circ}$. $\underline{n}_o = 1.658$, $\underline{n}_e = 1.486$, and $\underline{n}'_e = 1.618$, for which $\Delta \underline{n} = 0.040$. Estimates of lamella thicknesses have been made using Equation 24 for microtwinning lamellae in both calcite and dolomite. The value of ΔS is obtained using either a quartz wedge or rotation compensator. Of course, no colors are seen with the lamella horizontal and with the vibration directions of host and twin parallel to the nicol directions in the microscope, and it is necessary to rock the lamella

through extinction on the north-south axis of the stage and observe the colors on either side of the true horizontal position. For any rotation of the lamella from the true horizontal position, the apparent thickness of the slice as seen in the microscope increases as $\underline{t}/\cos(d\theta)$, where \underline{t} is the true thickness and $d\theta$ is the angle of tilt from the horizontal. For $d\theta$ equal to 5° the change in \underline{t} is not very great. On the other hand the change in Δn depends on the direction of tilt. Take the special case where the axis of rotation lies parallel to the trace of the lamella in the plane of the thin section. By differentiating the last equation

$$d(\Delta n) = -dn'_e = \frac{\sin\theta \cos\theta d\theta}{\left(\frac{\cos^2\theta}{n_o^2} + \frac{\sin^2\theta}{n_e^2}\right)^{3/2}} \cdot \frac{n_o^2 - n_e^2}{n_o^2 n_e^2}$$

All terms in the expression on the right are positive, and $d(\Delta n)$ thus depends on the sign of $d\theta$.

For θ equal to $26\frac{1}{4}^\circ$ and the indices of calcite the constant part of this equation equals 0.150. The apparent thicknesses on either side of the true horizontal position are thus not the same. In practice, the color 'average' for these two positions has been used to compute \underline{t} from Equation 24.

The values of \underline{t} obtained in this manner are compared with measurements under oil immersion (x 1000) of the width of the color spectrum produced at the tapered edge of the

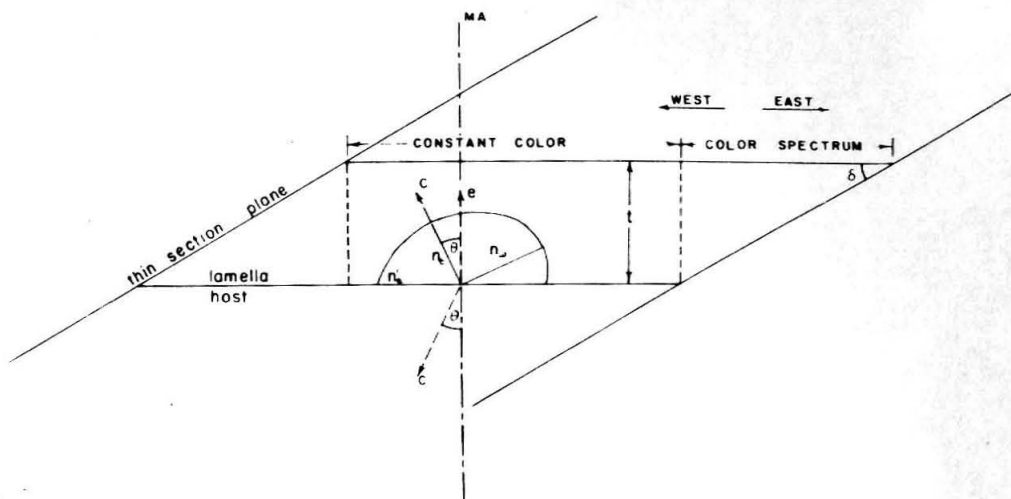


Figure 37. Positions of the color spectrum associated with the tapered edge of the lamella and the constant interference color across the constant thickness part of the lamella. Orientation of the indicatrix (for calcite) in the horizontal lamella is also shown in the position where both \bar{c} and \bar{e} the pole to the lamella \bar{e} lie in the east-west plane. \underline{n}_e represents the true extraordinary index (1.486), \underline{n}_o the ordinary index (1.658), \underline{n}'_e the apparent extraordinary index of the horizontal lamella (1.618). For calcite, $\theta = 26\frac{1}{4}^\circ$. For a horizontal $\bar{f} \{02\bar{2}1\}$ lamella in dolomite, $\theta = 62\frac{1}{2}^\circ$, $\underline{n}_e = 1.515$, $\underline{n}_o = 1.700$, and $\underline{n}'_e = 1.550$. The values of \underline{n}'_e are computed from the equation on p. 200.

lamella (fig. 37). The measured widths are multiplied by $\sin \delta$ where δ is the angle between the lamella and the plane of the thin section, to get the true lamella thickness t . The results of these measurements are given in Table 3. Measurements on both calcite and dolomite are included.

TABLE 3

Comparison of Lamellae Thicknesses Determined
by Optical and Direct Measurement

Meas. No.	ΔS	Δn	t_{opt}	δ	Spectrum width	t_{meas}	min-eral
1.	500-570 m μ	0.150	3-4 μ	37°	5 μ	3 μ	D*
2.	325 m μ	0.150	2 μ	50°	3 μ	2 μ	D
3.	640-650 m μ	0.150	4 μ	15°	14 μ	4 μ	D
4.	400 m μ	0.150	3 μ	44°	3 μ	2 μ	D
5.	250-300 m μ	0.150	1.7-2 μ	44°	3 μ	2 μ	D
6.	500-550 m μ	0.150	3-4 μ	44°	4 μ	3 μ	D
7.	820 m μ	0.150	6 μ	50°	8 μ	6 μ	D
8.	325 m μ	0.040	8 μ	43°	12 μ	8 μ	C
9.	83 m μ	0.040	2 μ	43°	3 μ	2 μ	C

*D = dolomite, C = calcite.

The general agreement between thicknesses based on the two types of observations is taken as proof that the lamella is composed of a thin slice of crystal whose optical orientation in relation to the host crystal is given by the normal twin law, as shown in Figure 37 .

In a survey of thin sections of limestones used in the fabric studies reported on above (about 35 sections) it was found that the majority of microtwinned lamellae showed interference colors of low first order (gray to black). This indicates lamella thicknesses in calcite of one micron or less. The retardation corresponding to such low order colors is very difficult to measure with the quartz wedge, so that a compensator (in this case an Ehringhaus Compensator with quartz combination plate) must be used. On the other hand, thin lamellae in dolomite may easily be measured below a thickness of one micron, since the birefringence of a lamella in dolomite in a nearly horizontal position is greater (0.150) than that of calcite (0.040).

Optical Effects Produced by Superposition
of Several Thin Lamellae

Introduction

In some situations, when thin lamellae are inclined at a low angle to the plane of a thin section and are closely spaced, they overlap* so that light travelling through the crystal must pass through several superimposed lamellae as well as thicker slices of host crystal. The question arises as to what information may be obtained by observing the interference colors produced by the superimposed thin plates, when they are oriented in the same manner as for determining thicknesses of single lamellae. The purpose of the calculations

*See Figure 31.

given below is to demonstrate that only the average and not the cumulative thickness for the lamellae is shown by their interference colors. It also develops that a good approximation to the exact calculation is obtained by neglecting path differences produced in waves travelling in the host crystal, if these crystal slices are much greater in thickness than the twins. This consideration allows the cumulative interference effects produced by any number of lamellae to be calculated in a relatively simple manner. The exact two lamellae calculations written out below proceeds by a straightforward treatment of optical effects produced by each lamellae and layer of host crystal successively. After this development the approximate calculation is carried out. In all of these calculations dispersion, absorption, and reflection are neglected.

Fresnel (1821) was the first to consider the problem of optical effects produced by several superimposed crystal plates. In particular he treated the case of two superposed anisotropic crystal plates between crossed nicol prisms. Airy (1833) extended this calculation to the situation where the two plates have their principal planes inclined at an angle to one another, and used the results in determining the optic sign of crystals. The problem treated here is somewhat different, as will be made clear below.

Suppose a crystal containing several closely spaced, thin e-lamellae in calcite (or f-lamellae in dolomite) is

oriented with the universal stage so that the lamellae overlap along the axis of the microscope. Suppose also that the lamellae are nearly horizontal, and let the host crystal be at extinction. Under these conditions, the allowed vibration directions of the twinned parts of the crystal will in general make some angle α with those of the host (and also the directions of polarization in the microscope). This situation is illustrated in Figure 38. In this position the lamellae will show some combination of interference colors, and in order to understand the combined interference effects produced with this configuration of crystal plates, we consider first the simplest case, that of two superimposed lamellae with vibration directions parallel, separated by a much thicker slice of host crystal in different orientation and arranged between crossed nicols as in Figure 38.

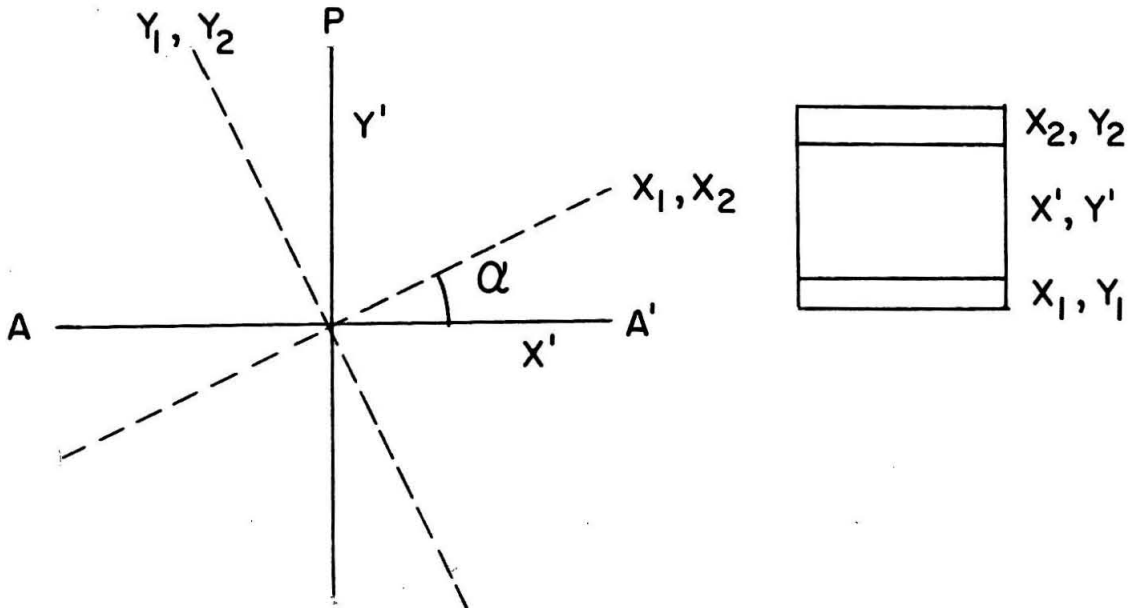


Figure 38. Relationship of lamellae vibration directions ($x_1, x_2; y_1, y_2$) to host crystal vibration directions (x', y'), and the planes of polarization of the nicols (PP' and AA').

Exact calculation for the two-lamellae case

Suppose that a plane polarized light wave with electric displacement $D = D_0 \sin \omega t$ ($\omega = \frac{2\pi c}{\lambda}$)* vibrating parallel to PP' impinges on the lowest lamella (1-subscripts) and is resolved into two components vibrating along x_1 and y_1 . After passing through the lamella, the components of D along these directions are:

$$\begin{aligned} D_{x_1} &= D_0 \sin \alpha \sin(\omega t + \phi_1^x) \\ D_{y_1} &= D_0 \sin \alpha \sin(\omega t + \phi_1^y), \end{aligned} \quad (25)$$

where ϕ_1^x and ϕ_1^y are the phase shifts of the waves vibrating along the x and y axes respectively. $\phi_1^x - \phi_1^y$ is the phase difference produced between the two waves in traversing the first lamella. After passing through the interposed slice of host crystal the components are:

$$\begin{aligned} \text{along } x' : D_{x'} &= D_0 \sin \alpha \cos \alpha [\sin(\omega t + \phi_1^x + \phi^{x'}) - \sin(\omega t + \phi_1^y + \phi^{y'})] \\ \text{along } y' : D_{y'} &= D_0 [\sin^2 \alpha \sin(\omega t + \phi_1^x + \phi^{x'}) + \cos^2 \alpha \sin(\omega t + \phi_1^y + \phi^{y'})] \end{aligned} \quad (26)$$

where $\phi^{x'}$ and $\phi^{y'}$ are the phase shifts introduced by the host crystal. Emerging from the second thin lamella the components of D along the directions x_2 and y_2 are:

* c is the velocity of light in vacuum.

$$\begin{aligned} \text{along } \underline{x}_2: D_{x_2} &= D_0 \sin^3 \alpha \sin (\omega t + \phi_1^x + \phi^{y'} + \phi_2^x) \\ &+ D_0 \sin \alpha \cos^2 \alpha [\sin(\omega t + \phi_1^x + \phi^{y'} + \phi_2^x) + \sin(\omega t + \phi_1^x + \phi^{x'} + \phi_2^x) \\ &\quad + \sin (\omega t + \phi_1^y + \phi^{x'} + \phi_2^x)] \quad (27) \end{aligned}$$

$$\begin{aligned} \text{and along } \underline{y}_2: D_{y_2} &= D_0 \cos \alpha [\sin^2 \alpha \sin(\omega t + \phi_1^x + \phi^{y'} + \phi_2^y) \\ &+ \cos^2 \alpha \sin(\omega t + \phi_1^y + \phi^{x'} + \phi_2^x)] - D_0 \sin^2 \alpha \cos \alpha [\sin(\omega t + \phi_1^y + \phi^{x'} + \phi_2^y) \\ &\quad - \sin (\omega t + \phi_1^y + \phi^{x'} + \phi_2^x)] \end{aligned}$$

ϕ_2^x and ϕ_2^y likewise being the phase shifts introduced in the second lamellae along the x and y directions respectively. When these components are resolved along the direction AA' the expression for D in this direction is:

$$\begin{aligned} D_A &= D_0 \sin^3 \alpha \cos \alpha [\sin(\omega t + \Delta_1) - \sin(\omega t + \Delta_1') \\ &\quad + \sin(\omega t + \Delta_3') - \sin(\omega t + \Delta_4')] \quad (28) \\ &+ D_0 \sin \alpha \cos^3 \alpha [\sin(\omega t + \Delta_2) + \sin(\omega t + \Delta_3) \\ &\quad - \sin(\omega t + \Delta_4) - \sin(\omega t + \Delta_2')] \end{aligned}$$

where

$$\begin{aligned} \Delta_1 &= \phi_1^x + \phi^{y'} + \phi_2^x ; & \Delta_1' &= \phi_1^x + \phi^{y'} + \phi_2^y \\ \Delta_2 &= \phi_1^y + \phi^{y'} + \phi_2^y ; & \Delta_2' &= \phi_1^y + \phi^{y'} + \phi_2^x \\ \Delta_3 &= \phi_1^x + \phi^{x'} + \phi_2^x ; & \Delta_3' &= \phi_1^x + \phi^{x'} + \phi_2^y \\ \Delta_4 &= \phi_1^y + \phi^{x'} + \phi_2^x ; & \Delta_4' &= \phi_1^y + \phi^{x'} + \phi_2^y \end{aligned}$$

Now separating the time varying part of the above expression from that involving the phases, one gets, after some manipulation,

$$\begin{aligned} \frac{D_A}{D_0} = & - \left[A_1 \sin \frac{\omega \Delta_{12}}{4} + A_2 \sin \frac{\omega \Delta_{34}}{4} + A_3 \sin \frac{\omega (\Delta_{12} + \Delta_{34})}{8} \right] \sin \omega t \\ & + \left[A_1 \cos \frac{\omega \Delta_{12}}{4} + A_2 \cos \frac{\omega \Delta_{34}}{4} + A_3 \cos \frac{\omega (\Delta_{12} + \Delta_{34})}{8} \right] \cos \omega t, \end{aligned} \quad (29)$$

where

$$\begin{aligned} A_1 &= \sin 2\alpha \cos \frac{\pi \Delta S_1}{\lambda} \sin \frac{\pi \Delta S_2}{\lambda} \\ A_2 &= \sin 2\alpha \sin \frac{\pi \Delta S_1}{\lambda} \sin \frac{\pi \Delta S_2}{\lambda} \\ A_3 &= \sin 4\alpha \sin \frac{\pi \Delta S_1}{\lambda} \sin \frac{\pi \Delta S_2}{\lambda} \sin \frac{\pi \Delta S'}{\lambda} \\ \Delta_{12} &= \Delta_1 + \Delta_1' + \Delta_2 + \Delta_2' \\ \Delta_{34} &= \Delta_3 + \Delta_3' + \Delta_4 + \Delta_4' \end{aligned}$$

In Equation 29 the various phase differences have been re-written as follows:

$$\begin{aligned} \phi_1^x - \phi_1^y &= \Delta S_1 \\ \phi^{x'} - \phi^{y'} &= \Delta S' \\ \phi_2^x - \phi_2^y &= \Delta S_2 \end{aligned}$$

The expression for the intensity of light transmitted by the analyser is given by the sum of the squares of the terms in square brackets in Equation 29 (see Ditchburn, 1952,

p. 386). After some further calculation and rearrangement of terms the resulting intensity ratio I can be written as:

$$\begin{aligned}
 I = \left(\frac{D_A}{D_O} \right)^2 &= \sin^4 2\alpha \left[\sin^2 \frac{\pi}{\lambda} (\Delta S_1 + \Delta S_2) \cos^2 \frac{\pi \Delta S'}{\lambda} \right. \\
 &\quad \left. + \sin^2 \frac{\pi}{\lambda} (\Delta S_1 - \Delta S_2) \sin^2 \frac{\pi \Delta S'}{\lambda} \right] \\
 &+ \frac{1}{2} \sin^2 4\alpha \left[\sin^2 \frac{\pi \Delta S_1}{\lambda} + \sin^2 \frac{\pi \Delta S_2}{\lambda} \right] \sin^2 \frac{\pi \Delta S'}{\lambda} \quad (30) \\
 &+ \sin^2 2\alpha \left[4 \cos^2 2\alpha \sin^2 \frac{\pi \Delta S_1}{\lambda} \sin^2 \frac{\pi \Delta S_2}{\lambda} \sin^2 \frac{\pi}{\lambda} (\Delta S_1 + \Delta S_2) \right. \\
 &\quad \left. + \cos^4 2\alpha \sin^4 \frac{\pi}{\lambda} (\Delta S_1 + \Delta S_2) \right]^{1/2} \cdot \sin \left(\frac{2\pi \Delta S'}{\lambda} + \Phi \right)
 \end{aligned}$$

and where

$$\sin \phi = \frac{\cos^2 2\alpha \sin^2 \frac{\pi}{\lambda} (\Delta S_1 + \Delta S_2)}{\left[4 \cos^2 2\alpha \sin^2 \frac{\pi \Delta S_1}{\lambda} \sin^2 \frac{\pi \Delta S_2}{\lambda} \sin^2 \frac{\pi}{\lambda} (\Delta S_1 + \Delta S_2) + \cos^4 2\alpha \sin^4 \frac{\pi}{\lambda} (\Delta S_1 + \Delta S_2) \right]^{1/2}}$$

When $\Delta S'$ is made equal to zero (i.e., the interposed host crystal is removed or is optically isotropic), the result (eqn. 30) reduces to the familiar relation for the intensity of light transmitted by two superimposed anisotropic plates between crossed nicols (Ditchburn, 1952, p. 386):

$$I = \sin^2 2\alpha \sin^2 \frac{\pi}{\lambda} (\Delta S_1 + \Delta S_2) . \quad (31)$$

For $\Delta S_1 = \Delta S_2 = 0$, ($\Delta S' \neq 0$), I is zero, since the host crystal is in a position of extinction.

Equation 30 is graphically represented in Figure 39. Data used in plotting the curve were obtained with the

Figure 39. Graphical representation of Equation 30. Along the horizontal axis is plotted $\pi \Delta S / \lambda$, with the vertical axis the intensity I. $\alpha = 22.5^\circ$. At the top of the drawing the range of $\pi \Delta S / \lambda$ throughout the visible spectrum is plotted for a number of specific values of ΔS_1 . The relationship of the variables given in Equation 30 is $\Delta S_2 = 2 \Delta S_1$, $\Delta S' = 25 \Delta S_1$.

Figure 40. The intensity I given by Equation 30 for $\alpha = 5^\circ$, $\Delta S_2 = 2 \Delta S_1$, $\Delta S' = 25 \Delta S_1$.

Figure 41. Illustration of contributions of the various terms in Equation 30. (a) First two terms of the expression, designated I_1 and I_2 ; (b) the third term of Equation 30 (I_3). $\alpha = 5^\circ$, $\Delta S_2 = 2 \Delta S_1$, $\Delta S' = 25 \Delta S_1$.

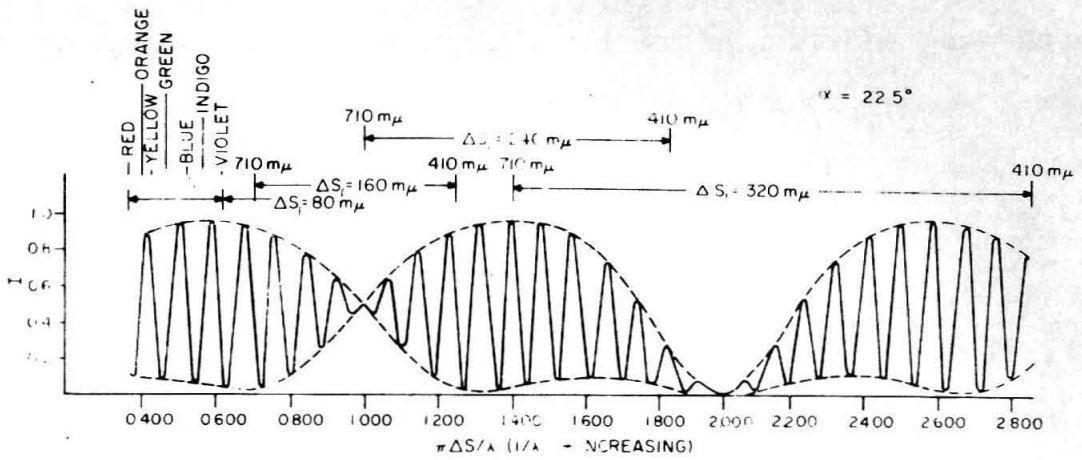


Figure 39

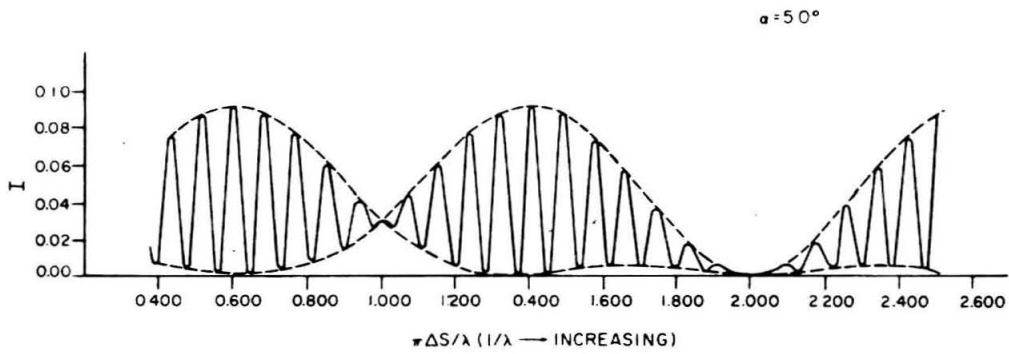


Figure 40

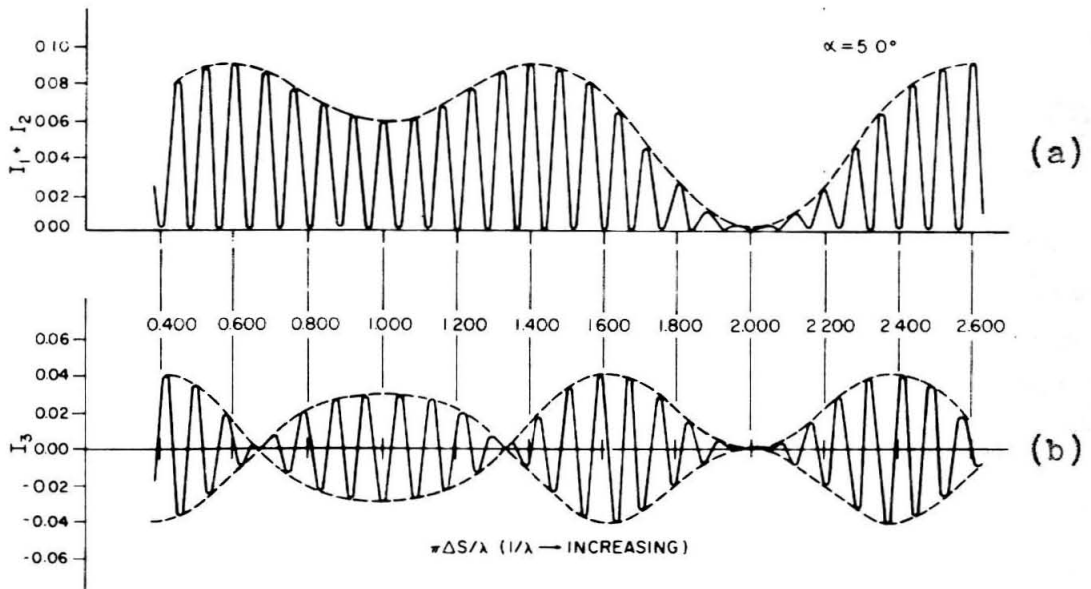


Figure 41

Burroughs 220 digital computer.* Since Equation 30 contains five parameters ΔS_1 , ΔS_2 , $\Delta S'$, α and λ , it has been necessary in plotting the curve in two dimensions to assume a relationship between the first three of these, and to consider fixed values of α . Thus, ΔS_2 has been taken equal to $2\Delta S_1$, and $\Delta S'$ equal to $25 S_1$. The example in Figure 39 is for $\alpha = 22.5^\circ$. $1/\lambda$ increases to the right along the horizontal axis along which $\pi\Delta S/\lambda$ is plotted. The vertical axis is the intensity I. Equation 30 gives a curve, outlined by the dashed boundary line, which is symmetric about $\Delta S/\lambda = m/\pi$, there being mirror symmetry in the curve for each set of values $m = 0, 2, 4, \dots$, and $m = 1, 3, 5, \dots$.

It is convenient to think of the variation of I as a function of $1/\lambda$ for a fixed value of ΔS_1 . Thus in Figure 39 regions are marked off for the variation of I throughout a range of λ corresponding to the visible spectrum (410-710 $m\mu$) for ΔS_1 equal to 80, 160, 240, 320, and 400 $m\mu$ (in calcite these would correspond to lamella thicknesses of 2, 4, 6, 8, and 10 microns respectively). Equation 30 then states, for example, that for a choice of ΔS_1 equal to 80 $m\mu$ the resultant visible color would be a combination of orange-yellow, greenish-blue, and violet.

* Computation of the curves was carried out on the computer at the California Institute of Technology, using the standard fixed point subroutines for $\sin x$ and $\cos x$ with x given in right angles. $\pi\Delta S_1/\lambda$ was taken as the independent variable, with $\Delta S_2 = 2\Delta S_1$, and $\Delta S' = 25\Delta S_1$, and values were calculated at an interval of 0.0072727272 right angles or 0.0114239733 radians. Sample values were checked against 6-place hand computed values.

As it stands Equation 30 is very cumbersome to deal with, but a simplification of this result is possible which has practical importance. When α is small, the first term of Equation 30 is of order α^4 , while the second two are of order α^2 (for $\alpha = 10^\circ$, the coefficient of the first term is about 0.07 that of the second, and 0.12 that of the third). The latter two terms thus dominate in the expression for I which becomes:

$$I \approx 8\alpha^2 \left[\sin^2 \frac{\pi \Delta S_1}{\lambda} + \sin^2 \frac{\pi \Delta S_2}{\lambda} \right] \sin^2 \frac{\pi \Delta S'}{\lambda} + 4A\alpha^2 \sin \left(\frac{2\pi \Delta S'}{\lambda} + \Phi \right) \quad (32)$$

where A has been written for the square root factor in the third term of Equation 30. The resultant intensity is thus composed of color contributions from each of the thin lamellae, represented by the first term on the right of Equation 30, and a contribution which depends in a very complex manner upon ΔS_1 , ΔS_2 , and λ , but which oscillates with very high frequency ($\Delta S' \gg \Delta S_1$ and ΔS_2) about zero because of the unsquared sine factor in the second term. The effect of the third term may be evaluated by referring to Figures 40 and 41. Figure 40 represents the total intensity I plotted as a function of $\pi \Delta S / \lambda$ for α equal to 5° , and with the relationships between ΔS_1 , ΔS_2 , and $\Delta S'$ previously designated. The curve in Figure 11a shows the first two terms of the intensity given by Equation 30, or effectively only the second term for this choice of α , and Figure 41b is the third term. The surprising fact

which may be noted from comparison of Figures 40 and 41 is that the positions of the maxima and minima in the boundary curves (dashed lines connecting closely spaced maxima) of these expressions are not shifted relative to each other by subtracting out the third term. The amplitudes of the maxima are also unaltered, but the value of one of the minima in the boundary curve is increased by a factor of two. This means that the net effect of the third term in determining the colors visible in the microscope is to alter the intensity of some colors already present. The distribution of wave lengths is not changed. Thus if one were to analyse the light for the distribution of wave lengths present there would be no difference observed in the results predicted by Equation 30 if the last term of this expression were neglected. Practically speaking differences in color would be observed which, for example, would be more prominent for a choice of $\Delta S_1 = 160 \text{ m}\mu$, but almost unobservable for $\Delta S_1 = 320 \text{ m}\mu$. (Compare with fig. 39.)

A good approximation for I, under the restriction that α is small is thus

$$I \sim \left[\sin^2 \frac{\pi \Delta S_1}{\lambda} + \sin^2 \frac{\pi \Delta S_2}{\lambda} \right] \sin^2 \frac{\pi \Delta S'}{\lambda} \quad (33)$$

Equation 33 shows that light transmitted by the analyser consists of a sum of colors (for incident white light) representing each thin lamella separately. The effect of the factor $\sin^2\left(\frac{\pi \Delta S'}{\lambda}\right)$ can be evaluated by considering that the terms enclosed in square brackets form the amplitude of I as a function of $\frac{\Delta S'}{\lambda}$.

The actual wave lengths present are thus governed for the most part by maxima and minima in $\sin^2 \left(\frac{\pi \Delta S'}{\lambda} \right)$, but the separate color intensities are controlled by the terms involving ΔS_1 and ΔS_2 . When $\Delta S'$ is very great, individual maxima and minima in Equation 33 fall very close together so that essentially a "continuous" spectrum is visible, with the intensity of individual wavelengths governed by the factor involving ΔS_1 and ΔS_2 . In this case, I given by Equation 33 indicates the colors present to be functions only of ΔS_1 and ΔS_2 .

A second special case is $\alpha = \pi/4$, for which Equation 30 becomes exactly

$$I = \sin^2 \frac{\pi}{\lambda} (\Delta S_1 + \Delta S_2) \cdot \cos^2 \left(\frac{\pi \Delta S'}{\lambda} \right) + \sin^2 \frac{\pi}{\lambda} (\Delta S_1 - \Delta S_2) \cdot \sin^2 \left(\frac{\pi \Delta S'}{\lambda} \right) \quad (34)$$

Thus the light transmitted by the analyser for this setting of the crystal plates is a mixture of the additive and subtractive colors of the two thin plates, when $\Delta S'$ is very great.

Experimental test of the results for two superposed lamellae

The effects depicted by Equations 33 and 34 have been qualitatively verified in the following manner. Four thin pieces of muscovite ($\Delta S = 2020, 2640, 1100, \text{ and } 570 \text{ m } \mu$ as determined approximately with an Ehringhaus calcite compensator in white light) were cut in rectangular strips with the principal plane of the indicatrix parallel to the long dimension of the strips. The two thicker mica sheets separated by an Iceland spar rhomb ($\Delta S = 3.08 \times 10^5 \text{ m } \mu$) were then arranged with the principal planes of the mica sheets parallel

and making an angle α of about 45° with the traces (in the cleavage plane of the rhombohedron) of the vibration directions in the calcite crystal. This arrangement of plates was then placed on a glass slide on the microscope stage and rotated until the calcite crystal was in a position of extinction (optic planes of the mica sheets lying NW-SE). This is the arrangement for which Equation 34 is valid. A calcite compensator* was then inserted in the accessory slot of the microscope tube and rotated until compensation was achieved. Two positions of compensation could be observed (under reduced illumination and with some difficulty) one corresponding to a retardation of about $4600 \text{ m}\mu$, and the other at about $500 \text{ m}\mu$, which are the values Equation 34 predicts to be observed. This variance from true additive and subtractive colors might occur because of variations in thickness of the mica sheets (maximum observed variation of $40 \text{ m}\mu$ in each) or misinterpretation of the positions of compensation, which for the additive color was particularly difficult.

To observe the optical effects predicted by Equation 33 the thinner mica plates were used. These were arranged with the

* With thick muscovite plates the zeroth order fringe at compensation divides into two equally spaced zeroth order fringes, an effect due to dispersion in the muscovite. The true compensation position was determined for a given direction of rotation with the compensator by inserting greater and greater thicknesses of crystal and observing the separation of the zero positions.

calcite rhomb as described above, except that the angle α was made small (around 10°). It was found through trial and error that mica sheets with relatively low values of ΔS yielded the clearest results in this situation. Using the compensator, compensation was achieved at values of ΔS equal exactly to 1100 and 570 m μ , as predicted by Equation 33.

Extension of the calculations to the case of three or more lamellae

The exact calculation of the intensity of light transmitted through two lamellae with an intervening plate of crystal in different orientation described above is cumbersome, and its extension to the case of three or more lamellae would be impractically tedious. An approximation method (suggested by B. Kamb, oral communication) has therefore been employed to treat these cases. The purpose of this section is to extend the conclusions expressed by Equations 33 and 34 to situations of three or more superposed lamellae. The case of two lamellae is discussed first to show the validity of the approximate method.

The physical arrangement of lamellae under the microscope between crossed nicols is the same as before. Starting with Equation 25, it may be shown that the intensity of light vibrating parallel to AA' (fig. 38) after passing through the first lamella is given by:

$$I_A = \sin^2 2\alpha \sin^2 \left(\frac{\pi \Delta S_1}{\lambda} \right) \quad (35)$$

and that parallel to PP' by

$$I_p = 1 - \sin^2 2\alpha \sin^2 \left(\frac{\pi \Delta S_1}{\lambda} \right) \quad (36)$$

As an approximation it is now assumed that the two beams of light emerging from the first thin plate, after passing through the thick slice of host crystal, are non-coherent in the sense that interference effects in white light are not produced between them due to their large optical path difference in the host (see Ditchburn, 1952, p. 118). With this assumption, it is no longer necessary to consider the phase difference produced by the thick plate. The upper lamella is thus illuminated by two beams of light vibrating in mutually perpendicular planes whose intensities are given by Equations 28 and 29. The interference calculation is now repeated for the second lamella considering each incident beam separately, and replacing factors like D_o of Equation 25 by the square root of the appropriate Equation 35 or 36. The resulting intensity of light vibrating parallel to AA' can thus be shown to be:

$$I'_A = \sin^2 2\alpha \sin^2 \left(\frac{\pi \Delta S_1}{\lambda} \right) \left[1 - \sin^2 2\alpha \sin^2 \left(\frac{\pi \Delta S_2}{\lambda} \right) \right] + \sin^2 2\alpha \sin^2 \left(\frac{\pi \Delta S_2}{\lambda} \right) \left[1 - \sin^2 2\alpha \sin^2 \left(\frac{\pi \Delta S_1}{\lambda} \right) \right] \quad (37)$$

and parallel to PP'

$$1 - \sin^2 2\alpha \left\{ \sin^2 \left(\frac{\pi \Delta S_1}{\lambda} \right) \left[1 - \sin^2 2\alpha \sin^2 \left(\frac{\pi \Delta S_2}{\lambda} \right) \right] + \sin^2 \left(\frac{\pi \Delta S_2}{\lambda} \right) \left[1 - \sin^2 2\alpha \sin^2 \left(\frac{\pi \Delta S_1}{\lambda} \right) \right] \right\} \quad (38)$$

With some manipulation Equation 37 can be rewritten as:

$$I'_A = \frac{1}{2} \sin^4 2\alpha \left[\sin^2 \frac{\pi(\Delta S_1 + \Delta S_2)}{\lambda} + \sin^2 \frac{\pi(\Delta S_1 - \Delta S_2)}{\lambda} \right] + \frac{1}{2} \sin^2 4\alpha \left[\sin^2 \frac{\pi \Delta S_1}{\lambda} + \sin^2 \frac{\pi \Delta S_2}{\lambda} \right] \quad (39)$$

Comparing Equation 39 with Equation 30 it can be seen that the approximation method yields results in essential agreement with those of the exact method, the differences being that the complicated third term of Equation 30 is not present in Equation 39 (its effects become small for small α , see p. 214), and the factors involving $\Delta S'$ are absent in Equation 39. These two equations also differ by a factor of $\frac{1}{2}$ which appears in the second term of Equation 30. As has already been discussed, the factors of $\Delta S'$ in Equation 30 become less important with increasing values of $\Delta S'$. For small α the first term of Equation 39 is small compared to the second, and the equation is essentially the same as Equation 33. Setting $\alpha = \pi/4$, an expression like Equation 34 is obtained.

Calculations for the third, or for any number of succeeding plates may now be carried through treating each plate in the manner described above, neglecting the phase differences produced by the intervening slices of host crystal. For three lamellae the expression for the intensity of light vibrating parallel to AA' is given by

$$\begin{aligned}
 I_A'' = & \sin^2 2\alpha \left[\sin^2 \frac{\pi \Delta S_1}{\lambda} \left(1 - \sin^2 2\alpha \sin^2 \frac{\pi \Delta S_2}{\lambda} \right) \right. \\
 & + \sin^2 \frac{\pi \Delta S_2}{\lambda} \left(1 - \sin^2 2\alpha \sin^2 \frac{\pi \Delta S_1}{\lambda} \right) \left. \right] \\
 & \times \left[1 - \sin^2 2\alpha \sin^2 \frac{\pi \Delta S_2}{\lambda} \right] \\
 & + \left\{ 1 - \sin^2 2\alpha \left[\sin^2 \frac{\pi \Delta S_1}{\lambda} \left(1 - \sin^2 2\alpha \sin^2 \frac{\pi \Delta S_2}{\lambda} \right) \right. \right. \\
 & + \left. \left. \sin^2 \frac{\pi \Delta S_2}{\lambda} \left(1 - \sin^2 2\alpha \sin^2 \frac{\pi \Delta S_1}{\lambda} \right) \right] \right\} \\
 & \times \sin^2 2\alpha \sin^2 \frac{\pi \Delta S_3}{\lambda} \quad (40)
 \end{aligned}$$

When α is sufficiently small Equation 40 yields

$$I_A'' = 8\alpha^2 \left[\sin^2 \frac{\pi \Delta S_1}{\lambda} + \sin^2 \frac{\pi \Delta S_2}{\lambda} + \sin^2 \frac{\pi \Delta S_3}{\lambda} \right] \quad (41)$$

which predicts that the observed color intensities are functions of the retardations of each of the lamellae separately. In the other extreme, for $\alpha = \pi/4$, Equation 40 reduces to

$$\begin{aligned}
 I_A'' = & \frac{1}{4} \left[\sin^2 \frac{\pi}{\lambda} (\Delta S_1 + \Delta S_2 + \Delta S_3) + \sin^2 \frac{\pi}{\lambda} (\Delta S_1 + \Delta S_2 + \Delta S_3) \right. \\
 & + \sin^2 \frac{\pi}{\lambda} (\Delta S_1 - \Delta S_2 + \Delta S_3) \quad (42) \\
 & \left. + \sin^2 \frac{\pi}{\lambda} (\Delta S_1 - \Delta S_2 - \Delta S_3) \right]
 \end{aligned}$$

Thus for this case, additive and subtractive colors of all combinations of the lamellae are seen. Comparing Equations 33 and 34 with Equations 41 and 42 suggests that when this kind of analysis is extended to the case of N thin plates superposed as described above, the colors from each plate independently are seen when the angle between the permitted vibration directions of the lamellae and interposed slice is

small, and a mixture of their additive and subtractive colors are visible when the angle is near 45° .

Applying this result to the problem of determining thicknesses of twinned material by observation of interference colors, it is seen that a median, not a cumulative thickness for the lamellae may be obtained using the procedure outlined previously.

Summary of results of previous sections

The so-called nontwinned lamellae parallel to $\{01\bar{1}2\}$ in calcite and $\{02\bar{2}1\}$ in dolomite show interference colors and four types of interference fringes. Using the interference colors displayed by the lamellae, their optical thicknesses may be determined, and these agree well with measurements made by direct means. This shows that the lamellae are extremely thin twins, usually about one micron or less in thickness. A technique is described for obtaining the orientation of shallowly inclined lamellae which makes use of the fact that the twinned crystal can be placed in a position of extinction between crossed nicols. The technique is useful in eliminating the "blind-spot" from e-lamella diagrams prepared from one thin section. Calculations show that when using the new orientation method and the interference color technique, only the average and not a cumulative interference color produced by a series of superposed lamellae may be ob-

tained. It is suggested on the basis of this work that the term nontwinned lamellae be replaced by microtwinned lamellae, which more correctly indicates the true nature of these features.

APPENDIX I

CRYSTALLOGRAPHIC NOTATION AND A SUMMARY OF
EXPERIMENTALLY DETERMINED GLIDING
ELEMENTS IN CALCITE

Two different systems of crystallographic notation have been used in this thesis. The conventional notation adopted by Turner et al. (1954, p. 886) is used throughout, except in the sections discussing dislocations and mechanical twinning where the Miller or rhombohedral system of indexing is employed. In Turner's notation, letter symbols have been adopted for various directions and planes as follow:

For crystal axes: \underline{c} (vertical) [0001]

$\underline{a}_1, \underline{a}_2, \underline{a}_3$ (horizontal)

For crystal planes: $\underline{c} = (0001)$

$\underline{m} = \{10\bar{1}0\}$

$\underline{r} = \{10\bar{1}1\}$

$\underline{e} = \{01\bar{1}2\}$

$\underline{f} = \{02\bar{2}1\}$

Individual planes of a form are differentiated by subscripts, as $\underline{r}_1 = (10\bar{1}1)$; $\underline{r}_2 = (1\bar{1}01)$; $\underline{r}_3 = (01\bar{1}1)$. Faces of a different form that have a common zone axis are given the same numbered subscript. Thus $\underline{r}_1 = (10\bar{1}1)$; $\underline{e}_1 = (10\bar{1}2)$; $\underline{f}_1 = (\bar{2}021)$, and the zone axis is \underline{a}_2 . All of these relations are depicted

in the equal area projection shown in Figure 42 . Planar structures noted in individual calcite grains are identified by their angular relations to one another and to the c-crystallographic axis. The following angles, measured between poles of faces are important (Palache, Birman and Frondel, 1951, p. 143)

$$\begin{array}{ll}
 \underline{c} \wedge \underline{r} & = 44\frac{1}{2}^{\circ} & \underline{e}_1 \wedge \underline{f}_2 & = 78\frac{1}{2}^{\circ} \\
 \underline{c} \wedge \underline{e} & = 26\frac{1}{4}^{\circ} & \underline{a}_1 \wedge \underline{r}_1 & = 52^{\circ} \\
 \underline{c} \wedge \underline{f} & = 63^{\circ} & \underline{a}_2 \wedge \underline{r}_1 & = 90^{\circ} \\
 \underline{e}_1 \wedge \underline{e}_2 & = 45^{\circ} & \underline{f}_1 \wedge \underline{f}_2 & = 79^{\circ} \\
 \underline{r}_1 \wedge \underline{r}_2 & = 75^{\circ} & \underline{c} \wedge \underline{c}' & = 52\frac{1}{2}^{\circ} \quad (\underline{c}' \text{ is } \underline{c}\text{-axis} \\
 & & & \text{of the twin)} \\
 \underline{e}_1 \wedge \underline{r}_2 & = 70\frac{3}{4}^{\circ} & \underline{e}_1 \wedge \underline{r}_2 & = 38^{\circ}
 \end{array}$$

In Appendix III where the problem of the growth of mechanical twins in calcite is treated in the light of dislocation theory, it is convenient to index the planes according to rhombohedral axes. The relationship between the rhombohedral and hexagonal indices for some important planes is the following: $(111) = (0001)$; $(110) = (01\bar{1}2)$; $(100) = (10\bar{1}1)$; $(11\bar{1}) = (02\bar{2}1)$. The direction $[110] = [\underline{r}:\underline{f}]$. In this coordinate system a lattice vector of the true unit cell is $\frac{1}{2} \underline{a} [112]$, where \underline{a} is the length of the side of the unit rhombohedron containing two CaCO_3 molecules.

A special notation has been developed by Handin et al. (1957) to describe internally rotated lamellae (Turner et al.,

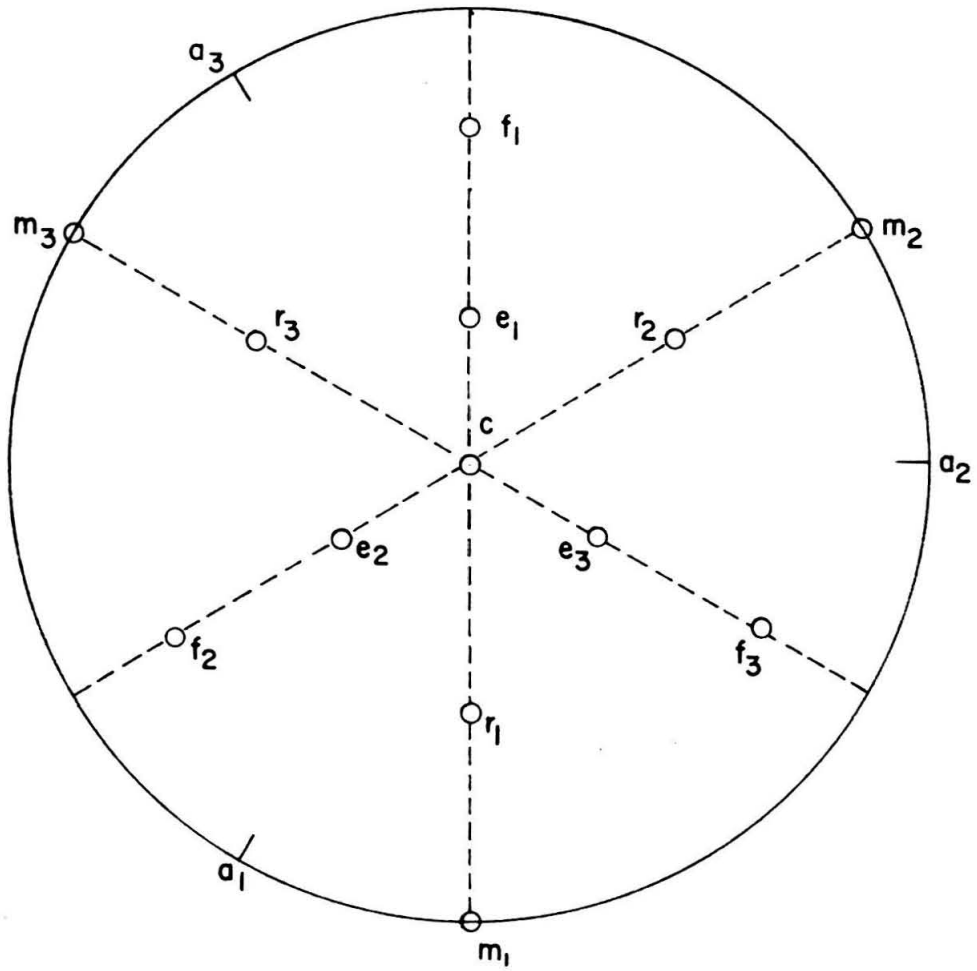


Figure 42. Equal area projection (upper hemisphere) showing poles of common faces and crystal axes in calcite (after Turner et al., 1954).

1954). An internally rotated lamella is designated L, and specific rotated lamellae defined with respect to their original undeformed orientation in the lattice are designated \underline{r}_2 , \underline{f}_3 , etc. Thus the symbol $L_{m_k}^{n_j}$ identifies a lamella m_k internally rotated by glide on the plane n_j . The notation can be extended to describe more complex gliding, but need not be considered here (see Handin et al., 1957).

Experimental studies on single crystals of calcite have disclosed a variety of glide mechanisms which may operate at various temperatures. These results are presented by both Turner et al. (1954) and Higgs and Handin (1959), and a summary of their findings is tabulated below.

TABLE 4

Experimentally Determined Glide Relations in Calcite

<u>Glide plane</u>	<u>Glide direction</u>	<u>Sense</u>	<u>Type</u>	<u>Temperature</u>
\underline{r}_1 {10 $\bar{1}$ 1}	$[\underline{r}_1:\underline{f}_2]^*$	negative & positive**	tr.	20°-500° C (neg), 800° C (neg & pos)
\underline{f}_1 { $\bar{2}$ 021}	$[\underline{r}_1:\underline{f}_2]$	negative	tr.	20°, 600° C
\underline{a}_2 { $\bar{1}$ 2 $\bar{1}$ 0}	?	?	tr.	?
\underline{c} (0001)	?	?	tr.	800° C
\underline{e}_1 {01 $\bar{1}$ 2}	$[\underline{e}_1:\underline{r}_2]$	positive	tw.	20°-500° C
\underline{r}_1 {10 $\bar{1}$ 1}	$[\underline{f}_1:\underline{r}_2]$	positive	tw.	20° C

* $[\underline{r}_1:\underline{f}_2]$ designates the edge between \underline{r}_1 {10 $\bar{1}$ 1} and \underline{f}_2 {2 $\bar{2}$ 01}.

** The sense of glide in e-twinning in calcite is "positive" and for f-twinning in dolomite "negative." Similar definitions hold for translation gliding.

APPENDIX II

GLIDE MECHANISMS OBSERVED IN THE DARWIN ROCKS

Though mechanical twinning is the most obvious mode of deformation in the rocks studied here, other glide mechanisms can be deduced from analysis of nonhomogeneously deformed single crystals containing kink bands and warped lamellae. The microscopic techniques used to do this are analogous to those developed by Turner et al. (1954). The method depends on the fact that when a crystal is deformed by translation or twin gliding, lamellae present before deformation are rotated relative to the crystal lattice during the gliding process. Careful measurement of the position of such "internally rotated" structures relative to the c-axis of the crystal can thus be used to deduce the operative glide mechanisms if the deformation is not too complicated.

In the highly deformed Darwin rocks, close examination reveals that twinning lamellae present in many grains are warped and twisted. The purpose here is to examine how such nonhomogeneous distortion is accommodated in the crystals.

There are at least two methods whereby the crystal lattice could undergo such bending: (1) the crystal could deform in plastic bending by means of slip similar to the way in which a thick sheaf of papers is bent (Cottrell, 1953, p. 29) or (2) the crystal could twin or untwin to vary the

thickness of twinning lamellae and bring about bending (Basinski and Christian, 1954). A consequence of (1) is that pre-existing lamellae should be internally rotated in parts of the crystal where slip has occurred. For slip on a single system the axis of external rotation (bending) lies in the glide plane and normal to the glide direction. The poles of the gliding plane and the internally rotated lamellae in all positions of rotation will fall on a great circle when plotted on either a stereographic or equal area net. In practice if the bending is due to unequal slip on two or more glide systems, the method becomes difficult to apply and the exact mode of deformation often cannot be deduced. If bending is accomplished by operation of (2) then it can be shown (Basinski and Christian, 1954, p. 103) that the effect of side ways steps in the twin boundary is to bend the host and twin lattices, there being a rotation of $\frac{b}{t}$ about the normal to the twin direction for each step in the twin boundary. b is the magnitude of the Burgers vector of the twinning dislocation (see appendix III, this thesis), and t is the total thickness of parent and twin crystal measured normal to the twin plane. If in two neighboring sections perpendicular to the twin plane there are n twins of thicknesses p_1 and p_2 , then there are $2n$ twin boundaries and the total number of twinning steps between the two sections is $(p_1 - p_2)\frac{n}{h}$ (h is the minimum step height). The total rotation between the two sections

is $\Delta\theta = \underline{s}(p_1 - p_2)/\underline{t}$, where $\underline{s} = \underline{b}/\underline{h}$ the twinning shear (0.69 for calcite). $\Delta\theta$, p_2 , p_1 , and \underline{t} can then be measured in the crystal. $\Delta\theta$ computed using this equation can be compared with that measured.

In attempting to determine possible gliding elements responsible for warping in individual crystals, simply deformed grains were chosen for examination. Since the gross deformation the Darwin rocks have undergone is not very well known, it is not possible quantitatively to relate the microscopic deformation to the bulk strain. In addition, an entire grain can, and does participate in the deformation, so that no undeformed reference areas exist, as occur in and near the end cups in experimentally deformed specimens, which may be used to establish absolutely the glide systems in operation.

The procedure followed here is to plot orientation data from each part of a warped grain on a stereographic projection, arbitrarily choosing one portion to be the "reference" area. The axis of external rotation is then found relative to the crystal axes in the reference portion. The results of measurements on 12 grains are presented in Tables 5 and 6. Table 5 refers to grains where bending is thought to be predominantly accomplished by translation gliding, and Table 6 to those grains where change in thickness of the twins might account for the deformation. In the tables starred symbols refer to data in the "rotated"

portion unstarred in the reference portion of each grain. No statistical significance can be attached to the relative frequency of occurrence of each of these modes of bending, because the grains were not randomly picked during traverses of the thin sections.

The data given in Tables 5 and 6 indicate that:

(1) in many grains the observed bending may result from translation gliding on planes observed to operate in laboratory experiments, i.e., $\underline{r}\{10\bar{1}1\}$ and $\underline{f}\{02\bar{2}1\}$ (appendix I), and on some that are not commonly observed in experiments, i.e., positive $\underline{r}\{10\bar{1}1\}$ gliding and $\underline{c}(0001)$ and $\underline{m}\{10\bar{1}0\}$ gliding. (2) Examples of bending through accommodation to changes in thickness of twins can be found, but in the cases investigated the computed angles of bending are relatively much greater than those observed. This is probably due principally to the crudeness of the measurements, but some influence of translation gliding in the bending cannot be discounted. (3) In the rocks used in this study, anomalously oriented lamellae such as those described by Borg and Turner (1953) are commonly associated with non-homogeneously deformed grains.

TABLE 5.

Summary of Translation Gliding Relations
in Grains from the Darwin Fold

<u>Description</u>	<u>Bending Data</u>	<u>Angles</u>	<u>Possible Types of Glide</u>
Two sets of equally developed microtwinned lamellae	Bending axis for \underline{c} , \underline{a}_3 $\underline{c} \ \underline{c}^* = 15^\circ$	$\underline{c} \wedge \underline{e}_1 = 26$ $\underline{c} \wedge \underline{e}_2 = 26$ $\underline{c}^* \wedge \underline{e}_1^* = 31$ $\underline{c}^* \wedge \underline{e}_2^* = 32$	\underline{f}_2 or \underline{r}_2 active with bending about \underline{a}_3
Two sets of lamellae, \underline{e}_1 visibly twinned, of variable width; \underline{e}_2 microtwinned	Bending axis is \underline{a}_3 $\underline{c} \wedge \underline{c}^* = 14^\circ$	$\underline{c} \wedge \underline{e}_1 = 25$ $\underline{c} \wedge \underline{e}_2 = 25$ $\underline{c}^* \wedge \underline{e}_1^* = 28$ $\underline{c}^* \wedge \underline{e}_2^* = 25$	Translation on any plane with \underline{a}_3 as zone axis, i.e., \underline{r}_2 , \underline{f}_2 , \underline{m}_2
Three areas of different orientation; \underline{e}_1 is 25% twinned, \underline{e}_2 is microtwinned	Axis of bending nearly coincides with the \underline{a}_3 -axis $\underline{c} \wedge \underline{c}^* = 40^\circ$ $\underline{c} \wedge \underline{c}^{**} = 13^\circ$ $\underline{c}^* \wedge \underline{c}^{**} = 28^\circ$	$\underline{c} \wedge \underline{e}_1 = 36$ $\underline{c} \wedge \underline{e}_2 = 26$ $\underline{c}^* \wedge \underline{e}_1^* = 18$ $\underline{c}^* \wedge \underline{e}_2^* = 40$ $\underline{c}^{**} \wedge \underline{e}_1^{**} = 33$ $\underline{c}^{**} \wedge \underline{e}_2^{**} = 27$	\underline{r}_2 , \underline{f}_2 or \underline{m}_2 are possibly glide planes
One set of lamellae \underline{e}_1 , 20% twinned, constant width	Bending about \underline{a}_1 $\underline{c} \wedge \underline{c}^* = 10^\circ$	$\underline{c} \wedge \underline{e}_1 = 30$ $\underline{c}^* \wedge \underline{e}_2^* = 29$	Glide on \underline{r}_3 , \underline{f}_3 , \underline{m}_2
\underline{e}_1 , \underline{e}_2 each 5% twinned	Bending axis is near pole to \underline{m}_3 for \underline{c}	$\underline{c} \wedge \underline{e}_1 = 37$ $\underline{c} \wedge \underline{e}_2 = 32$ $\underline{c}^* \wedge \underline{e}_1^* = 31$ $\underline{c}^* \wedge \underline{e}_2^* = 26$	Glide on either \underline{c} or \underline{m}_3

TABLE 5 (CONT.)

<u>Description</u>	<u>Bending Data</u>	<u>Angles</u>	<u>Possible Types of Glide</u>
One set of microtwinned lamellae \underline{e}_1	Bending axis is 22° from \underline{a}_3 . \underline{e}_1 has moved along the great circle $\overline{\underline{r}_3 \underline{c}_1 \underline{r}_2}$ $\underline{c} \wedge \underline{c}^* = 20^\circ$	$\underline{c} \wedge \underline{e}_1 = 26$ $\underline{c}^* \wedge \underline{e}_1^* = 11$	Negative \underline{r}_2 glide. \underline{a}_3 is perpendicular to glide line. \underline{e}_1^* is thus a $L_{\underline{e}_1}^{\underline{r}_2}$ lamella (Appendix I)
\underline{e}_1 5% twinned \underline{e}_2 microtwinned visible twins or irregular width	$\underline{c} \wedge \underline{c}^* = 14^\circ$ bending axis for \underline{c} is approximately \underline{a}_2	$\underline{c} \wedge \underline{e}_1 = 26$ $\underline{c} \wedge \underline{e}_1 = 27$ $\underline{c}^* \wedge \underline{e}_1^* = 33$ $\underline{c}^* \wedge \underline{e}_2^* = 33$	Positive (?) \underline{r}_2 glide could account for the observed bending of the crystal and for the observed internal rotation of lamellae
Crystal is 50% twinned on \underline{e}_1 , twin bands vary in width	$\underline{c} \wedge \underline{c}^* = 36^\circ$ axis of bending exactly coincides with pole to \underline{m}_2	$\underline{c} \wedge \underline{e}_1 = 32^\circ$ $\underline{c}^* \wedge \underline{e}_1^* = 20^\circ$ $\underline{e}_1 \wedge \underline{e}_1^* = 10^\circ$	Glide on \underline{c} (0001) (?) Internal rotation data indicate glide in opposite directions in two parts of the crystal. \underline{e}_1 follows the great circle $\overline{\underline{e}_3 \underline{e}_1 \underline{a}_3}$.
$\underline{e}_1, \underline{e}_2$ both microtwinned \underline{r}_3 cleavage	$\underline{c} \wedge \underline{c}^* = 32^\circ$ axis of bending is 9° from pole to \underline{m}	<u>Parts I, II</u> $\underline{c} \wedge \underline{e}_1 = 22, 19$ $\underline{c} \wedge \underline{e}_2 = 35, 31$ $\underline{e}_1 \wedge \underline{e}_2 = 48, 45$ $\underline{c} \wedge \underline{r}_3 = 48, 43$ $\underline{r}_3 \wedge \underline{e}_1 = 40, 34$ $\underline{r}_3 \wedge \underline{e}_2 = 56, 46$	Glide on \underline{c} (0001) or $\{\overline{1}2\overline{1}0\}$ with glide direction [0001] angular changes in rotated sector compatible with negative translation on \underline{r}_1 .

TABLE 6

Twin Accommodation Bending in Crystals
from the Darwin Fold

<u>Description</u>	<u>p₁(mm)</u>	<u>p₂(mm)</u>	<u>t(mm)</u>	<u>θ_{obs}</u>	<u>θ_{calc}</u>	<u>Internal rotation data</u>
Amount of twinning changes from 35% to 20% across bend. Axis of bending perpendicular to glide direction in <u>e₁</u>	0.01	0.005	0.015	8°	13°	<u>c</u> ^ <u>e₁</u> = 28 <u>c*</u> ^ <u>e₁*</u> = 28
40% twinned on <u>e₁</u> , contains micro-twinned lamellae <u>e₂</u> . Axis of bending is perpendicular to glide direction in <u>e₁</u>	0.01	0.005	0.015	9°(?)	13°	<u>c</u> ^ <u>e₁</u> = 32 <u>c</u> ^ <u>e₂</u> = 25 <u>c*</u> ^ <u>e₁*</u> = 25 <u>c*</u> ^ <u>e*</u> = 30
20% twinned on <u>e₁</u> with <u>a₂</u> as axis of rotation for <u>c</u> and <u>e₁</u>	0.1	0.05	0.15	7°	13°	

APPENDIX III

DISLOCATION MODEL FOR THE GROWTH OF
MECHANICAL TWINS IN CALCITE

Introduction

It is reasonable to suspect that the plastic behavior of calcite--twinning, translation gliding, and work hardening--must be explicable in terms of the theory of dislocations. This is because one is faced with essentially the same problems as are posed in explaining the plastic behavior of metals. For one thing, it is geometrically difficult to imagine all atoms on a particular slip or twin plane moving simultaneously during slip or twinning, since thermal fluctuations throughout the crystal would be likely to cause movement sooner in one place than another (Cottrell, 1953, p. 7). A second reason is that there are large discrepancies between experimentally determined critical shear stresses for twinning and translation gliding and values for the theoretical shear strength of perfect crystal determined using the approximation of Frenkel* (see Cottrell, 1953, p. 9).

*The Frenkel method states that the critical stress at which slip takes place in a crystal is $\tau_c = \mu/2$, where μ is the shear modulus, which for calcite is different for various planes and directions. μ can be computed from the

The discrepancy for twinning is much greater than for translation gliding. Low experimentally observed values for twinning in metals, particularly cadmium and zinc, have been interpreted as indicating (Cahn, 1954) that most investigators have measured stresses required to thicken already existing twins, not the stresses required to initiate twinning lamellae. It has in fact been recently proposed (Bilby and Entwisle, 1954) that the nucleation of mechanical twins is controlled by large local stresses which are set up in a crystal around inhomogeneities of various kinds (dislocations, impurities) and that twinning does not obey a critical resolved shear stress law. Garber (1947) has shown that stresses required to initiate twins in optically perfect calcite are very high ($\gg 20 \text{ kgm/cm}^2$, see Cahn, 1954, p. 427), but available experimental data on twinning in calcite single crystals (see footnote, p. 235) indicate low values of the critical resolved shear stress for twinning.

There is some direct evidence that movement of dislocations is responsible for translation gliding and

single crystal compliance constants, which are usually referred to the crystallographic axes, by using the formulae $s'_{ijkl} = \lambda_{i\alpha} \lambda_{j\beta} \lambda_{k\delta} \lambda_{l\gamma} s_{\alpha\beta\delta\gamma}$ (Nye, 1957, p. 137). For e-twinning $\tau_c = 0.35 \times 10^5 \text{ kgm/cm}$, and $\tau_{\text{obs}} = 20 \text{ kgm/cm}^2$; for r-gliding $\tau_c = 0.45 \times 10^5 \text{ kgm/cm}^2$ and $\tau_{\text{obs}} = 180-1800 \text{ kgm/cm}^2$. Experimental data are taken from Turner et al. (1954, p. 889).

twinning in calcite. Keith and Gilman (1959) have produced arrays of etch pits on glide planes around indentation points of various kinds of dies. The glide planes depicted in this manner are the same as those deduced in the more elaborate experiments of Turner et al. (1956). Etch pits were also produced along microtwinning (?) e-lamellae (their figure 21).

The present study shows that at least geometrically the proper arrays of dislocations can be found to account for the twinning movements in calcite which satisfy the conditions of the so-called "pole mechanism" of Cottrell and Bilby (1951). The treatment is thus the same as has been proposed to account for twinning in metals. This approach is physically more satisfactory than the usual one invoked in explaining twinning in carbonate minerals which merely describes the twin process as one of simple shear with gliding on successive ionic layers in the proper sense and amount to develop a twinned lattice from an original or host lattice (Higgs and Handin, 1959). However, a dislocation theory of twinning as applied to calcite is still restricted in its description of the actual process, as the theory can account only for the shear components of the twinning movements together with possible movements perpendicular to the twinning plane. The structure of the twin boundary is not described, and no specific treatment of the required rotations of CO_3 - groups during twinning is pro-

vided by the theory. Before turning to a discussion of the "pole mechanism" and its application to calcite, a previous theoretical treatment of twinning in calcite is discussed.

Previous Work on the Mechanism
of Twinning in Calcite

Lifshits and Obriemov (1948) have studied twinning in calcite using a model which does not explicitly postulate the existence of dislocations to account for the twinning. However, dislocations are created by allowing very large elastic strains, comparable in magnitude to the twinning shear, to exist near the point of application of load (a knife edge) without causing fracture. This allows atoms just under the loading point to be sheared through large distances, and so to fall into twinned position one by one thus creating a twinning dislocation (Cahn, 1953, p. 378). By these means it has been possible to qualitatively account for the observations of Garber (1947) on the stages of development of twins in calcite (p.177 this thesis).

The Pole Mechanisms

Outline of the theory

Cottrell and Bilby (1951) have proposed a mechanism for the production of mechanical twins in metals by dislocation movements, the essential idea being that a single dislocation accounts for the twinning deformation on successive twin planes. The mechanism requires that three dislocations meet at a node in the lattice. Designate these three by their Burgers vectors \bar{b}_1 , \bar{b}_2 , and \bar{b}_3 . Then at the node the relation

$$\bar{b}_1 + \bar{b}_2 + \bar{b}_3 = 0 \quad (i)$$

must be satisfied (Cottrell and Bilby, 1951, p. 57⁴). Let \bar{b}_3 be the dislocation accounting for the twinning movements (in this theory the macroscopic shear of only atom centers and CO_3 groups associated with the twinning). If the twin plane is specified by its vector normal \bar{k} , and $(\bar{b}_3 \cdot \bar{k}) = 0$, the twinning dislocation is free to continuously move in the twin plane provided neither of the other two dislocation lines lie in the plane and interfere with its motion. The "pole" mechanism arises from the case where the other two dislocation lines thread the twin plane (\bar{b}_1 and \bar{b}_2 thus acting as "poles" to the twin plane). Relation (i) requires that if $\bar{b}_3 \cdot \bar{k} = 0$, $(\bar{b}_1 + \bar{b}_2) \cdot \bar{k}$ must equal zero as well. There is thus a component of each of the pole

dislocations

$$\bar{h} = (\bar{b}_1 \cdot \bar{k})\bar{k} = - (\bar{b}_2 \cdot \bar{k})\bar{k} \quad (ii)$$

perpendicular to the twin plane which allows the line of \bar{b}_3 to be displaced by \underline{h} ($=|\bar{h}|$) for each revolution about the poles. If \underline{h} is equal to the spacing between successive twin planes, then \bar{b}_3 can sweep out twinned material on successive planes as it climbs up the spiral ramp created by the pole dislocation.

The problem is therefore one of finding the proper array of dislocations meeting at a node. In particular the requirements to be satisfied are (Cottrell and Bilby, 1951, p. 576):

- (1) The sweeping dislocation (twinning dislocation) must produce the correct shear displacement to generate the transformed structure on the sweeping (twin) plane.
- (2) The Burgers vector of the pole dislocation must have a component perpendicular to the sweeping planes that is equal to their spacing.
- (3) The pole dislocation must be anchored strongly enough so that it does not move under the stress causing the sweeping dislocation to move.

- (4) The sweeping and pole dislocations, together with perhaps other dislocations must form a node and in the node the sweeping dislocation must be free to move in the sweeping plane which is intersected by the pole.

Bilby (1953) has reached a general conclusion that a generating node of the kind required above can always be found in any crystal lattice. In the following, Bilby's result will be particularized for the case of calcite.

Bilby (1953) shows that a generating node between two Bravais lattices \underline{P} and \underline{C} with vectors $\bar{P}(n) = n^j \bar{p}_j$ and $\bar{C}(n) = n^j \bar{c}_j$ (sum over repeated indices $i = 1, 2, 3$) is

$$-\bar{P}(n) + \bar{C}(n) + (\bar{C}(n) \cdot \bar{k}) (\Gamma \bar{i} + \epsilon \bar{k}) . \quad (\text{iii})$$

\bar{k} and \bar{i} are mutual orthogonal vectors, \bar{k} being perpendicular to the twin plane, and \bar{i} parallel to the direction of the twin shear. Γ describes the twin shear and ϵ a contraction or extension parallel to \bar{k} . $-\bar{P}$ is the pole dislocation in \underline{P} and \bar{C} is the pole dislocation in \underline{C} , with $(\bar{C} \cdot \bar{k})(\Gamma \bar{i} + \epsilon \bar{k})$ the twinning dislocation.

The theory applied to calcite

For calcite Γ is equal to $\tan \psi'$ (fig. 44), and $\epsilon = 0$. In order to investigate the various possibilities for \bar{P} and \bar{C} in calcite, we proceed by specifying the twin dislocation Burgers vector as $(\bar{C} \cdot \bar{k})(\tan \psi' \bar{i})$, choosing \bar{C} in the original lattice and then solving Equation iii for \bar{P} . Acceptable possibilities for \bar{P} are complete or partial dislocations with $\bar{P} \cdot \bar{k}$ equal to \underline{h} and which do not have large misfit energies in the twin lattice. A restriction on the vectors \bar{C} in the original lattice is possible. The requirement that the deformation in twinning be plane perpendicular to the shear plane in twinning indicates that the Burgers vector \bar{C} must originally lie in the shear plane, for otherwise the transformation associated with \bar{C} will not produce plane disformation of the type required.

For calcite there are three possibilities for \bar{C} which have reasonably short Burgers vectors and are complete dislocations in the \bar{C} lattice. These are $\underline{a}[110]$,* $\frac{1}{2}\underline{a}[112]$, and $2\underline{a}[111]$. A fourth lattice vector $2\underline{a}[100]$ is excluded because it lies in the twin plane (110) (i.e. $\bar{P} \cdot \bar{k} = 0$). Proceeding as indicated above, the various vectors obtained from Equation iii for \bar{P} are tabulated below.

* See Appendix I.

TABLE 7

$\bar{C}(n)$	$\bar{C}(n)$ in rhomb. coordinates	$\bar{P}(n)$	$\bar{P}(n)$ in rhomb. coordinates
$h \bar{k} - \frac{1}{2} h \tan \psi'$	$\underline{a}[110]$	$h \bar{k} + \frac{1}{2} h \tan \psi'$	$\underline{a}[110]$
$-\frac{1}{2} h (\bar{k} + \cot \beta \bar{i})$	$\frac{a}{2}[112]$	$-\frac{h}{2} [\bar{k} + (\cot \beta - \frac{1}{2} \tan \psi') \bar{i}]$	nearly $\frac{1}{2} \underline{a}[110]$
$-2 h (\bar{k} + \tan \psi' \bar{i})$	$2\underline{a}[111]$	$-2h [\bar{k} + (\tan \zeta - 2 \tan \psi') \bar{i}]$	neither a partial nor a complete dislocation

In the above table, the angles, β , ψ' , ζ are defined in Figure 44. It appears that the only suitable choice for \bar{C} is a vector of the type $\underline{a}[110]$ for this yields a vector in the twin lattice which is exactly $\underline{a}[110]$.

It can now be established that all conditions on the node given above are satisfied. The first is satisfied by hypothesis. The second is accounted for if the dislocations \bar{C} and \bar{P} ($\underline{a}[110]$) are of screw character. Condition (3) only requires that the pole dislocation in each lattice be immobile under the stresses causing the twin dislocation to move. Dislocations with Burgers vectors $\underline{a}[110]$ are mobile in both the twin and original lattice (they are associated with translation gliding on (100), i.e., \underline{r}) but experiments indicate the resolved shear stress for their motion at least at low temperature is much greater than that needed to cause twinning. Hence the dislocations \bar{P} and \bar{C} are probably immobile under the stress required to move the sweeping dislocation.

Condition (4) is satisfied by Bilby's analysis together with (2), that is, specifying the pole dislocation to be of the pure screw type.

Generation of the twin dislocations

The theory outlined above and applied to calcite cannot account for the origin of twinned crystal from perfect crystal which otherwise contains only $a[110]$ screw dislocations. The theory also cannot describe the "reshuffles" which accompany twinning movements such as the rotation of CO_3 -groups. However it is possible to see how these twin dislocations may be generated in calcite. Consider an $a[110]$ screw dislocation in the original lattice which passes through a thin lamella of twinned material and emerges again on the opposite side of the twin. From the above analysis, $a[110]$ becomes a complete dislocation with Burgers vector $a[110]$ in the twin lattice and the difference between these two is precisely the Burgers vector of the twinning dislocation. Twin dislocations will thus be generated at the points of emergence of the pole dislocation from the twin. This argument is the same as that invoked to account for the origin of twin dislocations in metals (Cahn, 1954, p. 437).

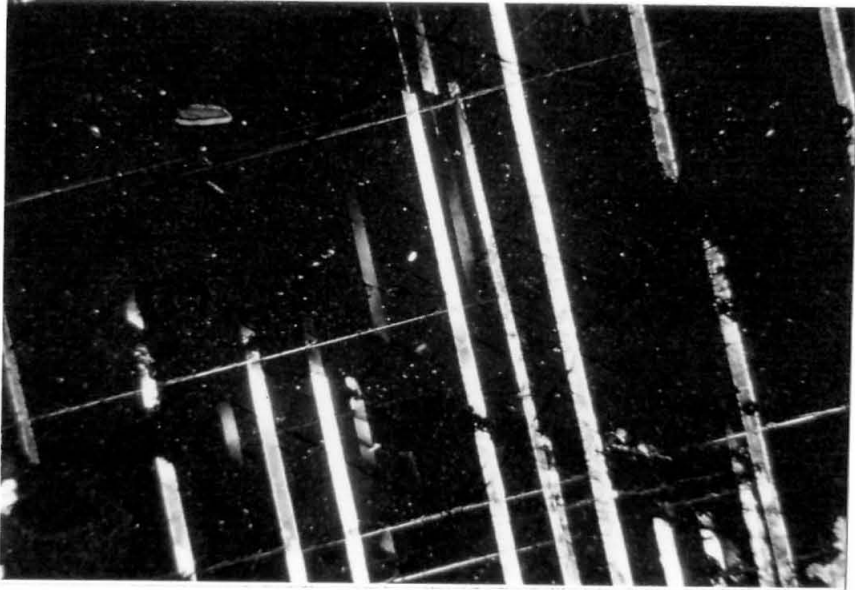


Figure 43. Photomicrograph. Tapered $\{02\bar{2}1\}$ twin lamellae in dolomite. In several of the bright bands crossing the dark field of the host crystal, the interference colors produced by the lamella range from lowest first order gray through blue of the second order. Because the lamellae are inclined approximately 40° to the plane of the thin section, these colors do not reflect the true thickness of the lamellae but some greater thickness than the true one. The true thickness varies from zero to approximately 2μ . Other bright lines crossing the photo at a small angle to the horizontal are thinly twinned $\{02\bar{2}1\}$ lamellae. Other faint dark lines are $\{10\bar{1}1\}$ cleavage.

Geometry of Twin Dislocations in Calcite

Microtwinned lamellae in calcite and dolomite generally exhibit some variation in thickness along the linear projected trace of the lamellae in thin section. This variation can easily be observed by noting changes in interference colors produced by the lamellae (see fig. 43). For a change in thickness the twin boundary must be stepped, and such a step is shown in the drawing of Figure 44, where a dashed line separates material in twin- and non-twin orientation. The step shown in the twin boundary is equal to the spacing between two successive (110) planes, equal to the step height h of the previous analysis. Frank and van Der Merwe (see Read, 1953, p. 109) have termed a step of this type in an otherwise coherent twin-nontwin interface a twinning dislocation. In Figure 44 the dotted atoms represent positions of transition between twinned and nontwin states of the lattice. This drawing must of course be regarded as qualitative only, as for example the transition disturbance is probably distributed over a much greater area of twin plane than shown in the drawing. Furthermore, it has tacitly been assumed that the structure of the twin boundary consists of a single twin-nontwin interface across which atoms and molecules are situated in twin position with respect to one another. Another possibility (Cahn, 1954, p. 383) is that there is

Figure 44. Schematic representation of a step in twin boundary (twinning dislocation) in calcite. Straight dashed line separates crystal in twin and non-twin orientation. Open circles are Ca atoms, planar groups of three circles CO_3 -groups (solid circles carbon atoms). At the step the dashed atoms and molecules are meant to represent approximately the positions of transition from host to twin orientation. $\beta = 36 \frac{3}{4}^\circ$, $\delta = 38 \frac{1}{4}^\circ$, $\zeta = 26 \frac{1}{4}^\circ$, $\psi' = 34 \frac{3}{4}^\circ$, $a = 6.42 \text{ \AA}$ (Turner et al., 1954, p. 887) $\underline{h} = 7.64 \text{ \AA}$. $\tan \psi' = 2 \tan(\delta/2)$.

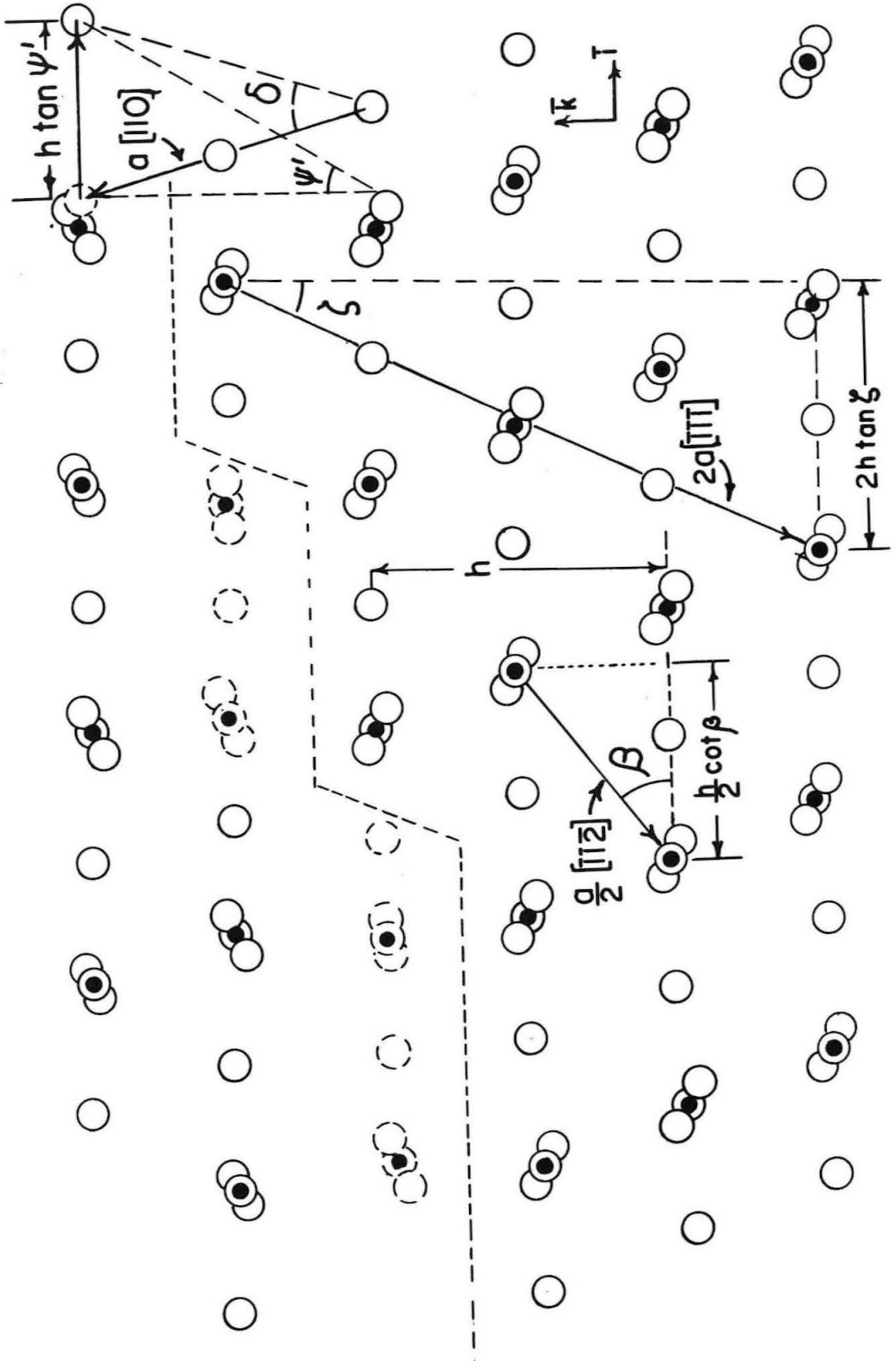


Figure 44

a layer at the twin interface where CO_3 -groups are parallel to the twinning plane. This structure actually differs from the one shown in Figure 44 by only a $26\frac{1}{4}^\circ$ counterclockwise rotation of CO_3 -groups at the twin boundary about an axis lying in the twin plane and perpendicular to the direction of twinning shear. A reshuffle of this type may accompany the twinning movements, but is not described in terms of the pole mechanism.

The existence of tapered twins (fig. 43) can provide important evidence for the mechanism of twinning discussed here. A consequence of the Cottrell-Bilby model is that twins are built up conically in a way analogous to the growth spirals on crystal faces, since the portion of the sweeping dislocation near the pole has a higher angular velocity and can sweep out twinned material more rapidly (Cottrell and Bilby, 1957). Incipient mechanical twins can thus always be expected to be somewhat lens shaped.

REFERENCES

- Adams, F. D., and Nicolson, J. T., 1900, An experimental investigation into the flow of marble: Philos. Trans. Roy. Soc., A195, 363-401.
- Airy, G. B., 1833, Trans. Cambr. Phil. Soc., 41, 313.
- Bailey, S. W., Bell, R. A., Peng, C. J., 1958, Plastic deformation of quartz in nature: Geol. Soc. Am. Bull., 69, 1443-1466.
- Bain, G. W., 1938, The central Vermont marble belt: New England Intercollegiate Geological Assn. Guidebook, 23 pp.
- Ball, S. H., 1907, A geologic reconnaissance in southwestern Nevada and California: U.S.G.S. Bull., 308, 218 pp.
- Balsley, J. R., 1941, Deformation of marble under tension at high pressure: Am. Geophys. Union Trans., 22, 519-525.
- Barrett, C. S., 1952, Structure of metals: McGraw-Hill Book Co., New York, 661 pp.
- Basinski, Z. S., and Christian, J. W., 1954, Crystallography of deformation by twin boundary movements in indium-thallium alloys: Acta Met., 2, 101-116.
- Bilby, B. A., 1953, On the mutual transformation of lattices: Phil. Mag., 44, 782-785.
- Bilby, B. A., and Entwisle, A. R., 1954, The formation of mechanical twins: Acta Met., 2, 15-19.
- Biot, M. A., 1957, Folding instability of a layered viscoelastic medium under compression: Proc. Roy. Soc., A242, 444-454.
- Bishop, J. F. W., 1953, A theoretical examination of the plastic deformation of crystals by glide: Phil. Mag., 44, 51.
- Bishop, J. F. W., A theory of the tensile and compressive textures of face-centered cubic metals: J. Mech. Phys. Solids: 3, 130, 259.

- Bishop, J. F. W., and Hill, R., 1951a, A theory of the plastic distortion of a polycrystalline aggregate under combined stresses: Phil. Mag., 42, 414-427.
- Bishop, J. F. W., and Hill, R., 1951b, A theoretical derivation of the plastic properties of a polycrystalline face-centered metal: Phil. Mag., 42, 1298-1307.
- Borg, I., and Turner, F. J., 1953, Deformation of Yule marble: Part VI--Identity and significance of deformation lamellae and partings in calcite grains: Geol. Soc. Am. Bull., 64, 1343-1352.
- Cahn, R. W., 1953, Soviet work on mechanical twinning, Nuovo Cimento Supplemento, 10, ser. 9, no. 4.
- Cahn, R. W., 1954, Twinned crystals: Advances in Physics, 3, no. 12, 363-445.
- Calnan, E. A., and Clews, C. J. B., 1951, The development of deformation textures in metals--Part III, Hexagonal structures: Phil. Mag., 42, 919-931.
- Chayes, F., 1956, Petrographic modal analysis: John Wiley & Sons, New York, 113 pp.
- Christie, J. M., 1958, Dynamic interpretation of the fabric of a dolomite from the Moine thrust zone in north-west Scotland: Am. Jour. Sci., 256, 159-170.
- Christie, J. M., and Raleigh, C. B., 1959, Origin of deformation lamellae in quartz: Am. Jour. Sci., 257, 385-407.
- Cloos, E., 1947, Oolite deformation in the South Mountain fold, Maryland: Geol. Soc. Am. Bull., 58, 483-918.
- Cloos, E., 1951, The physical features of Washington County: Department of Geology, Mines, and Water Resources, State of Maryland Report, 333 pp.
- Cottrell, A. H., 1953, Dislocations and plastic flow in crystals: Clarendon Press, Oxford, 223 pp.
- Cottrell, A. H., and Bilby, B. A., 1951, A mechanism for the growth of deformation twins in crystals: Phil. Mag., 42, 573-581.
- Crampton, C. B., 1956, Loch Shin limestone--comparison of dolomite and calcite fabrics: Edinburg Geol. Soc. Trans., 16, 334-337.

- DeSitter, L. U., 1956, Structural geology: McGraw-Hill Book Co., New York, 552 pp.
- Ditchburn, R. W., 1958, Light: Interscience Publishers, Inc., New York, 680 pp.
- Emmons, R. C., 1943, The universal stage: Geol. Soc. Am. Memoir 8, 205 pp.
- Erwin, H. D., and Gardner, D. L., 1940, Notes on the geology of a portion of the Calico mountains, San Bernardino County, California: California Jour. Mines and Geology, 36, 293-304.
- Fairbairn, H. W., 1949, Structural petrology of deformed rocks: Addison and Wesley Publishing Co., Cambridge, Mass., 344 pp.
- Fairbairn, H. W., and Hawkes, H. E., Jr., 1941, Dolomite orientation in deformed rocks, Am. Jour. Sci., 239, 617-632.
- Fresnel, A., 1821, Ann. Chim., 17, 167.
- Garber, R. I., 1947, The mechanism of calcite and nitre twinning under plastic deformation, J. Phys. USSR, 11, 55-66.
- Gay, T. E., and Wright, L. A., 1954, Geology of the Talc City area, Inyo County: Calif. Div. Mines Bull. 170, Map no. 12.
- Gilmour, P., and Carman, M. F., 1954, Petrofabric analysis of the Loch Tay limestone: Geol. Mag., 91, 49-60.
- Green, A. P., 1951, The use of plasticine models to simulate the plastic flow of metals: Phil. Mag., 42, 365-373.
- Griggs, D. T., 1936, Deformation of rocks under high confining pressures: Jour. Geol., 44, 541-577.
- Griggs, D. T., 1939, Creep of rocks: Jour. Geol., 47, 225-251.
- Griggs, D. T., 1940, Experimental flow of rocks under conditions favoring recrystallization: Geol. Soc. Am. Bull., 51, 1001-1022.

- Griggs, D. T., and Miller, W. B., 1951, Deformation of Yule marble, Part I: Geol. Soc. Am. Bull., 68, 853-862.
- Griggs, D. T., Turner, F. J., Borg, I., and Soska, J., 1951, Deformation of Yule marble: Part IV--effects at 150°C, Geol. Soc. Am. Bull., 62, 1385-1406.
- Griggs, D. T., Turner, F. J., Borg, I., and Soska, J., 1953, Deformation of Yule Marble: Part V--effects at 300°C: Geol. Soc. Am. Bull., 64, 1327-1342.
- Griggs, D. T., and Handin, John, eds., 1960, Rock deformation (A symposium): Geol. Soc. Am. Memoir 79, 382 pp.
- Griggs, D. T., Turner, F. J., and Heard, H., 1960, Deformation of rocks at 500° to 800° C.: in Rock Deformation (A symposium): Geol. Soc. Am. Memoir 79, 39-104.
- Hall, W. E., and Mackevett, E. M., 1958, Economic geology of the Darwin quadrangle, Inyo County, California: Calif. Division Mines Spec. Rept. 51, 73 pp.
- Handin, John, and Griggs, D. T., 1951, Deformation of Yule marble: Part II--predicted fabric changes: Geol. Soc. Am. Bull., 62, 863-885.
- Handin, John, and Fairbairn, H. W., 1955, Experimental deformation of Hasmark dolomite: Geol. Soc. Am. Bull., 66, 1257-1274.
- Handin, John, Higgs, D. V., Lewis, D. R., and Weyl, P. K., 1957, Effects of gamma radiation on the experimental deformation of calcite and certain rocks: Geol. Soc. Am. Bull., 68, 1203-1224.
- Handin, John, Higgs, D. V., and O'Brien, J. K., 1960, Torsion of Yule marble under confining pressure: in Rock deformation (A symposium), Geol. Soc. Am. Geol. Soc. Am. Memoir 79, 245-274.
- Higgs, D. V., and Handin, John, 1959, Experimental deformation of dolomite single crystals: Geol. Soc. Am. Bull., 70, 245-278.
- Hill, R., 1956, The mathematical theory of plasticity: Clarendon press, Oxford, 356 pp.

- Hills, E. S., 1953, Outlines of structural geology, John Wiley and Sons, Inc., New York, 182 pp.
- Hopper, R. H., 1947, Geologic Section from the Sierra Nevada to Death Valley, California: Geol. Soc. Am. Bull., 58, 393-432.
- Jaeger, J. C., 1956, Elasticity, Fracture and Flow: John Wiley and Sons, Inc., New York, 152 pp.
- Jaswon, M. A., and Dove, D. B., 1960, The crystallography of deformation twinning: Acta Cryst., 13, 232-240.
- Jones, K. A., 1959, A petrofabric method of fold analysis: Am. Jour. Sci., 257, 138-143.
- Kamb, W. B., 1958, Isogyres in interference figures: Am. Mineralogist, 43, 1029-1067.
- Kamb, W. B., 1959, Theory of preferred crystal orientation developed by crystallization under stress: Jour. Geol., 67, 153-170.
- Kamb, W. B., 1961, The thermodynamic theory of nonhydrostatically stressed solids: J. Geoph. Res., 66, 259-271.
- Karman, Th. von, 1910, Untersuchungen über Knickfestigkeit: Collected works of Theodore von Karman, v. 1, 90-140.
- Keith, R. E., and Gilman, J. J., 1959, Dislocation etch pits and plastic deformation in calcite: General Electric Research Laboratory Report No. 59-RL-2207, 19 pp.
- Kienow, S., 1942, Grundzüge einer Theorie der Faltungen und Schieferungsvorgänge: Fortschritte der Geologie und Paleontologie, Band 14, Heft 46, 129 pp.
- Knopf, E. B., and Ingerson, E., 1938, Structural petrology: Geol. Soc. Am. Memoir 6, 270 pp.
- Knopf, E. B., 1949, Fabric changes in Yule marble after deformation in compression: Am. Jour. Sci., 247, (a) 433-461; (b) 437-569.
- Ladurner, J., 1950, Beitrag zur Typisierung von Quarzfalten: Tschermaks Miner. u. Petrog. Mitt., F. 3, Band II, 47-66.

- Lifshits, I. M., and Obreimov, I. V., 1948, Some considerations of twinning in calcite (in Russian): Izv. Akad. Nauk. Ser. Phys., 12, No. 2, 67-80.
- McIntyre, D. B., 1951, The tectonics of the area between Grantown and Tomintoul (Mid-Strathspey): Quart. Journ. Geol. Soc., 57, 1-22.
- McIntyre, D. B., and Turner, F. J., 1953, Petrofabric analysis of marbles from Mid-Strathspey and Strathavon: Geol. Mag., 90, 225-240.
- Nadai, A. L., 1950, Theory of flow and fracture of solids: McGraw-Hill Book Co., New York, 572 pp.
- Nickelsen, R. P., and Gross, G. W., 1959, Petrofabric study of Conestoga limestone from Hanover, Pennsylvania: Am. Jour. Sci., 257, 276-286.
- Nye, J. F., 1957, Physical Properties of crystals: Clarendon Press, Oxford, 322 pp.
- Palache, C., Berman, H., and Frondel, C., 1951, Dana's system of mineralogy, vol. II: John Wiley and Sons, Inc., New York, 1124 pp.
- Ramberg, Hans, 1961, Relationship between concentric longitudinal strain and concentric shearing strain during folding of homogeneous sheets of rocks: Am. Jour. Sci., 259, 382-390.
- Ransome, F. L., 1910, Geology and ore deposits of the Bull Frog district, Nevada: U.S.G.S. Bull., 407, 130 pp.
- Read, W. T., 1953, Dislocations in crystals: McGraw-Hill Book Company, Inc., New York, 228 pp.
- Robertson, E. C., 1955, Experimental study of the strength of rocks: Geol. Soc. Am. Bull., 66, 1275-1314.
- Sander, B., 1911, Über Zusammenhänge zwischen Teilbewegung und Gefüge in Gesteinen: Tschermaks Mineralogische und Petrographische Mitteilungen, Bd. 30.
- Sander, B., 1930, Gefügekunde der Gesteine: Julius Springer, Wien, 352 pp.
- Sander, B., 1950, Einführung in die gefügekunde der geologischen körper: Julius Springer, Wien, Vol. II, 409 pp.

- Silver, L. T., 1955, The structure and petrology of the Johnny Lyon Hills area, Cochise county, Arizona: (unpublished) Ph.D. thesis, California Institute of Technology, 407 pp.
- Schmidt, E., and Boas, W., 1950, Crystal plasticity: Hughes and Co., London, 353 pp.
- Sokolnikoff, I. S., 1956, Mathematical theory of elasticity, 2nd. ed.: McGraw-Hill Book Co., New York, 373 pp.
- Stose, G. W., and Swartz, C. K., 1912, Pawpaw-Hancock folio #179; Maryland, West Virginia, Pennsylvania: U.S.G.S. Geologic Atlas of the United States.
- Taylor, G. I., 1938, Plastic strain in metals, Journ. Inst. Metals, 62, 307-324.
- Timoshenko, S., and Goodier, J. N., 1951, Theory of elasticity, 2nd ed.: McGraw-Hill Book Co., New York 602 pp.
- Thompson, N., and Millard, D. J., 1952, Twinning in cadmium, Phil. Mag., 43, 422-440.
- Turner, F. J., 1948, Deformation lamellae in quartz and calcite: Trans. Am. Geoph. Union, 29, 565-569.
- Turner, F. J., 1949, Preferred orientation of calcite in Yule marble: Am. Jour. Sci., 247, 593-621.
- Turner, F. J., 1952, Interpretation of marble fabrics in the light of recent experimental deformation: Congres Geol. Internat., 19th. Session Compt. Rend., sec. 3, fas. 3, 95-111.
- Turner, F. J., 1953, Nature and dynamic interpretation of deformation lamellae in calcite of three marbles: Am. Jour. Sci., 251, 276-298.
- Turner, F. J., 1955, Experimental evidence relating to symmetry of fabric and its bearing on the problem of lineation in tectonites (abs.): Geol. Soc. Am. Bull., 66, 1668.
- Turner, F. J., 1957, Lineation, symmetry, and internal movement in monoclinic tectonite fabrics: Geol. Soc. Am. Bull., 68, 1-18.

- Turner, F. J., and Ch'ih, C. S., 1951, Deformation of Yule marble: Part III--Observed fabric changes due to deformation at 10,000 atmospheres confining pressure, room temperature, dry: Geol. Soc. Am. Bull., 62, 887-905.
- Turner, F. J., Griggs, D. T., Heard, H., 1954, Experimental deformation of calcite single crystals: Geol. Soc. Am. Bull., 65, 883-934.
- Turner, F. J., Griggs, D. T., Heard, H., and Weiss, L. E., 1954, Plastic deformation of dolomite at 380° C: Am. Journ. Sci., 252, 477-488.
- Turner, F. J., Griggs, D. T., Clark, R. H., and Dixon, R. H., 1956, Deformation of Yule marble, Part VIII: Development of oriented fabrics at 300° C-500° C: Geol. Soc. Am. Bull., 67, 1259-1294.
- Weiss, L. E., 1954, A study of tectonic style: U. Cal. Publ. in Geol. Sci., 30, no. 1, 1-102.
- Weiss, L. E., 1958, Structural analysis of the basement system of Turoka, Kenya: Overseas Geology and Mineral Resources, 7, 3-35; 123-153.
- Wright, L. A., 1954, Geology of the Alexander Hills area, Inyo and San Bernardino counties: California Div. Mines Bull 170, Map sheet no. 17.